MEGAPOLI Scientific Report 11-04

Evaluation and Improvement of Regional Model Simulations for Megacity Plumes

MEGAPOLI Deliverable D5.3

Mikhail Sofiev, Marje Prank, Jaakko Kukkonen (Eds)

Mikhail Sofiev, Marje Prank, Jaakko Kukkonen, J. Vira (FMI)
Arjo Segers, Peter Builtjes, Hugo Denier van der Gon (TNO)
Ulrik Korsholm, Iratxe Gonzales-Aparicio, Roman Nuterman,
Alexander Mahura, Alexander Baklanov (DMI)
Spyros Pandis, Christos Fountoukis,
Alexandra Tsimpidi, Vlassis Karydis (FORTH)
and MEGAPOLI regional modelling teams

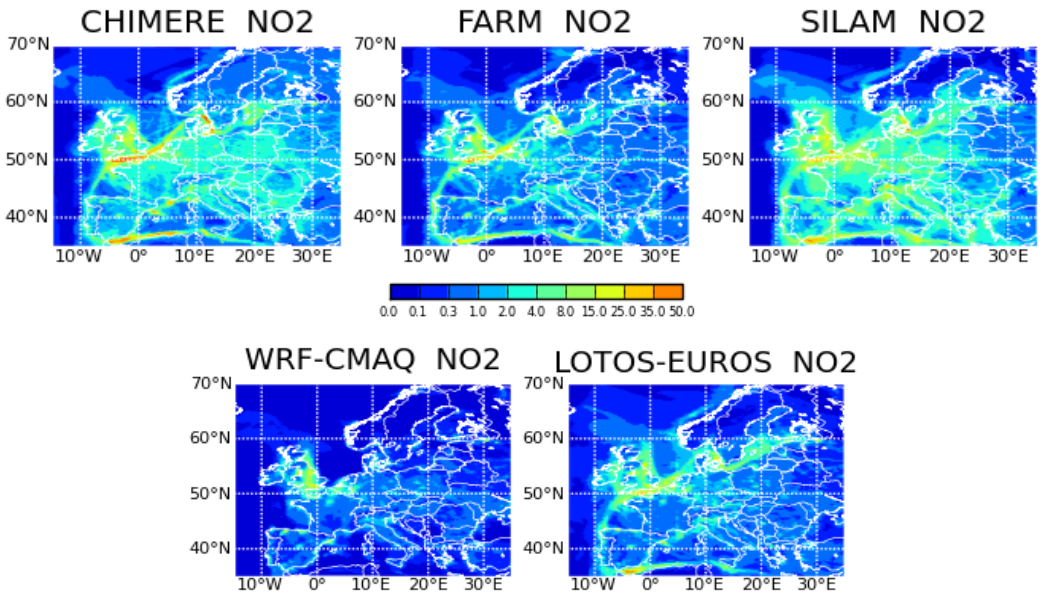

1.7.2009, NO_2 near-surface concentrations from MEGAPOLI regional ensemble

Helsinki, 2011

Colophon

Serial title:
MEGAPOLI Project Scientific Report **11-04**

Title:
Evaluation and improvement of regional model simulations of megacity plumes

Subtitle:
MEGAPOLI Deliverable D5.3

Editor(s):
Mikhail Sofiev, Marje Prank, Jaakko Kukkonen

Main Author(s):
M. Sofiev, M. Prank, J. Kukkonen

Contributing Author(s):
J. Vira (FMI),
A. Segers, P. Builtjes, H. Denier van der Gon (TNO),
U. Korsholm, I. Gonzales-Aparicio, R. Nuterman, A. Mahura, A. Baklanov (DMI),
S. Pandis, C. Fountoukis, A. Tsimpidi, V. Karydis (FORTH)
and MEGAPOLI regional modelling teams

Responsible institution(s):
Finish Meteorological Institute (FMI)
P.O.Box 503
00101 HELSINKI, Finland

Language:
English

Keywords:
Urban climate, anthropogenic heat flux, global climate model, energy balance, metabolism

Url:
http://megapoli.dmi.dk/publ/MEGAPOLI_sr11-04.pdf

Digital ISBN:
978-87-92731-08-1

MEGAPOLI:
MEGAPOLI-30-REP-2011-03

Website:
www.megapoli.info

Content:

Abstract

This report entitled "*Evaluation and improvement of regional model simulations of megacity*" plumes (MEGAPOLI Deliverable D5.3) addresses evaluation and improvement of regional model simulations of megacity plumes. The objectives of this report are:

- to evaluate the regional chemistry transport models using a unified European-wide observational dataset and standardised procedure of the model-measurement comparison
- to compare the model simulations with each other
- to evaluate the performance of multi-model ensemble in comparison with individual models
- to estimate the potential gains of the assimilation of observational information by means of adaptive ensemble methods.
- to evaluate the gaps of knowledge and the most important areas of improvement for the regional chemistry transport models

This report includes results from MEGAPOLI regional ensemble simulations, results from an extensive model review exercise, simulations using the LOTOS-EUROS model for Paris, and long-term simulations using the Enviro-HIRLAM model for the Paris metropolitan area.

This report outlines the outcome of the MEGAPOLI regional ensemble simulations for the intense campaign in Paris in 2009, as well as the ensemble simulations over the baseline year 2005. The datasets provided by the models are described and their first analysis and directions towards the model improvements are presented.

Five regional models have submitted their data for the campaign period of 2009 (CHIMERE, FARM, LOTOS-EUROS, SILAM, and WRF-CMAQ). Computations for 2005 were performed and supplied for the comparison and ensemble analyses by four models (CHIMERE, FARM, SILAM and LOTOS-EUROS).

In addition to the general similarity of the patterns computed with the above-mentioned models, the inter-comparison showed the systematic differences between the model predictions. The differences between the model predictions are of the same order of magnitude than the differences between the individual models and the observations. The reasons for the particular behaviour of each model are time-, region-, and model- specific and have to be analysed separately for each episode.

A series of ensemble based estimates have been generated based on the individual datasets: simple ones, such as arithmetic average and median, as well as observation based adaptive estimates using the Airbase observations.

1. Main Features of the Ensemble Setup

All models have provided the simulation results in agreement with the ensemble data specification described in the MEGAPOLI report 10-12 (deliverable 5.2). Period analysed in this report covers Paris summer campaign in 2009 (July 2009) and the baseline year 2005.

The Paris campaign period has been simulated and the results were submitted for the analysis by 5 modelling teams: CHIMERE (LISA), FARM (Arianet), LOTOS-EUROS (TNO), SILAM (FMI), and WRF-CMAQ (UH). The year 2005 computations were submitted by four groups: CHIMERE (LISA), FARM (Arianet), LOTOS-EUROS (TNO), and SILAM (FMI). An outlook of the models and their features can be found in the report on the MEGAPOLI Deliverable 7.2. An outlook of most of the models used in MEGAPOLI (including Enviro-HIRLAM, FARM, LOTOS-EUROS, SILAM and WRF-CMAQ) can be found in *Kukkonen et al. (2011).*

FMI has provided the ftp facility and hosted the dataset. The model predicted fields have been treated by the Ensemble Analysis Toolset developed in FMI. This tool comprises a set of software instruments for the model comparison with observations, inter-comparison with each other, as well as for the generation of both observation-independent and adaptive ensemble based estimates.

Some models could not provide the data for the ensemble construction but still performed certain evaluation and model-measurement comparison in line with the overall objectives of the WP 5. In particular, the campaign period was analysed by the CAMx (UA) and Enviro-HIRLAM models.

The observational dataset for the model-measurement comparison and adaptive ensemble treatment included: (i) the results of the Paris campaign, (ii) a complete set of in-situ observations available from the Airbase data bank managed by the European Environmental Agency, and (iii).AIRPARIF observations..

2. Simulations setup of the Individual Ensemble Members

Input meteorology and physiography: up to the model
Input emission: MEGAPOLI emission data, plus embedded dynamic modelled emission, if any.

Stack height, time: COST-728, time resolution: EMEP disaggregation.

Boundary conditions:

MATCH-MPIC for 2005 (gases)

GEMS/MACC MOZART global fields for 2009-2010 (gases).

Aerosol boundaries up to the model

Output file format: NetCDF, CF convention generally followed

Output domain: GEMS/MACC (15W-35E, 35N-70N)

Output grid resolution: (0.30 0.20)

Output vertical levels: screen level (2m/10m above the surface), 100m, 500m, 1000m, 3000m

Output variables:

- 3D concentrations of SO2, SO4, NO, NO2, NO3, HNO3, O3, NH3, HCHO, CO, NH4.
  Unit: µg <substance> m-3
- 3D concentrations of PM2.5, PM10, PPM2.5 (Primary PM2.5), EC (Elemental carbon), POC (Primary Organic carbon), SOA (secondary), SS (Sea salt), D (wind-blown Dust). Unit: µg PM m-3
- 2D dry and wet deposition of the above species. Unit: µg <subst/PM> m-2 hr-1
- Column-integrated PM10. Unit: µg PM m-2
- 3D wind u-component. Unit: m sec-1
- 3D wind v-component. Unit: m sec-1
- 2D boundary layer height. Unit: m
- 2D precipitation rate. Unit mm hr-1
- 2D cloud cover fraction. Relative unit [0..1]
- 2D surface temperature. Unit: K

Output temporal resolution: 1 hour

Computational domain: covering the output domain

Computational resolution: up to the model; re-project to the output grid if differs from it

Computational vertical: up to the model, project the fields to the output vertical levels

3. Hosting the datasets

Location of the data: ftp://ftp.fmi.fi, password protected. Information available at the site includes:

- individual model simulations in the above-outlined format
- ensemble based estimates: average, median, as well as the adaptive ensemble output

- illustrative plots of modelled variables for a selected set of times
- outcome of the comparison with the observations of both individual models and ensemble based estimates
    - time series plots for all individual models and estimates
    - statistical characteristics of the ensemble performance at all observational sites
    - Google-Earth-based visualization of the model-measurement comparison

4. Methods of Treatment of the Multi-Model Ensembles

A standard approach to treatment of a multi-model ensemble is to take an arithmetic average or, for the sake of higher robustness of the outcome, median, of individual models participating in the ensemble. Several applications of such techniques have demonstrated their efficiency. However, scientific information is scarce regarding why these simple methods work. A qualitative justification for that is based on the a-priori assumption that the model errors are non-correlated and zero-averaged. If it is true, the arithmetic average of several models will have smaller standard deviation of the error than each of the individual models. However, this assumption is strictly speaking never correct: model errors tend to correlate being higher in areas with poorly known emission of pollutants, complicated orography, etc. For many species the bulk of the RMSE (Root Mean-Square Error) is due to the model bias, not zero-mean scatter.

A step forward towards more accurate model combination into the ensemble based estimate would be utilization of observational data to evaluate the quality of each ensemble member and the evaluation of its ability to introduce an added value to the estimates performance (these two criteria are not identical). The results of the assessment can be used to assign certain weighting coefficients to the ensemble members. Specific methodology of assigning these weights can vary widely involving various optimization criteria and procedures.

In the current work, we analyse performance of several procedures. The following 5 methods are considered below. Notations are: $E(x,y,z,t)$ is the ensemble estimate, M_i is the value of the *i-th* model, N is the number of models, α_i is the weighting coefficient for the *i-th* model.

1. Arithmetic average of the individual ensemble members (hereinafter referred to as AVE)

(1) $$E(x,y,z,t) = \frac{1}{N}\sum_{i=1}^{N} M_i(x,y,z,t)$$

2. Median of the individual ensemble members (MED)

(2) $$E(x,y,z,t) = med\,(M_i(x,y,z,t))$$

3. Whole-domain least-square optimised RMSE (GLOB_LSQ):

(3) $$E(x,y,z,t) = \sum_{i=1}^{N} \alpha_i(t) M_i(x,y,z,t)$$

where the weights α_I are found by minimising the following cost function *J(t)*:

(4) $$J(t) = \sum_{k=1}^{K} \left(E(x_k,y_k,z_k,t) - O(x_k,y_k,z_k,t)\right)^2 \rightarrow \min_{\alpha}$$

4. Whole-domain optimised RMSE with additional constraints (GLOB_OPT). Ensemble is compiled as a linear combination (3) but the weights α_I are found by minimising the cost function *J* with additional constraints:

(5) $$J(t) = \sum_{k=1}^{K} \left(E(x_k,y_k,z_k,t) - O(x_k,y_k,z_k,t)\right)^2 \rightarrow \min_{\alpha \,|\, \alpha>0}$$

5. Local least-square optimised RMSE (LOC_LSQ). Ensemble is compiled independently for each grid cell as a linear combination of models (3), with the weights α_I are found by minimising the cost function *J* taking into account all stations with the inverse-distance weights:

(6) $$J(x,y,t) = \sum_{k=1}^{K} \frac{\left(E(x,y,z,t) - O(x_k,y_k,z_k,t_k)\right)^2}{(x-x_k)^2 + (y-y_k)^2} \rightarrow \min_{\alpha}$$

As seen from the above equations, the main quality criterion in all optimal ensemble treatment methods was the minimal value of the RMSE. The non-optimising methods AVE and MED were included for comparison as the most-common approaches.

Application of the optimising methods required a split of the observational dataset into the learning and control sub-sets. Since the number of sites of AIRBASE varies from about 100 up to more than 1000 depending on the substance it was possible to split the whole set in proportion 3:1, with the large subset used for determining the optimal weights and the smaller part used for evaluation of the obtained predictions.

5. Examples of the Model Results for Summer 2009

An outlook of the model results confirms the conclusions from the model ensembles analysed within the scope of other activities (such as COST-728 and AQMEII): the models tend to provide comparable predictions for the species routinely observed and verified – over the areas where such validation is established (i.e., near the surface). These are the primary gases, such as SO2, NO2, NH3, O3, some aerosols, such as sulphates and nitrates. More differences were observed for aerosol compounds. The biggest differences were found for rarely evaluated components, such as HCHO,

and for non-observable variables, such as dry deposition, which showed the largest scatter.

Evaluation of the quality of the input meteorological data is presented in the report for deliverable 7.3, so here we only provide some examples, which demonstrate that the models had comparatively similar input data flows, even for the diagnosed quantities, such as boundary layer height.

Examples of the corresponding fields are given in the below figures. They are grouped in the following order:

- The night- and day-time height of the boundary layer are presented in Figures 1-2
- The near-surface concentrations of the "basic" substances are given in Figures 3-5.
- The near-surface concentrations of HCHO as an example of not routinely verified substances and parameters are presented in Figures 6-7.
- The composite species (PM 2.5 and 10) are illustrated in Figures 8-10.
- Concentrations at 1000m altitude are given in Figures 11-13.

A detailed presentation of the obtained results and all model specifics and expected improvements are beyond the scope of the current short report. However, a few key points have already been clarified with regard to individual model behaviour.

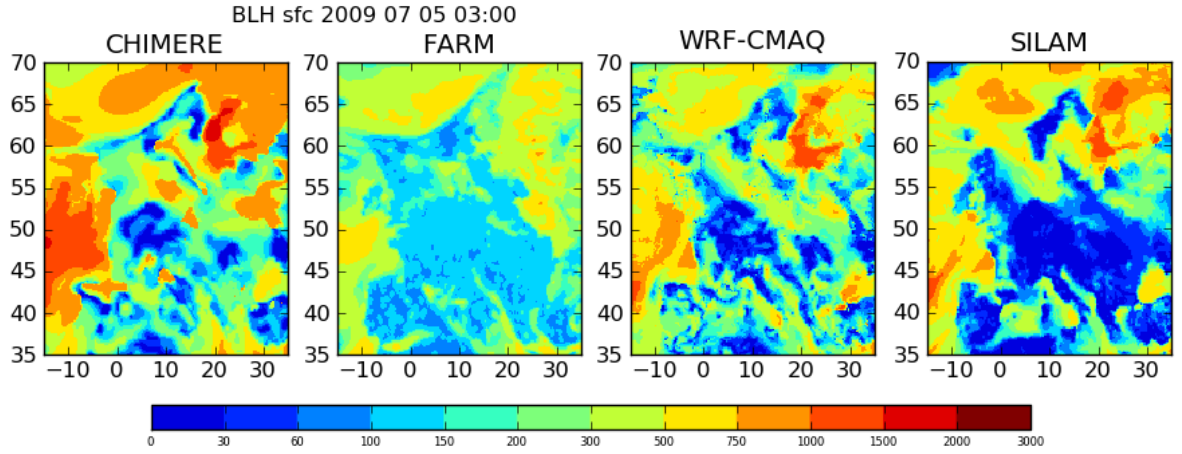

Figure 1: *Boundary layer height at night time diagnosed by the models, [m]*

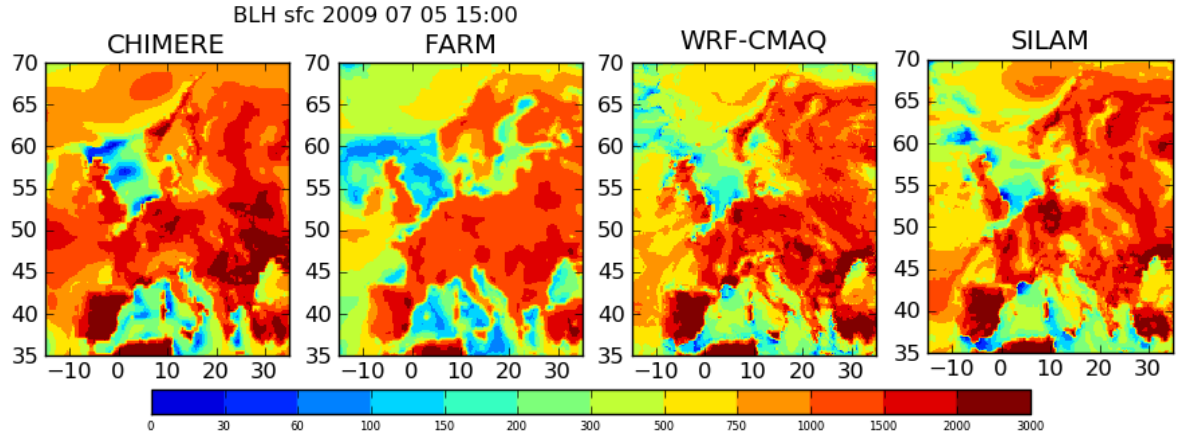

Figure 2: *Boundary layer height for daytime, diagnosed by the models, [m].*

Boundary layer height is diagnosed by the models from the basic meteorological variables. Such procedure is known to be uncertain, so that all models apply the lower limit for the boundary layer height in order to ensure the stability of the computational algorithms. Direct accommodation of the ABL height from NWP models can lead to unpredictable results. For instance, the ECMWF diagnostic frequently allows ABL height to be as low as 7-8 metres over very large areas in Central Europe over several hours, which seems unrealistic.

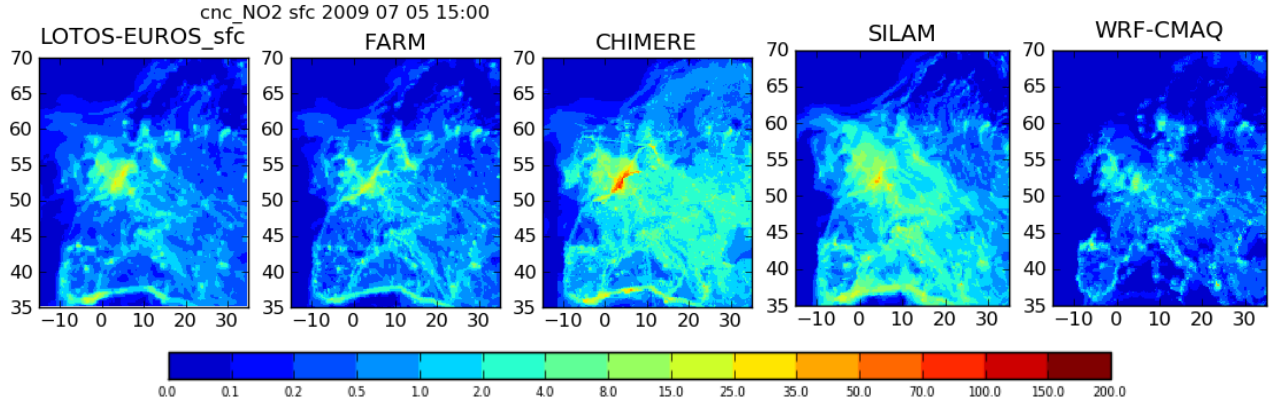

Figure 3: *Near surface concentrations of NO_2, [$\mu g\ m^{-3}$].*

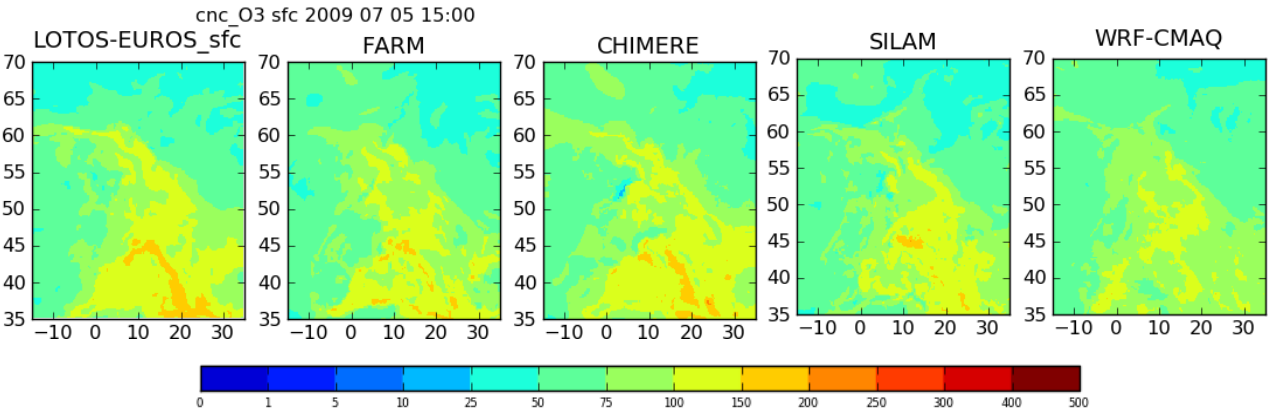

Figure 4: *Near surface concentrations of O_3, [$\mu g\ m^{-3}$].*

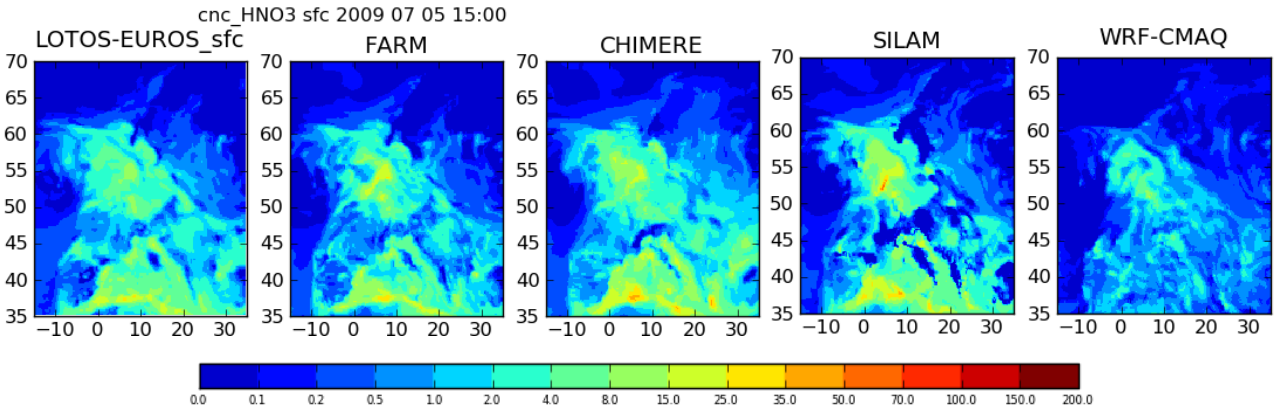

Figure 5: *Near surface concentrations of HNO_3, [$\mu g\ m^{-3}$].*

For primary gaseous species (NO_2, SO_2, NH_3) the general patterns shown by the models are quite similar, with differences being mainly in the absolute levels of the predicted concentrations. Model-wise, WRF-CMAQ tends to predict the lowest surface concentrations of these species, whereas SILAM demonstrates the lowest concentrations of the secondary inorganic aerosols.
Since such species are verified routinely and their behaviour is well known, good agreement between the models is not surprising. It also implies that application of the ensemble technique, unless optimising methods are used, brings little improvement in the quality scores for these species.

Patterns and absolute values of the substances and variables not verified routinely are among the most uncertain. For example, HCHO dry deposition (Figure 7) show strong differences between the models, some of which appeared to anti-correlate with each other, despite the near-surface concentrations are quite similar with each other. Some of these features have been traced down to specific model components. For instance, the low-deposition "holes" in the SILAM-predicted pattern (Figure 7) were attributed to incorrect diagnosing of the aerodynamic and laminar-layer resistances (the algorithm update is in progress). In other cases more in-depth investigations are needed.

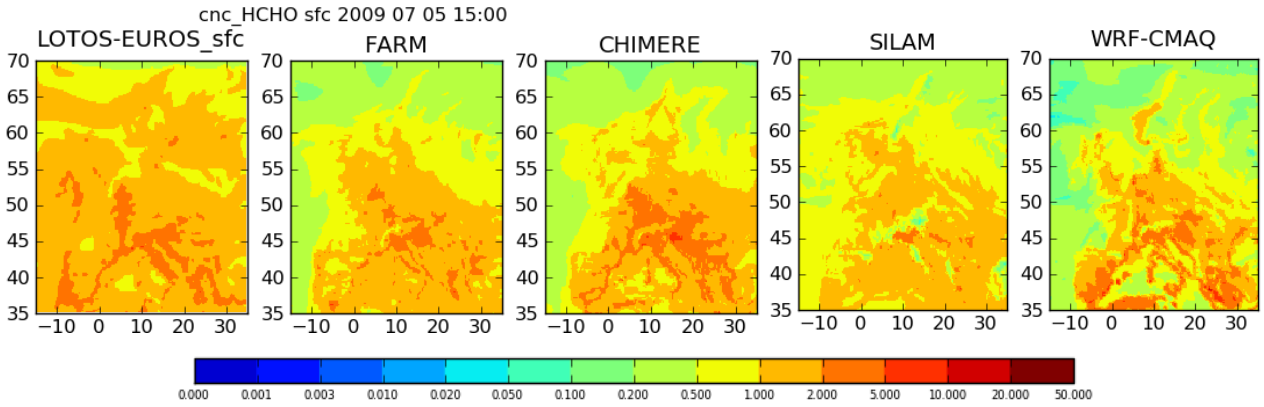

Figure 6: *HCHO near-surface concentrations [μg m^{-3}].*

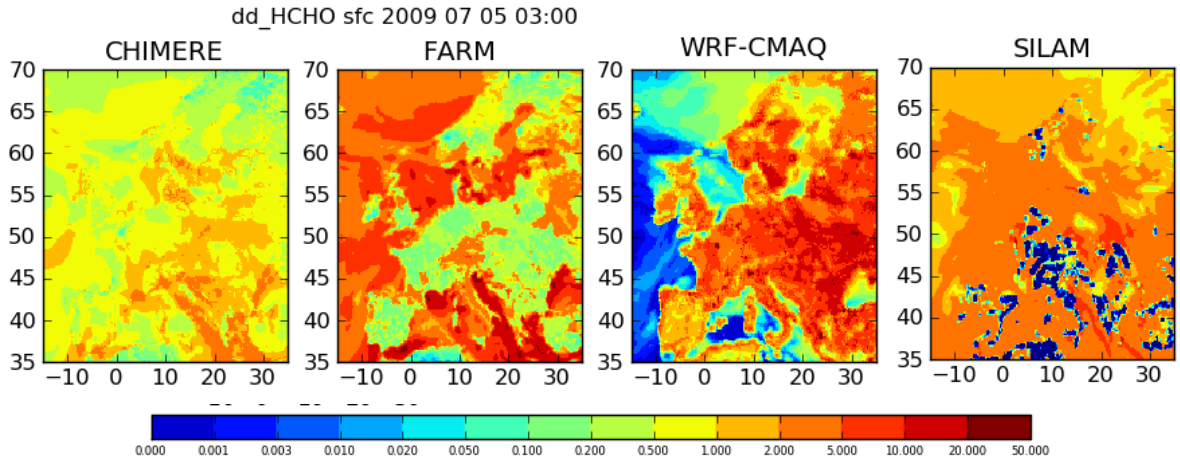

Figure 7: *Dry deposition of HCHO, [μg m^{-3}].*

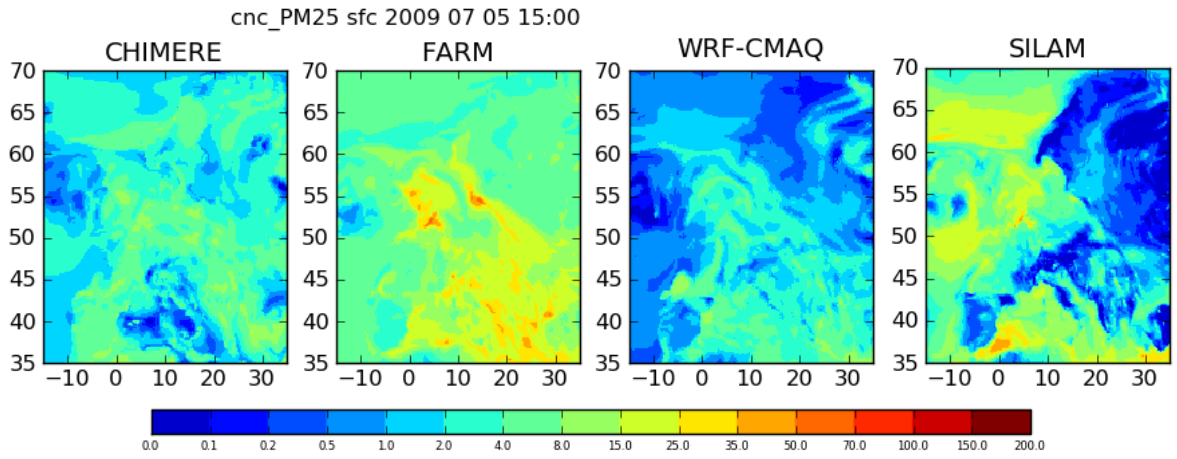

Figure 8: *Near-surface concentration of $PM_{2.5}$. [$\mu g\ PM\ m^{-3}$].*

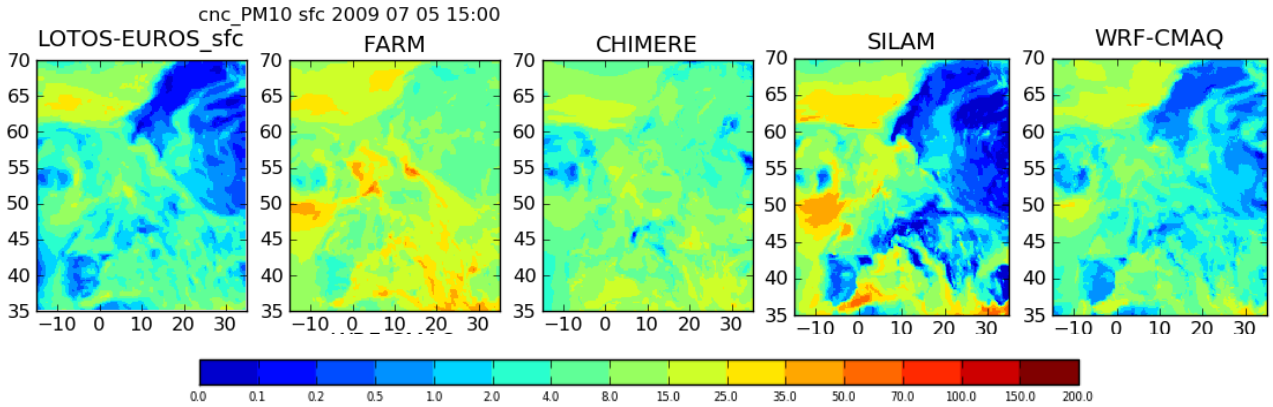

Figure 9: *Near-surface concentration of PM_{10}. [$\mu g\ PM\ m^{-3}$].*

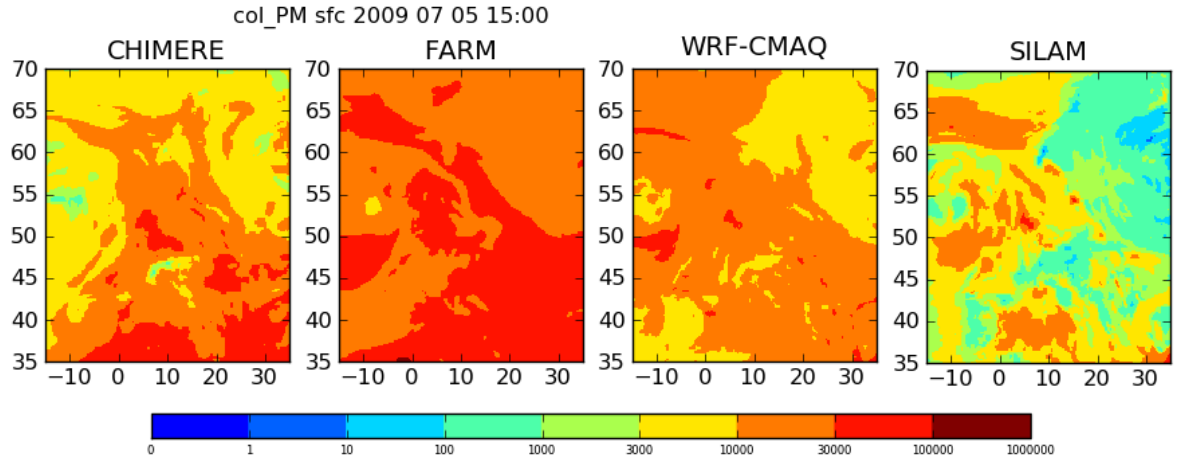

Figure 10: *Column-integrated concentration of total PM. [$\mu g\ PM\ m^{-2}$].*

Considering aerosol species, a significant divergence between the models should be noted – both quantitative (in the absolute levels predicted) and qualitative (the predicted distribution patterns vary widely). To a large extent this is the result of absence of several types of PM in some models (see the MEGAPOLI Deliverable 7.3 report for details).

FARM has shown the highest concentrations and depositions of all aerosols. To a certain extent it originates from the boundary conditions from GOCART where the sea salt contribution was over-estimated – but other possible reasons are also under investigation.

Detailed consideration of vertical profiles of concentrations was not possible due to limited number of vertical levels. However, the provided information suggests that the patterns at higher levels do not differ more substantially than those at the surface (examples in Figures 11-13). This is a significant difference from the COST-728 ensemble, where in many case fields agreeing at the surface were entirely different already at 1km altitude.

However, it was noted that in some cases the SILAM vertical profile had smaller gradient than the other models (e.g. compare Figure 3 and Figure 11). Possible reason for that is quite wide distribution of he emitted species, which followed the template suggested by EMEP (http://www.emep.int) but may be outdated for modern emission sources, which were subjected to several emission reduction measures since then.

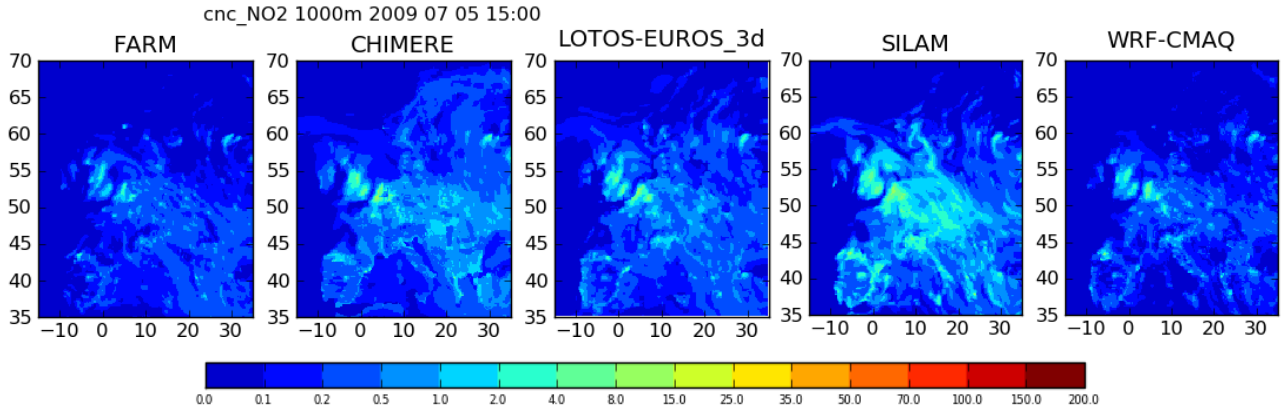

Figure 11: *Concentration of NO_2 at 1000m. [$\mu g\ m^{-3}$].*

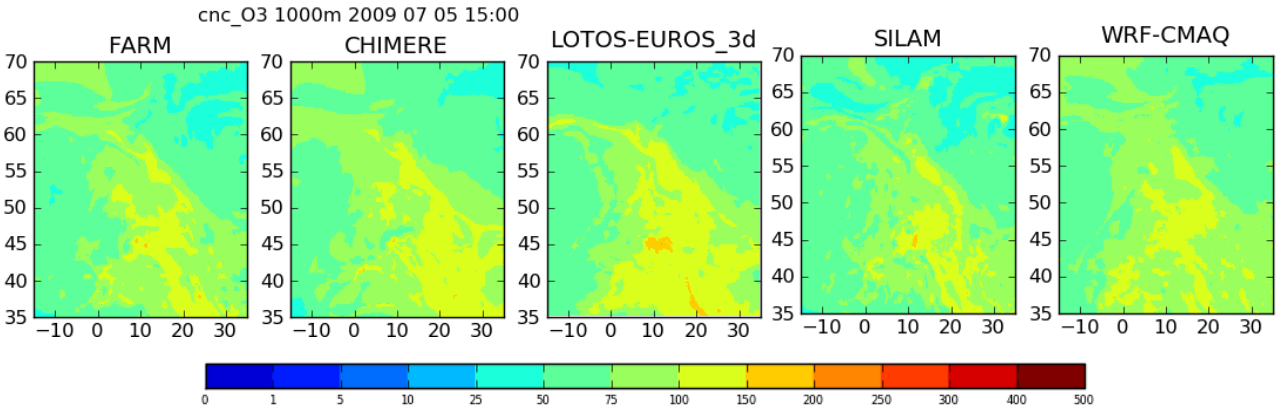

Figure 12: *Concentration of O_3 at 1000m. [$\mu g\ m^{-3}$].*

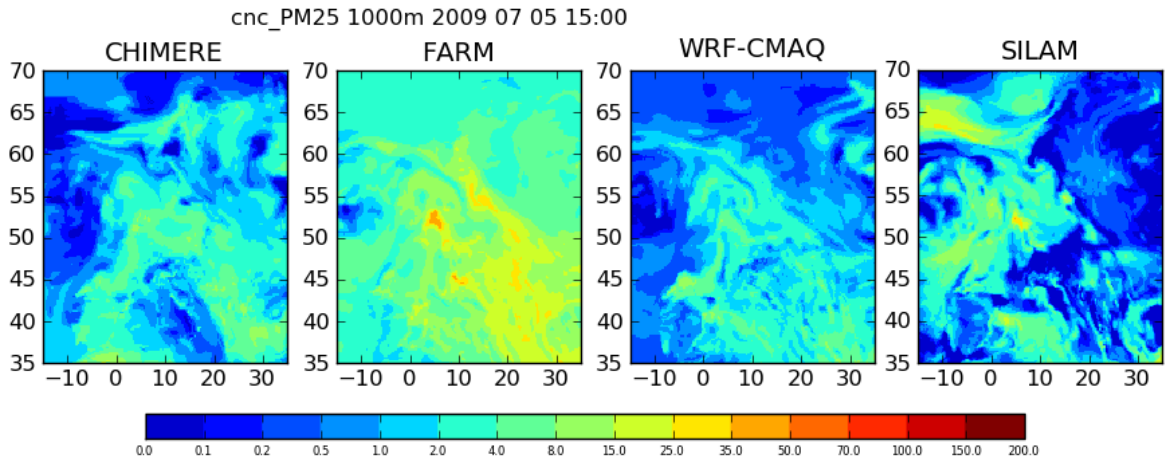

Figure 13: *Concentration of $PM_{2.5}$ at 1000m. [$\mu g\ PM\ m^{-3}$].*

6. Model-Measurement Comparison for Individual Models

Detailed numerical results for the model-measurement comparison for the individual models are provided as a supplementary material to this report in a form of Excel workbook (see the MEGA-POLI Web site). Here we highlight the important issue, which is frequently forgotten from the model evaluation: the spatial patterns of the model-measurement agreement.

The maps in Figure 14 provide an example of the Root Mean Square Error for the individual models computed for NO_2. The normalization is made with regard to the mean observed concentrations at each station. Therefore, the RMSE less than 100% of the observed value is marked by blue shades, whereas the poorly predicted sites with RMSE>100% are red. As follows from the Figure 14, most of the sites in Europe are predicted with the RMSE within 10-20% but still lower than the observed mean level. For the most polluted regions the relative error is somewhat lower, which is evidently explained by the higher normalising coefficient. The models performance also appeared to be quite similar to each other.

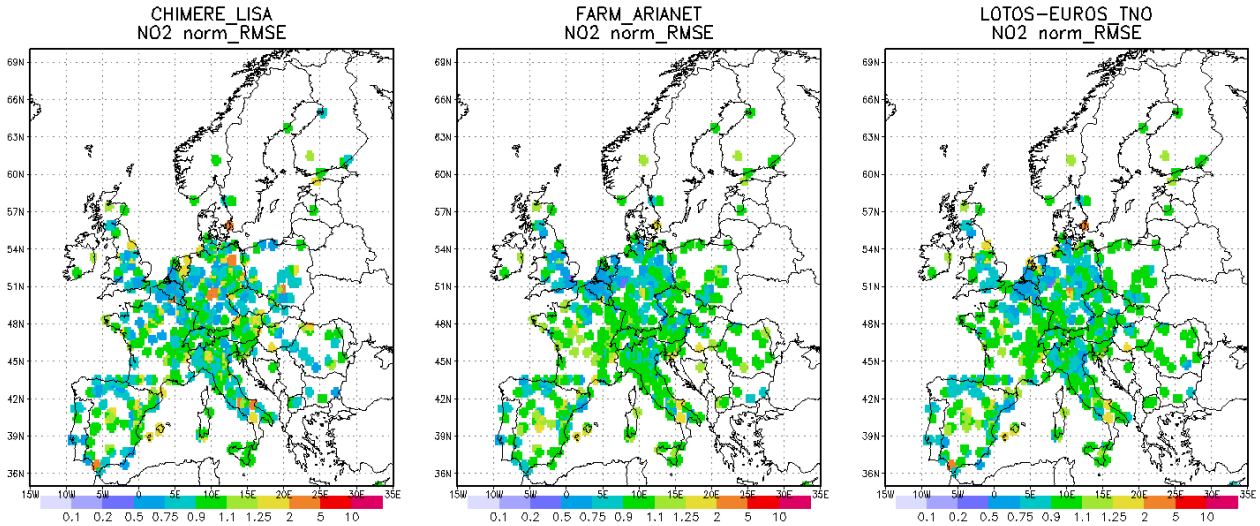

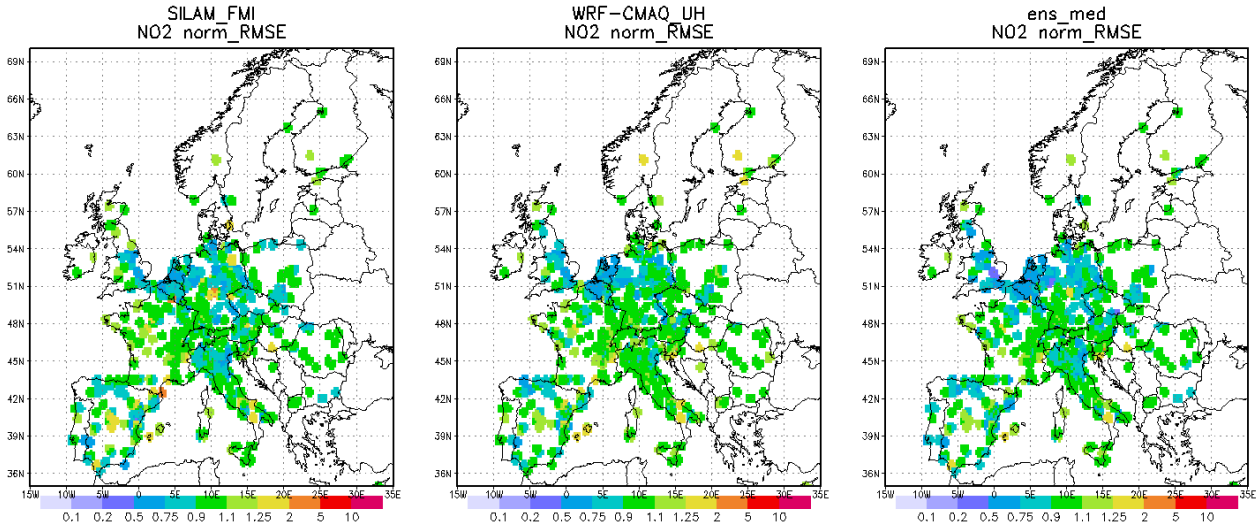

Figure 14: *RMSE for the individual models and ensemble median normalised with the mean observed value.*

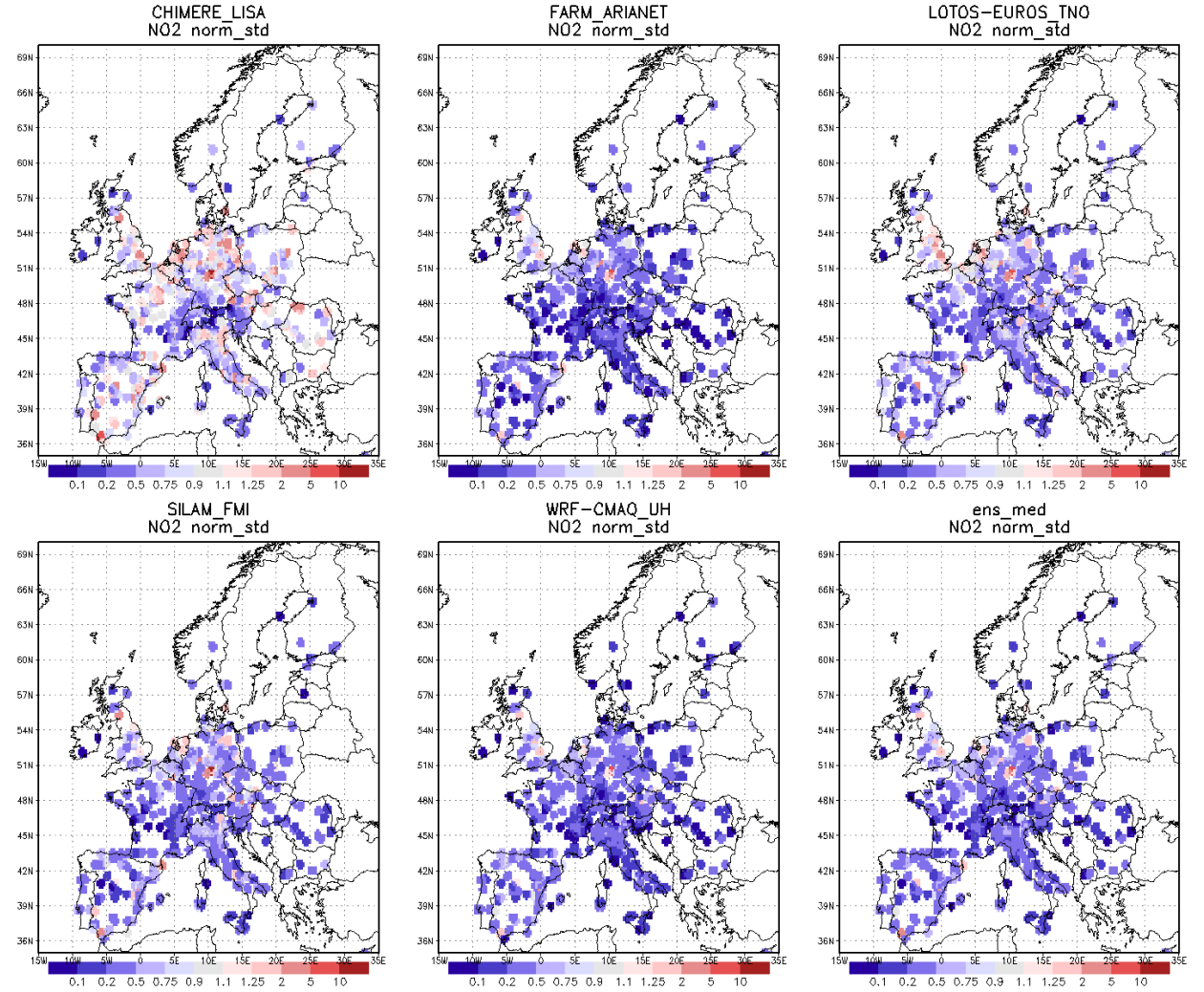

Figure 15: *Standard deviation of the model time series normalised with the standard deviation of the observed concentrations.*

The model ability to reproduce the observed dynamic range can be presented as a ratio of the standard deviations of the predicted and observed time series (Figure 15). As one can see, most of the models tend to under-predict the dynamic range, with an exception to CHIMERE, which has a clear spatial pattern of this parameter: under-predicting the variability in the Po Valley and over-predicting it in most of other polluted regions.

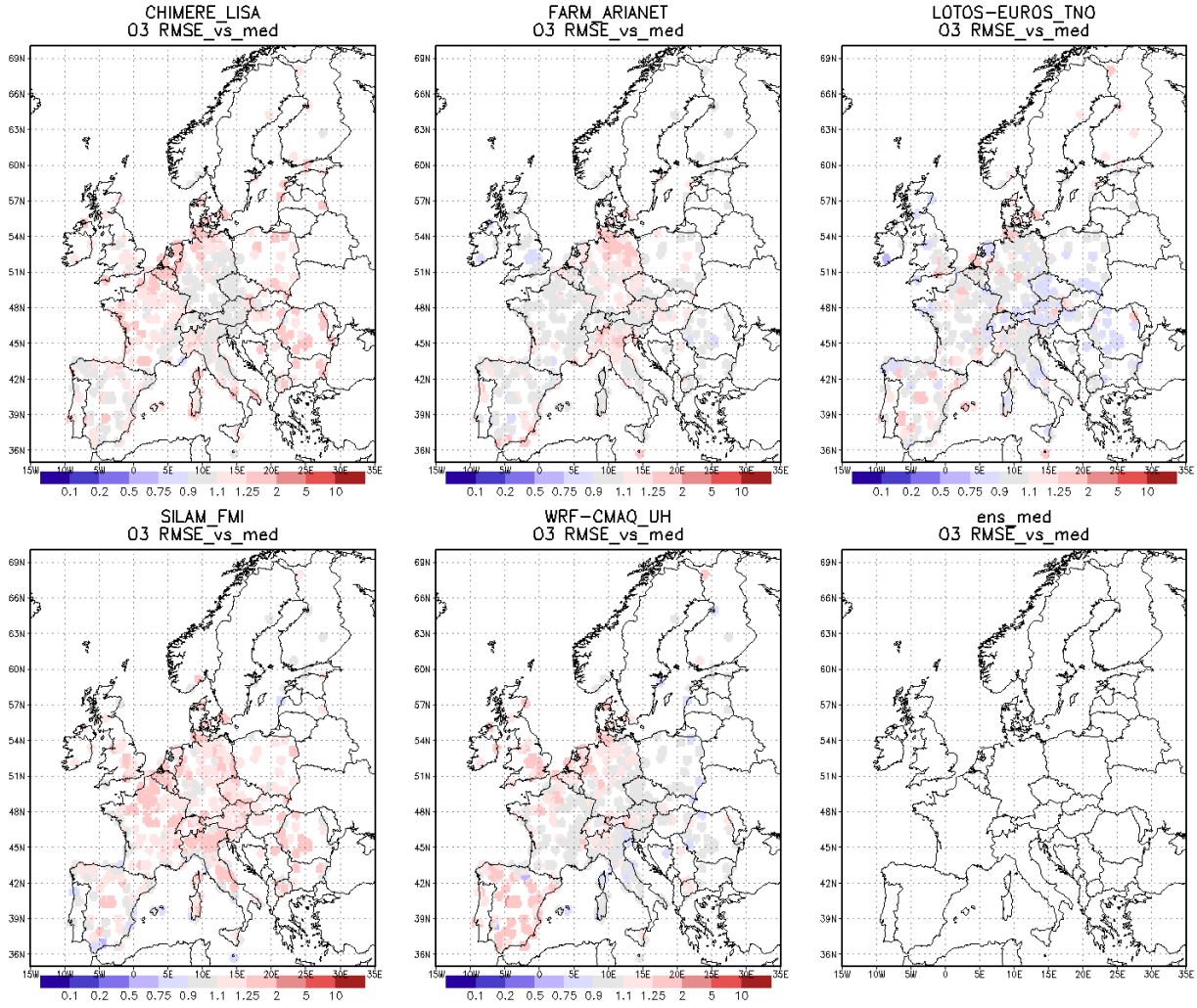

Figure 16: *RMSE for individual model scaled with of the RMSE of the ensemble median.*

To highlight the performance of the models with regard to each other and also the possibility to improve the predictions by applying the ensemble methods, the model RMSE was scaled with that of the ensemble median (Figure 16). As one can see, essentially all models show worse performance for O_3 than the median. Exception is the LOTOS-EUROS system, which even outperformed it at many sites of Eastern Europe but was still slightly trailing in the most-polluted areas and in the vicinity of the megacities, such as Paris, Po Valley, as well as in the highly polluted Benelux region.

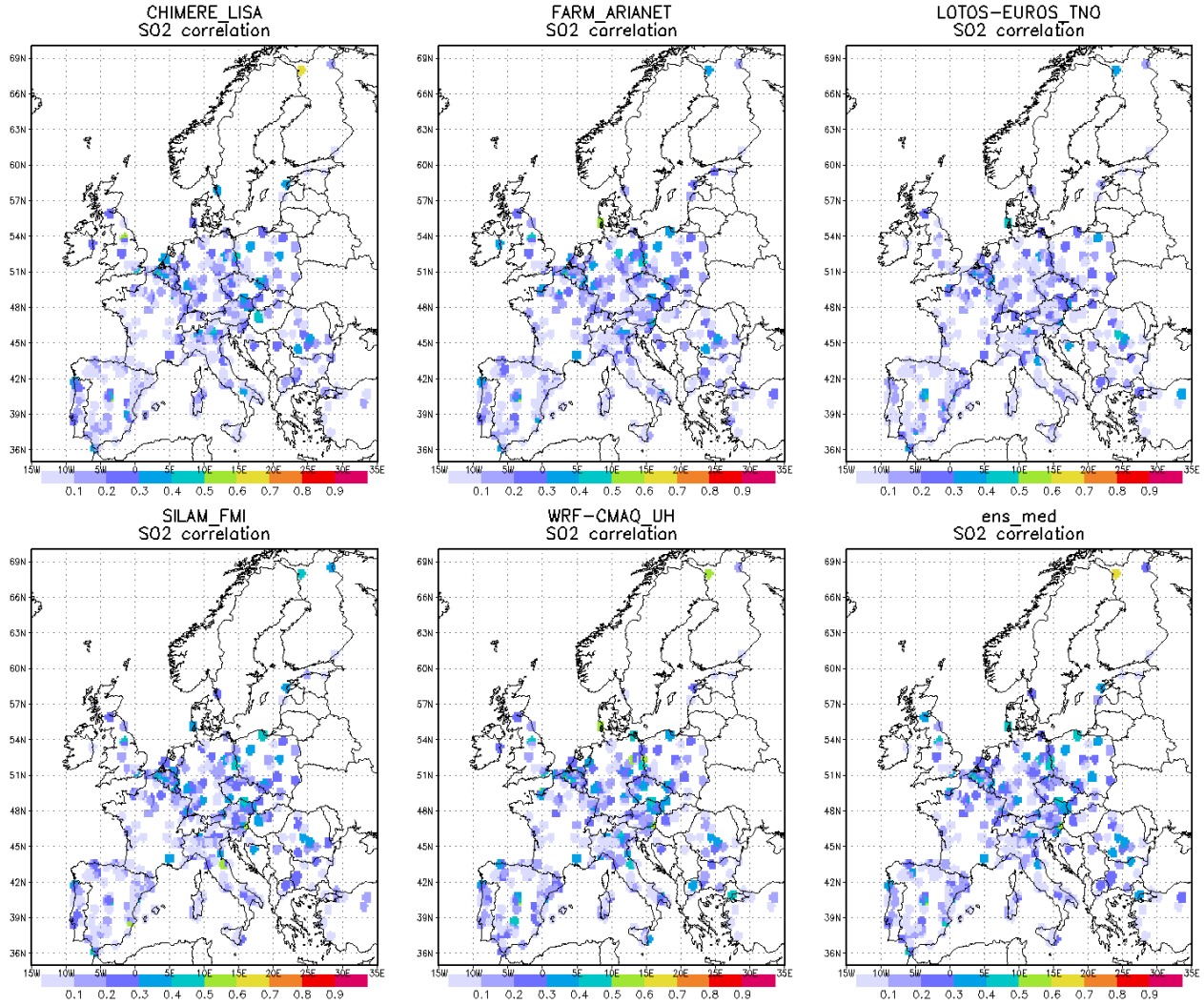

Figure 17: *Time correlation coefficient for SO_2 time series for individual models and ensemble median.*

An example of the most-difficult substance for all models is SO_2. As shown in Figure 17, time correlation coefficient is very low and the median does not show any noticeably better agreement. Nearly the only exception is the Northern Lapland where several models reached the correlation of 0.4-0.6. It is explained by a comparatively simple structure of the sources in the area, with a few large factories in Russia fully dominating the pollution pattern.

7. Improving the Model Predictions via Multi-Model Ensemble

This section illustrates the possibilities of improving the predictions of models by combining them into the multi-model ensemble. As introduced above, two types of ensemble treatment were considered: (i) arithmetic average and median, (ii) dynamic weighted averaging where the models weights are optimized so that the estimate best fits the monitoring data

7.1. Impact of treatment methods to ensemble quality

As seen from the examples in Figures 18-19, the under-estimation of some concentrations (in this case, NO_2 and PM_{10}) can be successfully handled by the optimising methods, which reported substantially higher levels in the polluted areas than the individual models. In particular, the regions around the megacities and industrial agglomerates, such as Ruhr area and Po Valley, have much higher predicted concentrations than reported by the individual models.

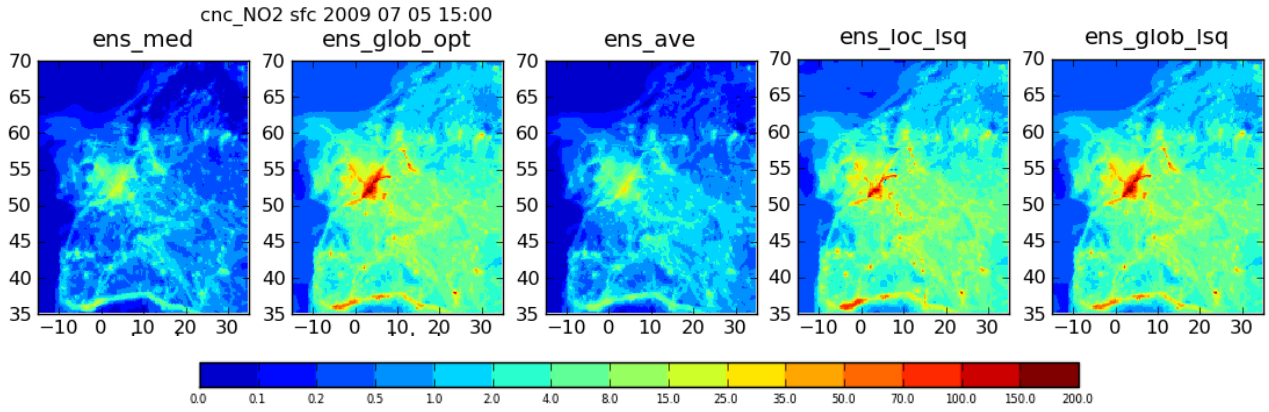

Figure 18: *Near-surface concentration of NO_2, [$\mu g\ m^{-3}$].*

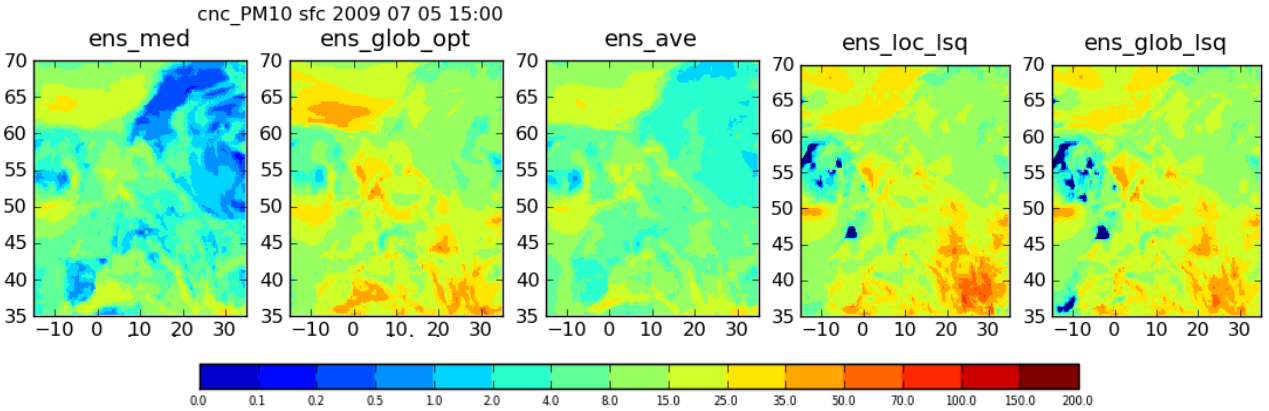

Figure 19: *Near-surface concentration of PM_{10}.*

7.2. Evaluation of the ensemble predictions against the control set of observations

Evaluation of the ensemble estimates against the control set of observations is presented below in relative terms – with regard to the ensemble median, whose performance was taken to be a reference. This way highlights the performance of the other ensemble based estimates in comparison with ensemble median. It was shown above that in most cases already the median outperformed the

individual models. In this section, we demonstrate that in some cases more sophisticated methods are justified since they can have substantially higher accuracy. An example of such case is shown in (Figure 20). As one can see, the ensemble average has nearly the same quality scores as the median, whereas the optimising methods provide substantial improvement over the most of Europe, including Paris area and Po Valley.

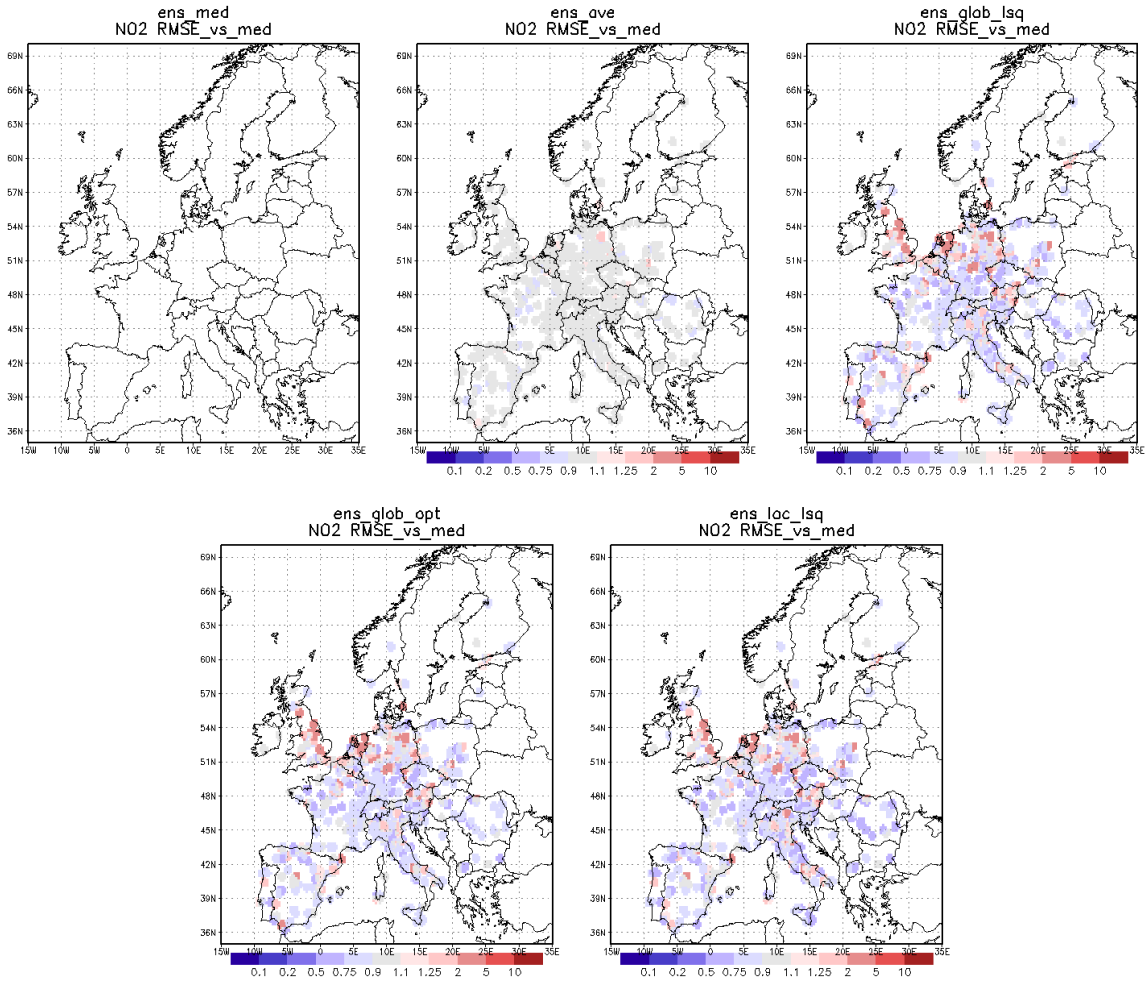

Figure 20: *RMSE of NO2 for the ensemble estimates scaled with RMSE of median.*

Slight improvement was obtained even for the SO_2 patterns but the gain was small (not shown).

These methods failed only in Benelux and eastern coast of UK, where the spatial variation of the fields was so large that the weighting coefficients selected to be optimal over a wide area appeared to be not suitable for these regions. This problem is being investigated.

One of the most substantial improvements from the optimised ensemble methods was obtained for PM_{10}, (Figure 21) where the optimising methods were able to eliminate the overall under-estimation of the concentrations and did it homogeneously over the whole Europe, so that the characteristic improvement over the median reached 20-30% in both clean and polluted regions. The effect is see in Figure 22, where both ensemble median and average are a factor of 3-10 lower than the observed

levels (with average being expectedly better) whereas the optimised estimates show both under-and over-estimation. The best results were shown by the locally optimised method, which best reproduced better the spatial pattern of the mean concentrations.

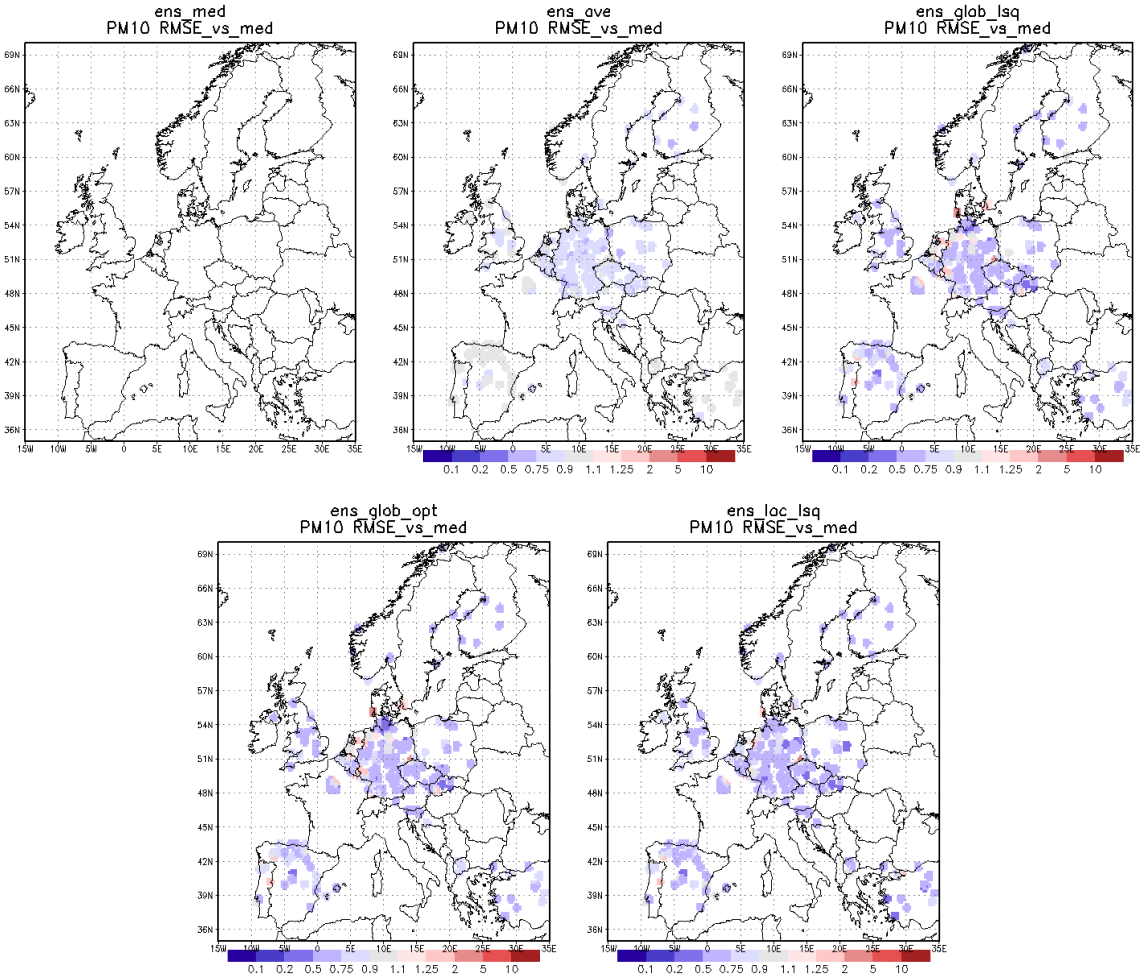

Figure 21: *RMSE of PM_{10} of the ensemble estimates normalised with RMSE of the median.*

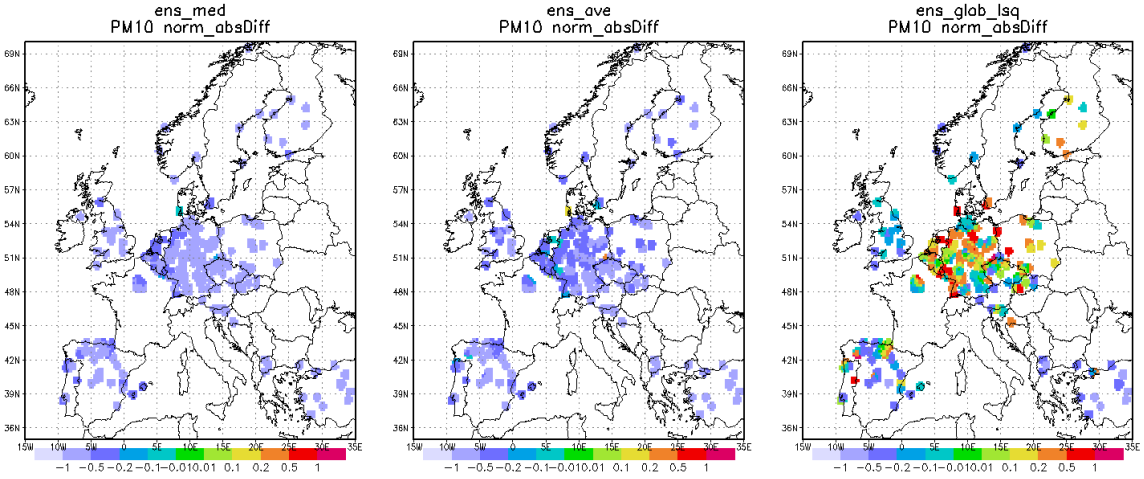

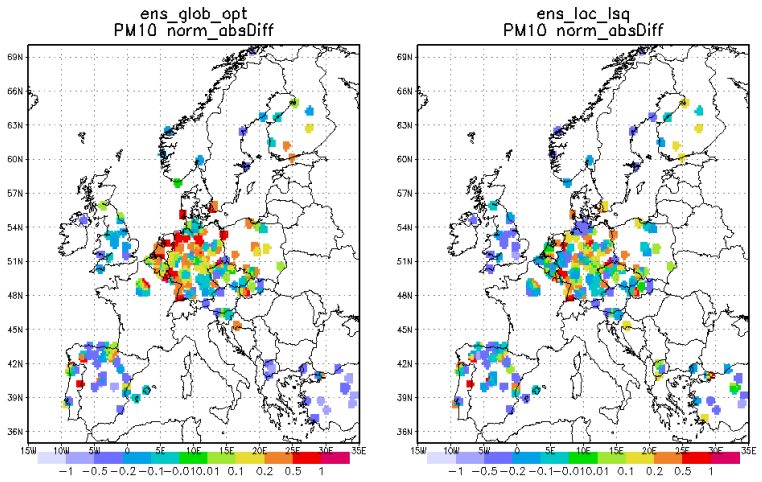

Figure 22:. *Bias of the ensemble estimates normalised with the mean observed concentrations of PM_{10}.*

8. Simulations of LOTOS-EUROS for Paris 2009-07

8.1. Model setup

For the Paris 2009-07 period, two simulations were performed with the LOTOS-EUROS model. The first run used the 2005 'base' emissions (MEGAPOLI Deliverable 1.2), and the second one used the 'nested mega-cities' emissions (MEGAPOLI Deliverable 1.6), which is basically a re-distribution of emissions between the mega-cities and the surrounding country. The domain was set to [5W, 15E] x [40N, 57N] which includes all the 4 MegaCities considered; resolution was set the same as the resolution of the emissions (1/8 deg. lon. x 1/16 deg.lat., about 6 km). The simulation period was July 2009, with a spin-up period of 2 weeks. Boundary conditions were taken from a run on the full European domain and a resolution of 0.3x0.2 deg, which is the same as used for the run over 2005. The global boundary conditions for these boundary conditions were provided by the project.

The analysis of the simulation focuses on particulate matter. The aerosol components of the model included primary and secondary inorganic aerosols and sea-salt. The aerosol concentrations will therefore always under-estimate the true values, since some particulate matter such as wind-blown dust and natural organic aerosols are missing; no bias-correction was applied to account for this.

8.2. Concentration fields

Figure 23 shows the average PM10 concentrations at ground level during July 2009, simulated using the two considered emission inventories. The general patter of the mean values is the same for

both simulations (left panels), except for the Paris area. The difference reaches values of 20-30 ug/m3 in the centre of the city. The re-distribution of the sources from city to rural has lead to lower emissions in the city and slightly higher emissions in the rest of the country; the latter is hardly visible in the average concentrations, however. The difference plot (right panel) shows that lower PM10 concentrations are also found for the mega-cities "London" and "Ruhr", although the magnitude is smaller. For the "Po", both higher and lower concentrations are visible, but since the aerosol concentrations are much higher here, the relative difference is rather small.

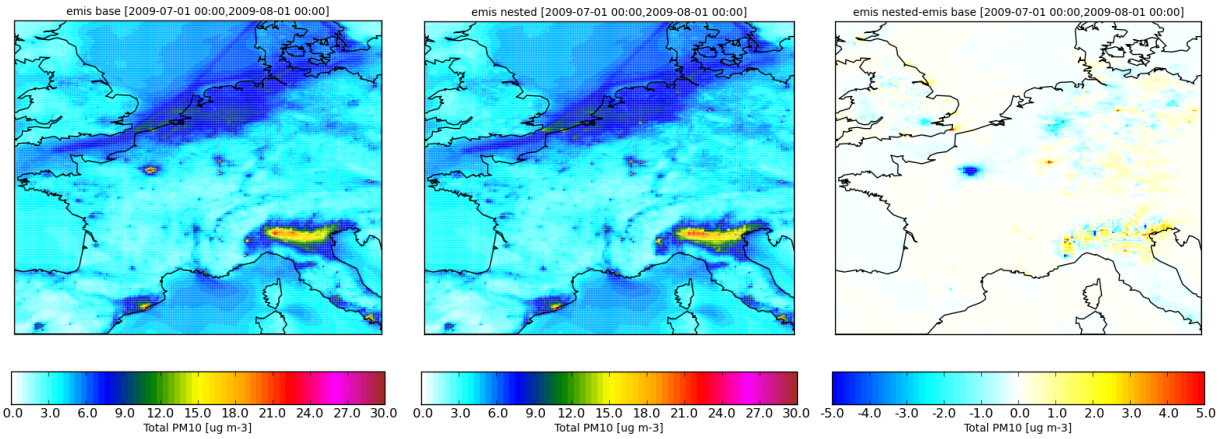

***Figure 23**: Average PM10 concentrations at ground level during July 2009.*
Left: simulation using base emissions. Middle: simulation using nested M.C. emissions.
Right: difference between the two.

8.3. Comparison with observations

For validation of the results, ground based observations from 15 background sites in and around Paris have been obtained from AirParif . As an illustration, Figure 24 shows the time series for total PM10 concentrations in site "Paris 18eme" for the complete month of July. The simulations using the base emissions (red line) show extreme high aerosol peaks throughout the month, while the simulation using the nested emissions are much smoother, similar to the observations.

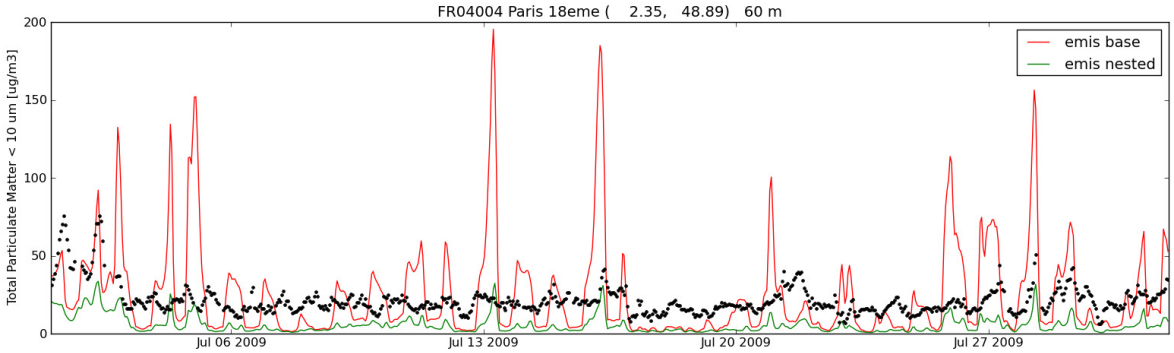

***Figure 24**: Observations and simulations of total PM10 in site "Paris 18eme".*

The average diurnal cycles for the same station are plotted in Figure 25, and show that the high

peaks for the base emissions occur during the night. This is an indication that the local emissions are over-estimated in this case, and accumulate into the stable boundary layer at night time. At daytime, the simulated concentrations are more similar for the two runs, with the 'base' run providing slightly higher concentrations as expected from the higher emissions in the Paris area.

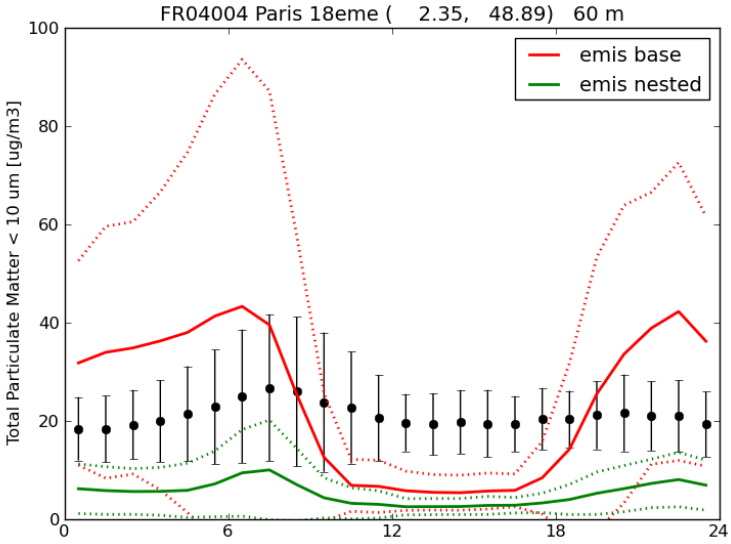

***Figure 25**: Diurnal cycles in site "Paris 18eme" during simulation period: mean (solid or bullets) plus and minus standard deviation (error bars or dotted lines).*

Similar results were obtained for the other urban and suburban sites in the region. For all these sites, the shape of diurnal cycle is better represented when using the 'nested' emissions, and does not show extreme high peaks during the night. At the four available rural background sites, hardly any difference between the two simulations was found.

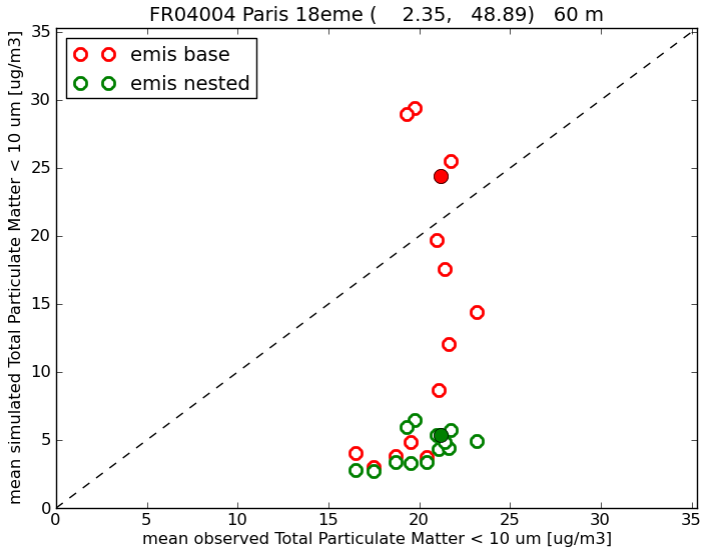

***Figure 26**: Average simulated concentrations of PM10 throughout the month versus observed values. The solid bullets indicate the values for site "Paris 18eme".*

Figure 26 shows a scatter plot of the average simulated concentrations versus the observed values.

Due to the missing semi-natural aerosols in the model, the observed concentrations are under estimated with about a factor 4 if the 'nested' emissions are used. The mean values for 'base' are sometimes comparable to the observed values, but due to the wrong diurnal cycles, the value of this agreement is limited.

9. Experiment on the Scalability of SILAM Model

9.1. Setup of the experiment

To investigate the impact of the computational grid resolution to air quality simulations, the air quality in Central Europe for July 2009 was simulated with SILAM model with 4 different model setups:

High resolution (hi res):
dx = 0.125
dy = 0.0625
time_step = 6 min
layer_thickness = 20. 40. 80. 200. 320. 680. 910. 1500. 1500.

Low horizontal resolution, high temporal and vertical resolution (lo xy res):
dx = 0.375
dy = 0.1875
time_step = 6 min
layer_thickness = 20. 40. 80. 200. 320. 680. 910. 1500. 1500.

Low horizontal and temporal resolution, high vertical resolution (lo xyt res):
dx = 0.375
dy = 0.1875
time_step 15 min
layer_thickness = 20. 40. 80. 200. 320. 680. 910. 1500. 1500.

Low resolution (lo xytz res):
dx = 0.375
dy = 0.1875
time_step 15 min
layer_thickness = 60. 280. 1000. 1410. 2500.

Simulations were made with both chemical schemes available in the model – CB4 and SILAM native acid-basic chemistry scheme. Primary PM and sea salt concentrations were also computed. All the simulations were nested in SILAM European run for the same period. The same meteorological and emission data was used for all runs. TNO MEGAPOLI emission data was used, which has the same resolution as the high-resolution model run. Model used ECMWF meteorological data with 0.25 degree resolution, which it interpolates to the computation grid.

Spatial patterns of concentrations and depositions and vertical distributions of pollutants were compared for the different model setups, together with the total dry and wet deposition in the computation domain and the fluxes out of the domain. Model measurement comparison was made for Airbase and AirParif measurements of CO, NH3, NO, NO2, O3, PM2.5, PM10 and SO2 surface concentrations.

9.2. Differences in total budget

For most species the difference between the model setups in the out-of-grid transport and total dry and wet deposition in the whole domain during the computations stays below 10%. For primary PM the differences in deposition and amount transported out of the domain stay below 2 %, showing that the transport, diffusion and deposition processes in SILAM model are well scalable and not dependent on computational resolution. The differences for sea salt are ~5%, the somewhat larger difference originating from the meteo-driven emission, which required interpolation of the wind speed. The changes in the secondary organic aerosol production are within 10%. For total PM, the differences are less than 5%.

The largest differences (up to 2-3 times) occur for the short lived chemical species and species which concentrations dependent on chemical equilibrium (OH, HO2, CH3O2, NO3 radical). It results in noticeable differences for some most common pollutants: ~20% changes between the low and high resolution computations in amounts of CO, O3 and NO transported out of the domain. For NO2 and SO2 the differences in the budget between the different setups are within 5%.

9.3. Comparison of the patterns

In most cases the pollution patterns look very similar between the model runs with different setups. The high resolution results expectedly show sharper gradients and higher peak values for the pollutant concentrations, as well as lower ozone concentrations in polluted areas (Figure 27)

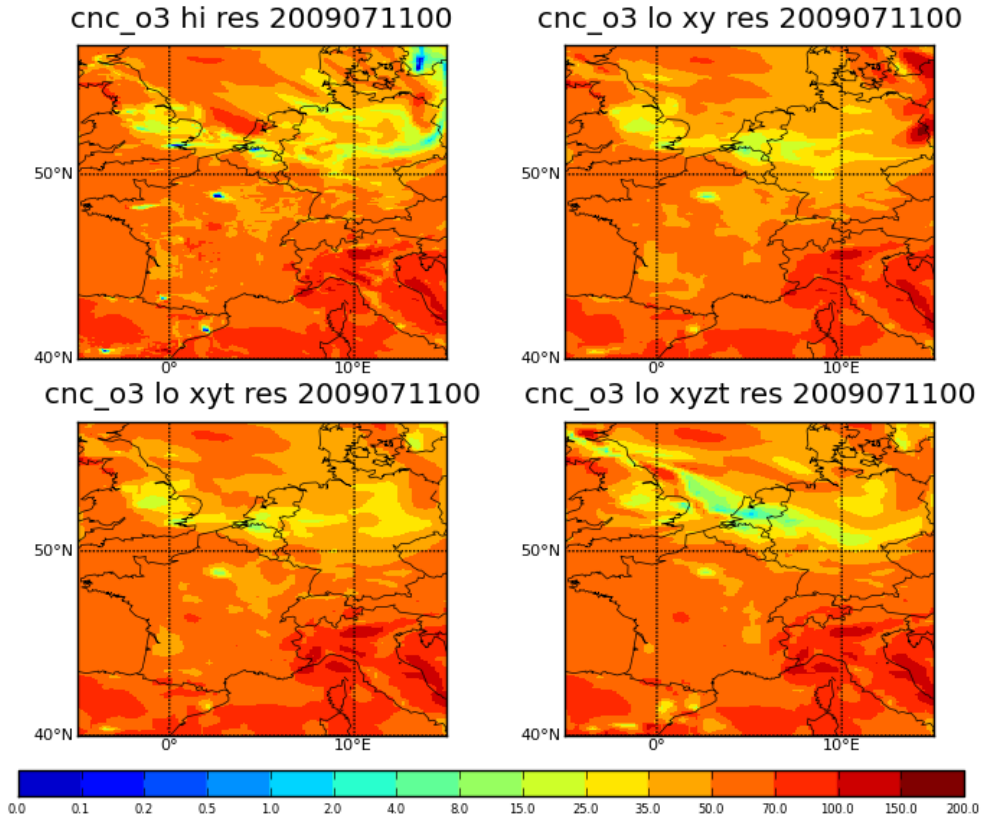

Figure 27: *O3 surface concentration at 03 07 2009 23:00 (upper left – high resolution, upper right – low horizontal resolution, lower left – low horizontal and temporal resolution, lower right – low horizontal, vertical and temporal resolution).*

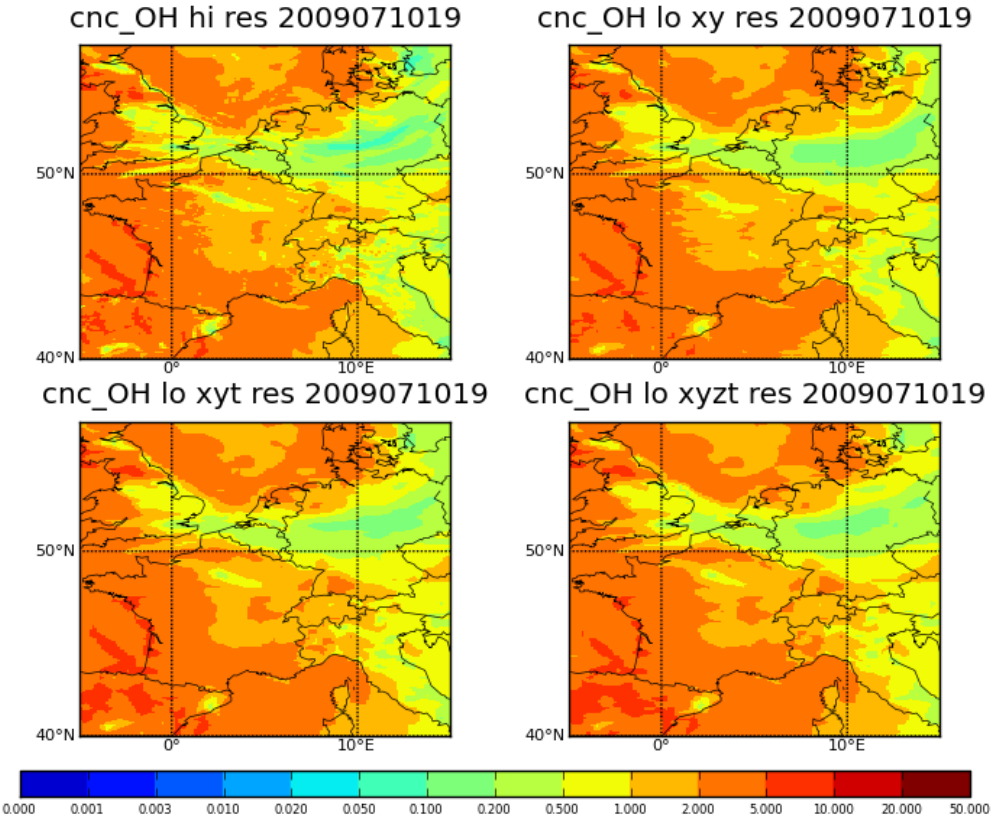

Figure 28: *OH surface concentration at 10 07 2009 19:00 (upper left – high resolution, upper right – low horizontal resolution, lower left – low horizontal and temporal resolution, lower right – low horizontal, vertical and temporal resolution).*

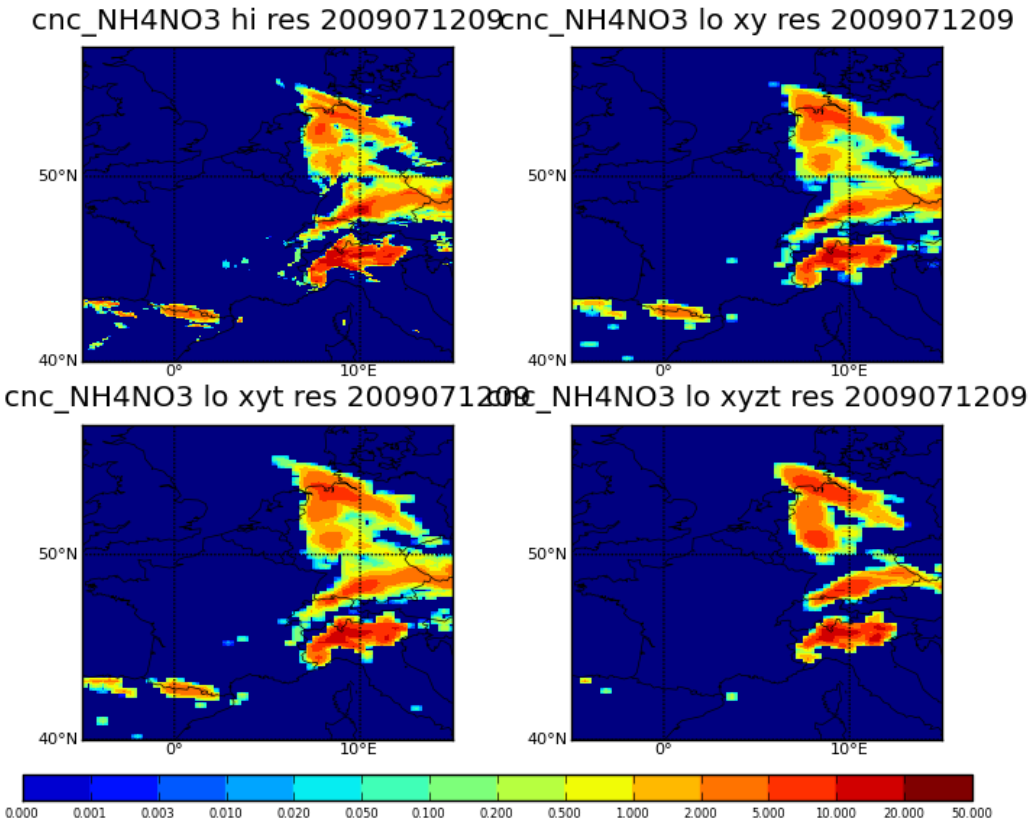

Figure 29: *NH4NO3 surface concentration at 12 07 2009 9:00 (upper left – high resolution, upper right – low horizontal resolution, lower left – low horizontal and temporal resolution, lower right – low horizontal, vertical and temporal resolution).*

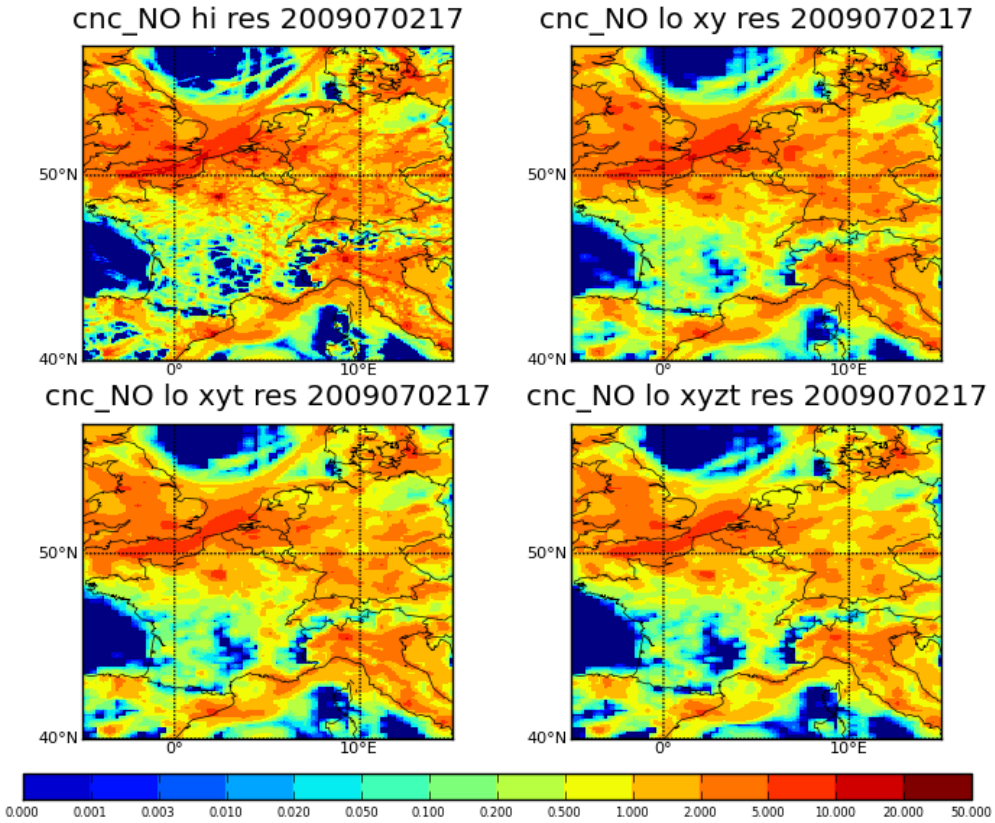

Figure 30: *NO surface concentration at 02 07 2009 17:00 (upper left – high resolution, upper right – low horizontal resolution, lower left – low horizontal and temporal resolution, lower right – low horizontal, vertical and temporal resolution).*

9.4. Model-measurement comparison

Raising the resolution of the computations brings the dynamic range of the modelled values closer to that of the measurements (Figure 31). However, that does not always lead to improvement of the model scores. Figures-31-32, for instance, show that in most of the domain the temporal correlation coefficient for O3 concentrations is the highest and also the root mean square error is the lowest for the computations with the low horizontal resolution. The high resolution run only outperforms the low resolution one in Italy. Interestingly, the low horizontal resolution leads to the best results (Figure 33), whereas the shortest time step is still preferable. The low resolution results also agree better with the measurements for NO and SO2.

The higher resolution does improve the results for CO (Figure 31, upper left panel) but for NO2 it is rather mixed (Figure 34). The wide areas of France Italy, part of UK and Switzerland were improving but other areas, e.g. Po Valley, English Channel and part of Benelux were reproduced worse by the high-resolution computations.

The results for PM are at similar level for all model setups.

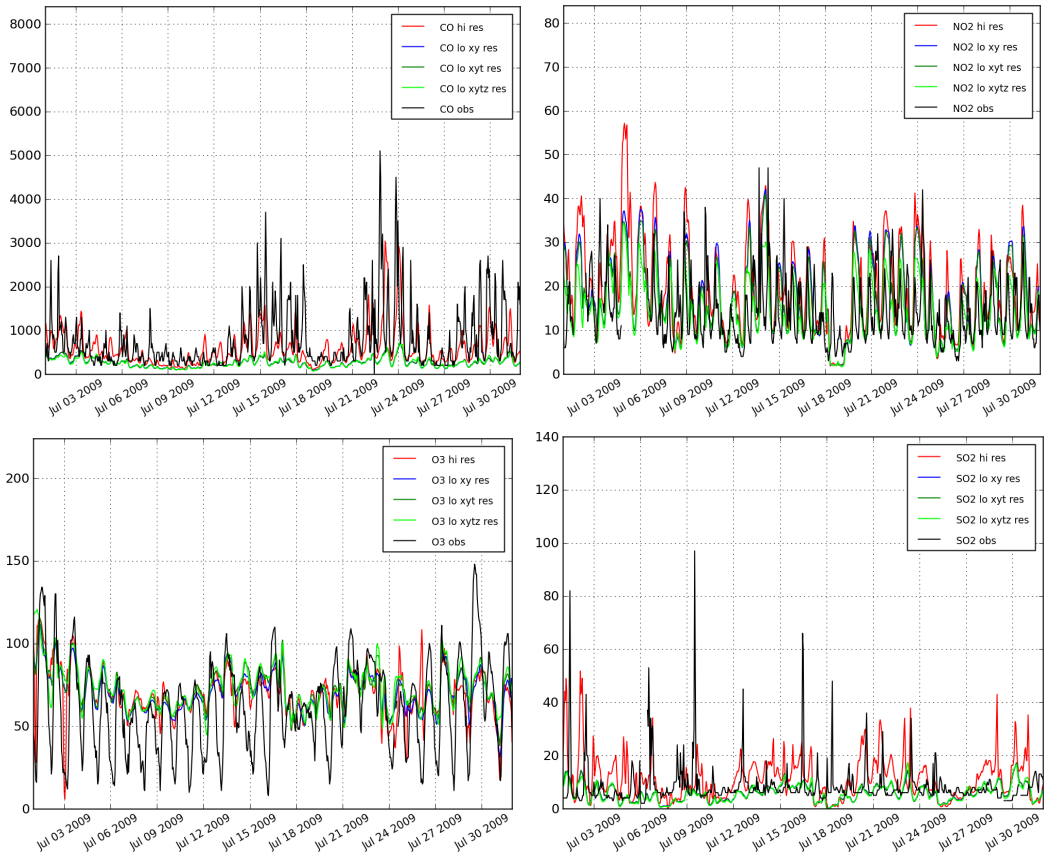

Figure 31: *Examples of time series of modelled and measured surface concentrations: upper left - CO; upper right – NO2; lower left - O3; lower right – SO2.*

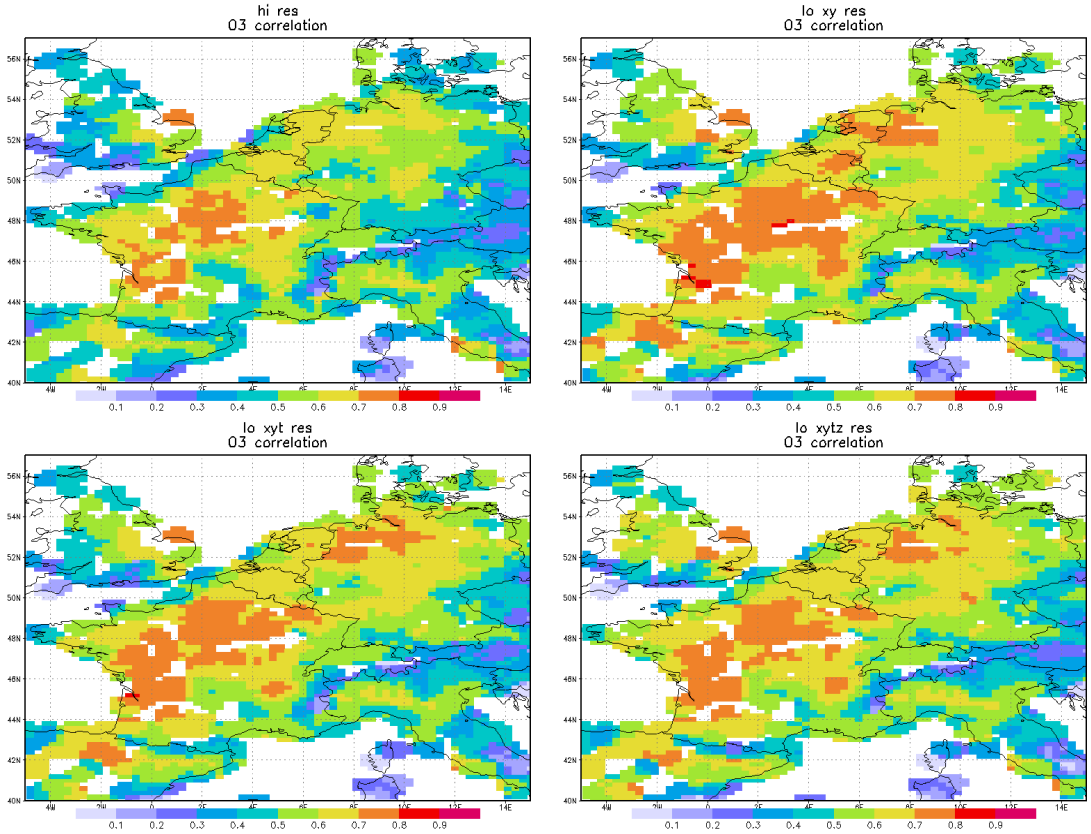

Figure 32: *Temporal correlation coefficient for O3 surface concentrations.*

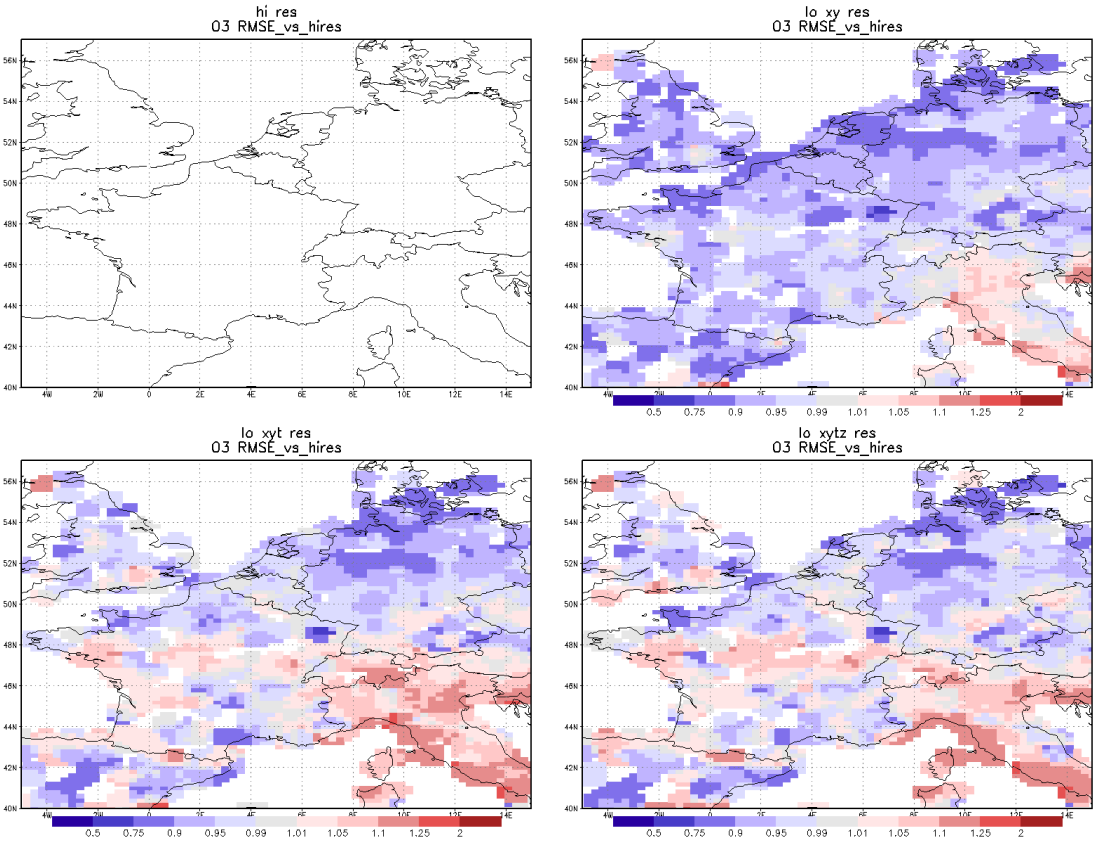

Figure 33: *Root mean square error, RMSE of O3 surface concentration divided with that of the high resolution computations.*

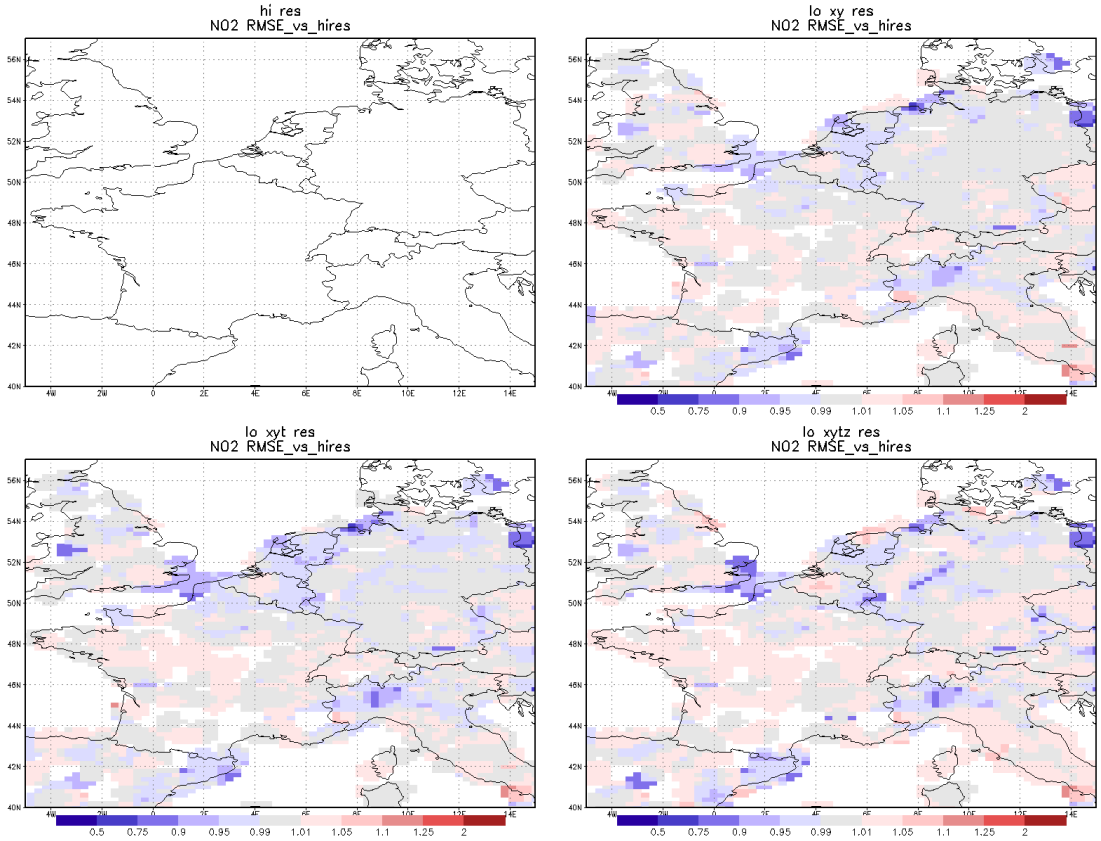

Figure 34: *Root mean square error of NO2 surface concentration divided with that of the high resolution computations.*

10. Evaluation and Improvement of Regional Enviro-HIRLAM Model Simulations of Megacity Plumes Including Aerosol Feedbacks

The main focus of the DMI team contribution for the deliverable D5.3 was to study, quantify and validate the possible effects of elevated pollutant concentrations from megacities on the meteorology on the regional scale. In particular, the influence of air pollution on cloud formation, precipitation and radiation was assessed and indicators relating meteorological patterns to urban air pollution episodes were developed through the application of the online coupled environment model Enviro-HIRLAM.

Two periods were considered in this chapter: (i) monthly averaged (for June 2009) changes in surface temperature due to aerosol indirect effects of primary urban aerosol emissions; and (ii) for the Paris MEGAPOLI summer campaign (July 2009) with comparative studies of the aerosol feedbacks versus urban heat island effects.

Additionally to this study the validation of the Enviro-HIRLAM model versus Paris monitoring data for a specific episodes was done by *Korsholm (2009*; http://www.dmi.dk/dmi/sr09-01.pdf).

Evaluation of the feedbacks of urban emissions on the chemical composition will be done sepa-

rately based on the online and off-line variants of model simulations.

10.1. Monthly averaged changes in surface temperature due to aerosol indirect effects of primary aerosol emissions in Western Europe

By Ulrik Korsholm, Alexander Mahura, Alexander Baklanov

Megacities emit aerosols and their pre-cursers and are transported downwind in urban plumes. Modifications of cloud properties due to anthropogenic aerosols may take place through modification of cloud reflectance and precipitation development, referred to as the first and second aerosol indirect effects respectively. These processes have received much attention on climatic time scales, since they represent one of the largest uncertainties in current climate models. There characteristic time scale, however, is the same as that of the clouds and significant differences may exist for various types of clouds. In this study we consider the monthly averaged effect of the first and second aerosol indirect effects. By comparing model runs with and without the indirect effects we found that a monthly averaged signal in surface temperature of about 0.5 °C exists. In particular the indirect effects led to stronger convection and heavier precipitation in some places and suppression of precipitation in other places. Changes in average cloud reflectivity and latent heat fluxes due to modification of cloud lifetime and precipitation led to changes in surface temperature. Comparison to temperature and dew point temperature measurement data showed that root mean square error and bias decreased near the surface, when averaged over all available measurement stations.

10.1.1. Introduction to the indirect aerosol effects study

Megacities (cities with more than five million inhabitants) affect temperature structure on several scales. On the global to regional scale energy production and consumption, transportation and industrial activities account for the main greenhouse gas emissions affecting global and regional climate and on the local scale the urban micro climate is affected by heterogeneity effects (roughness, heat fluxes, and canalization), shadowing and sheltering effects of buildings and radiation trapping.

The urban heat island (UHI) results from modifications in the surface energy balance. As rural vegetated areas are replaced by urban surfaces they dry out. Hereby, less incoming solar energy is consumed by evaporation of water located at the surface or in soils, plants, tress etc. Therefore, a larger fraction of the incoming solar energy is turned into heat. Urban materials accumulate larger amounts of solar energy than rural surfaces do and during night the accumulated energy is released, leading to reduction of the night time cooling. The UHI affects the urban microclimate but may also

have effects on larger scales. If large scale forcing is weak thermal motion induced by the UHI may initiate convective plumes (*Wong & Dirks, 1978; Masson et al., 2008; Hidalgo et al., 2008*) affecting the horizontal and vertical regional temperature structure upon down wind transport of heat.
Megacities are also characterized by large emissions of primary and secondary pollutants such as NO_x, O_3, volatile organic compounds as well as particles. Direct interaction between radiation and pollutants may cause strong local changes in temperature (Fan et al., 2008). Particles may be transported downwind in the urban plume into cloudy environments where they activate and contribute to an increase in cloud droplet number concentration. Such an increase leads to enhanced cloud reflectance through the first aerosol indirect effect (*Twomey, 1974*) and modification of precipitation development through the second aerosol indirect effect (*Albrecht, 1989*). Clouds exert strong constraints on tropospheric temperature and changes in reflectance and lifetime may be an important contributor in shaping the down wind temperature structure.
Modelling the effects of the aerosol indirect effects presents some difficulties due to the spatial and temporal scales which must be spanned. Aerosol and cloud microphysics take place on scales of the individual aerosols while cloud formation, transport and precipitation development have larger characteristic scales and require a good representation of the synoptic scales. Traditionally, models either contain a detailed description of chemistry, aerosols and cloud microphysics and a parameterized approach to dynamics or they contain detailed dynamics and highly parameterized microphysics.
In this study we have implemented representations of the first and second aerosol indirect effects in a short range weather model which contains a well tested parameterization of the autoconversion process (process by which cloud liquid water is transformed to rain drops). Quantification of the effect on thermal structure is not feasible in the present study due to a lack of suitable metrics for short lived species and because there is a strong dependency on the choice of auto conversion parameterization, i.e. many models should be included in such an exercise. The purpose of this work is to show the feasibility of the effects on the regional surface temperature structure on short time scales. This is done by comparing model simulations with and without representations of the first and second aerosol indirect effects. The simulations covered a full summer month and monthly averages were considered in order to exclude as much of the random signal as possible.

10.1.2. Enviro-HIRLAM model description

Enviro-HIRLAM (*Korsholm et al, 2008; Korsholm, 2009*) is an extension of the HIRLAM (High Resolution Limited Area Model) short range numerical weather prediction model system (*Unden et al., 2002*) to include gas-phase chemistry, aerosols and aerosol cloud interactions. Dispersion of aerosols and trace gases are done using the same parameterizations and the same grid as for mete-

orological variables. Prognostic variables comprise temperature, wind components, specific humidity, surface pressure, geopotential, trace gas mass concentrations and aerosol number and mass concentrations. The vertical coordinate is a hybrid between terrain following σ-coordinates and pressure levels while horizontal discretizations are done on an Arakawa-C grid. The dynamical core is based on the primitive equations and is solved numerically by using a semi-implicit semi-Lagrangian approach. For a more detailed description of HIRLAM the reader is referred to *Unden et al., 2002.*

Wet deposition (in-cloud, below cloud and snow scavenging) of aerosols is based on a scavenging coefficient which is dependent on precipitation rates (*Baklanov & Sorensen, 2001*). For gases uptake in falling rain (in-cloud and below cloud) and dissolution in cloud water (in-cloud) is taken into account. The scavenging coefficient follows *Seinfeld & Pandis (1994).* Dry deposition of gases and aerosols follow the *Wesely (1989)* resistance approach.

Cloud Radiative Properties

Atmosphere radiation interactions are highly parameterized and follows a modified version of the scheme described in *Sass et al. (1994).* The short wave (SW) clear sky flux at the top of the atmosphere is reduced by absorption due to the presence of stratospheric ozone, water vapour and due to Rayleigh scattering through vertical columns. Average CO_2, O_2 and aerosol absorption is also accounted for. If clouds are present the downward SW flux is reduced by cloud transmissivity and absorptivity. For a partly cloudy column the clear sky and cloudy fluxes are linearly combined. Cloud transmissivity and absorptivity depends on the cloud condensate content (CCC (kg m^{-3})) and cloud droplet effective radius (μm) (*Wyser et al., 1999*). For water clouds the effective radius is expressed as (*Wyser et al., 1999*):

$$R_e^3 = 3CCC/(4\pi\rho_{water}kN),$$

where ρ_{water} is the density of water (1000 kg m^{-3}), N is the cloud droplet number concentration and k is a factor of proportionality between R_e^3 and R_v^3 where R_v is the volume cloud droplet radius. Simultaneous measurements of R_e and R_v shows that k is different for marine (k=0.81) and continental (k=0.69) (*Martin et al., 1994*) conditions. The corresponding clean marine and continental values of N is 10^8 m^{-3} and $4 \cdot 10^8$ m^{-3} respectively. Hence, a CCC value of 1 g m^{-3} corresponds to Re = 9.6 μm over continental regions and Re = 14.4 μm over marine regions. Cloud transmissivity (T_r) is related to R_e as: $T_r = T_1/(T_1+M)$ where M (g m^{-2}) is the vertical integral of CCC from a given level to the top of the atmosphere multiplied by the ratio of cloud cover and maximum cloud cover in the column and $T_1 = a_t(c_t+\cos\theta)$ with θ the solar zenith angle, $a_t = c_{ta}*R_e+c_{tb}$ and c_t, c_{ta}, c_{tb} are constants. Similarly, the absorptivity (A) is related to R_e as: $A = a_a(c_{a1}+\cos\theta)\log(1+c_{a2}M)$, where a_a

$= c_{aa} * R_e + c_{ab}$, where c_{a1}, c_{a2}, c_{aa} and c_{ab} are constants. Hence, an increase in R_e leads to a increase in T_r and A and a corresponding decrease in cloud reflectivity. Therefore, clouds over marine regions are less reflective than clouds over continental regions. The horizontal and vertical variations in R_e is accounted for by weighing according to $R_e = fR_{e,cont} + R_{e,mar}(1-f)$, where $R_{e,cont}$ and $R_{e,mar}$ are the effective radii for continental and maritime regions respectively and the weight f is given as $f = f_{land}(\eta - \eta_0)(1 - \eta_0)$ for $\eta > \eta_0$ where η is the vertical hybrid coordinate used in HIRLAM, $\eta_0 = 0.7$ and f_{land} is the fraction of land; f = 0 otherwise. A minimum effective radius of 4 μm is imposed.

Cloud Microphysics Scheme

The STRACO (Soft TRAnsition and COndensation) cloud scheme (*Sass, 2002*) represents convective and stratiform cloud formation and contains a gradual transition between the two regimes. Subgrid scale variability of humidity is assumed to follow a predefined probability density function which differ in the two regimes and facilitates calculations of the cloud fraction (f_c). Trace gases and aerosol species are convected as water vapour except for condensation and evaporation to and from the aerosols are not accounted for, hence, the aerosols are passive in this respect.

Condensation, collection and autoconversion are assumed to have time scales faster than a model time step and is based on a bulk approach. In the version used here autoconversion in follows the scheme by *Rasch & Kristjansson (1998),* in which autoconversion depends on in-cloud specific cloud condensate (CCC/f_c), air and water density and is proportional to $N^{1/3} H(R_e - R_0)$, where H is the Heavy side step function and R_0=5 μm is a cut-off below which droplets are considered too small to initiate rain, hence, for $R_e < R_0$ H is zero and autoconversion stops.

Cloud droplet number concentration

The primary aerosol sulfate content was given by the emission inventory and the mass concentration was related to the number concentration of activated droplets (CDNC) by using the parameterization by *Boucher & Lohmann (1995),* which distinguishes between marine and continental regions:

$$CDNC_{marine} = 10^6 \cdot 10^{2.06+0.48\log(m_S)}$$

$$CDNC_{continental} = 10^6 \cdot 10^{2.24+0.26\log(m_S)}$$

where m_s is the sulfate mass concentration (μg m^{-3}). The sulfate mass concentration is treated as a prognostic variable in the model and the appropriate CDNC value is added to the clean background cloud droplet number concentration. Hereby, autoconversion of cloud water into rain and the reflectivity of the clouds are affected.

10.1.3. Experimental set-up

Enviro-HIRLAM model was run for a full summer month starting at May 30 2009 and ending at June 30 2009. This run is referred to as BASELINE. The first two days were discarded as spin-up and averages were taken over the period 1-30 June 2009. The forecasts were restarted every six hours at 00, 06, 12, 18 UTC and the forecast length was 24 hours. ECMWF (European Centre for Medium-Range Weather Forecasts) deterministic output was used for the boundary conditions which were updated every hour. The model domain covered western Europe in 0.15º x 0.15º horizontal resolution (154 x 148 grid points) using 40 levels in the vertical with the top level located near 10 hPa. The MEGAPOLI emission inventory (*van der Gon et al., 2009*) was used and sulfate emissions were extracted from PM_{10} according to the procedures used for generation of the inventory and interpolated to the model grid. No aerosol model of gas phase chemistry is included in these runs, which only considers the effect of primary aerosols.

In a second run, termed 12IE, the same procedure was taken as in the BASELINE run except the model now included representations of the first and second aerosol indirect effects. Monthly averages were taken by using the 00 and 03 hour forecasts from each restart in order to get full coverage of the month. Temperature spin-up in the model is typically a few hours and should not affect the averaging. In order to test this hypothesis the surface temperature was averaged using the 00 UTC forecast every day through the month to get full coverage. There were only very slight differences of no relevance to the conclusions of this study. The averaging of accumulated fields such as precipitation is done by using the 24hour accumulated values each day, while daytime and night time averages of activated aerosol number concentration are represented by 00 UTC and 12 UTC averages.

10.1.4. Meteorological situation

Figure 35a displays the time averaged mean sea level pressure. The domain was effectively split in a western and an eastern part, dominated by high pressure ridges and low pressure troughs respectively. The western part was dominated by cool northerly winds (Figure 35b) and relatively little precipitation while the eastern domain was dominated by northward moving thermal lows and therefore stronger precipitation mainly of convective origin (Figure 35c).

The Alps experienced rain up to 18 mm over 24 hours on average while further east up to 13 mm per 24 hours was found. Due to the northerly winds rainout occur just before the Alps and lee side lows are generated. Figure 2.1d shows the number concentration of activated aerosols at about 850 hPa. Maximum values of 0.2×10^8 are found in the eastern part due to strong emissions of sulfate from Belgrade, Budapest and Krakow. In the western part the effect of Paris and London are visible.

The strong average precipitation in the eastern part renders the aerosol effects weak since it takes much larger concentrations to affect the strong precipitation events and due to wash out of the aerosols. Therefore, the following analysis focuses on the western part of the domain where the largest impact of the aerosols is expected.

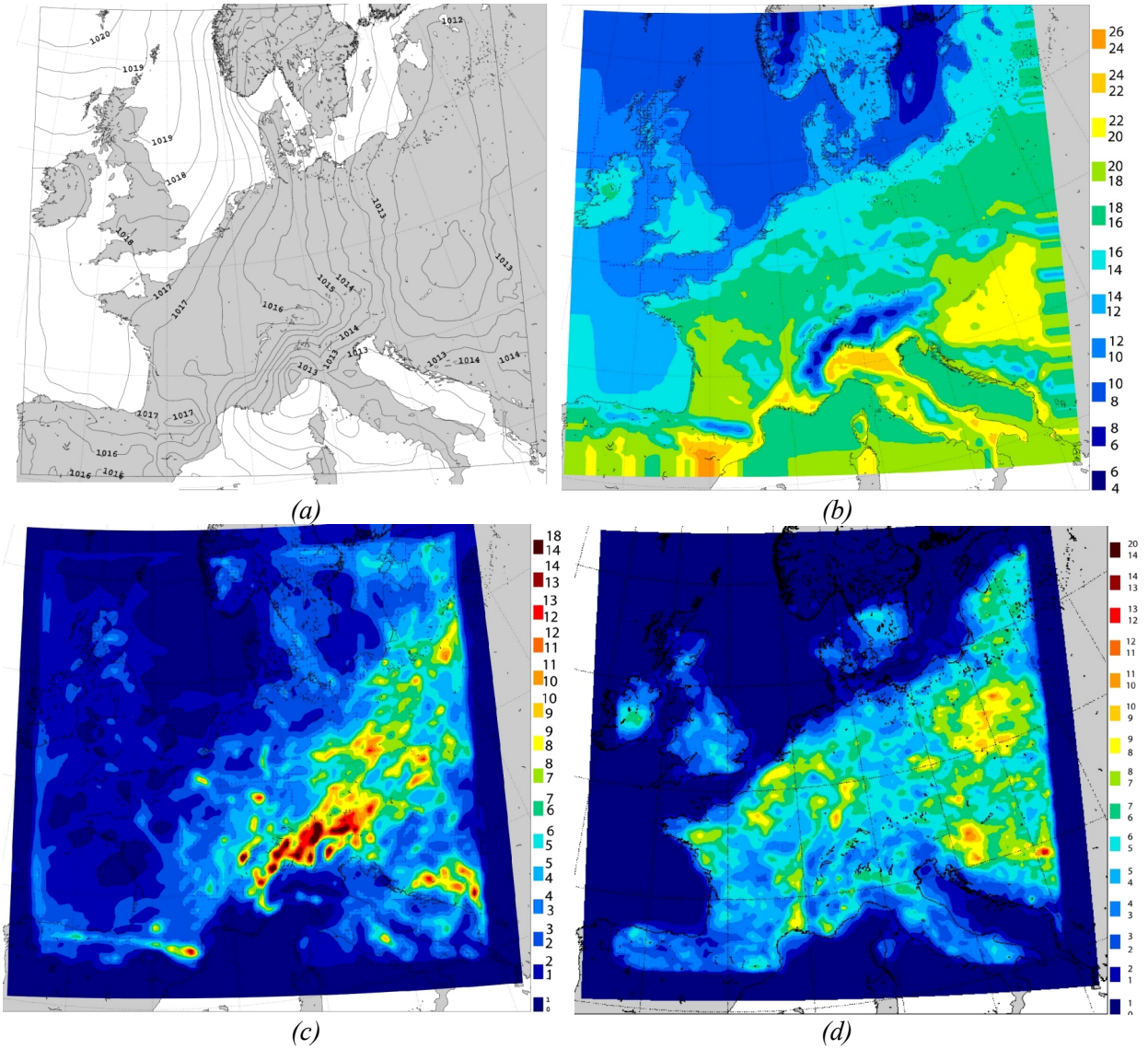

Figure 35: *(a) Mean sea level pressure (in hPa; at 0.5 hPa interval); (b) two-meter temperature (°C); (c) total precipitation (mm / 24 hours); and (d) number concentration (x 10^6 m^{-3}) of activated anthropogenic aerosols at approximately 850 hPa /plots show 12 UTC average over the forecast period 1-30 June 2009/.*

10.1.5. Results and discussion

In the following all differences are calculated as BASELINE minus 12IE and the first and second aerosol indirect effects are referred to as the indirect effects. Figure 36a displays the monthly averaged surface temperature (T_s, °C). Average cooling and warming of up to 0.5ºC was found while the domain averages remained close to zero, i.e. there was no "climate effect" found on this timescale in this modelling domain. On individual days the maximum and minimum changes were up to 5ºC. T_s is controlled by the surface radiation balance and the sensible and latent heat fluxes.

Incoming SW radiation below the tropopause is mainly affected by water vapour absorption and the presence of cloud layers that reflect in the short wave part of the spectrum (O_3 and CO_2 also have some influence, which remains fixed between the BASELINE and 12IE runs).

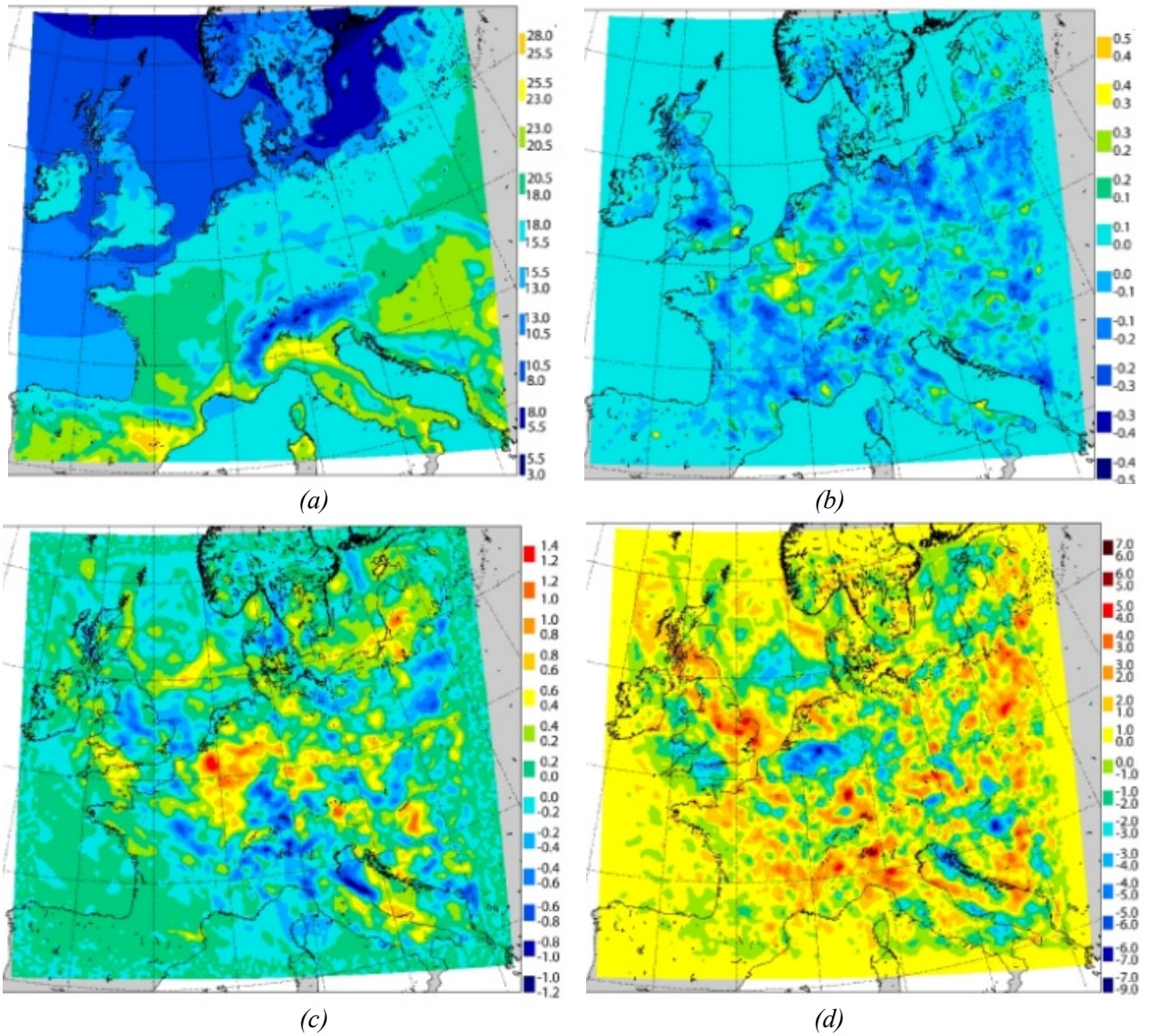

(a) *(b)*

(c) *(d)*

Figure 36: *(a) Surface temperature (°C), (b) difference in surface temperature (BASELINE minus 12IE), (c) net daily accumulated short wave radiation at the surface (x 10^6 W m^{-2}) and (d) cloud reflectivity (%) /all plots displays averages over the period 1-30 Jun 2009/.*

Cloud reflectivity is modified by the first aerosol indirect effect, while the second aerosol indirect effect affects the lifetime of the clouds through suppression of rain and thereby, has an average radiative impact.

The monthly averaged 24 hour accumulated net SW radiation at the surface is displayed in Figure 36b while the average cloud reflectivity is shown in Figure 36c. Cloud reflectivity is a pseudo satellite image for the visible range calculated for direct comparison with satellite images. The calculation begins at the lowest model level where the a reflectivity value is calculated based on effective cloud droplet radius which in turn depends on cloud liquid water and cloud droplet num-

ber concentration. This start value is then modified according to overlying clouds when looping through the layers (*Tijm, 2009*). Relative humidity only changes slightly and the changes in SW is therefore controlled by the modifications in cloud reflectivity. An increase in average cloud reflectivity leads to a decrease in direct SW at the surface and may be due to an increase in cloud lifetime, an increase in cloud water content or an increase in droplet number concentration.

The indirect effects were postulated in the context of boundary layer clouds with a relatively low concentration of cloud droplets and their effects in relation to deep convective clouds is not fully understood. Increased cloud water path allows the cloud to grow to greater heights and thus induce stronger convective cells which at a later time deliver larger precipitation fluxes. However, convective activity is also affected by T_s and thereby by increased reflectivity due to increased cloud lifetime. In particular evaporation of precipitation tends to stabilize the sub-cloud layer facilitating decoupling of the cloud layer and the surface. Furthermore, invigoration of convection may lead to increased entrainment of dry air and thereby to a decrease in cloud liquid water path (*Feingold et al., 1996; Lu & Seinfeld, 2005*). Hence, the aerosol indirect effects may act to increase or decrease convection and thereby precipitation, lifetime, liquid water path and T_s (*Platnick et al., 2000; Coakley et al., 2002; Han et al., 2002; Andrae et al., 2004*). The detailed mechanisms controlling the response is not fully understood, however, it seems from cloud resolving modelling studies that the rain rate, anthropogenic loading and the development of convective system have an influence.

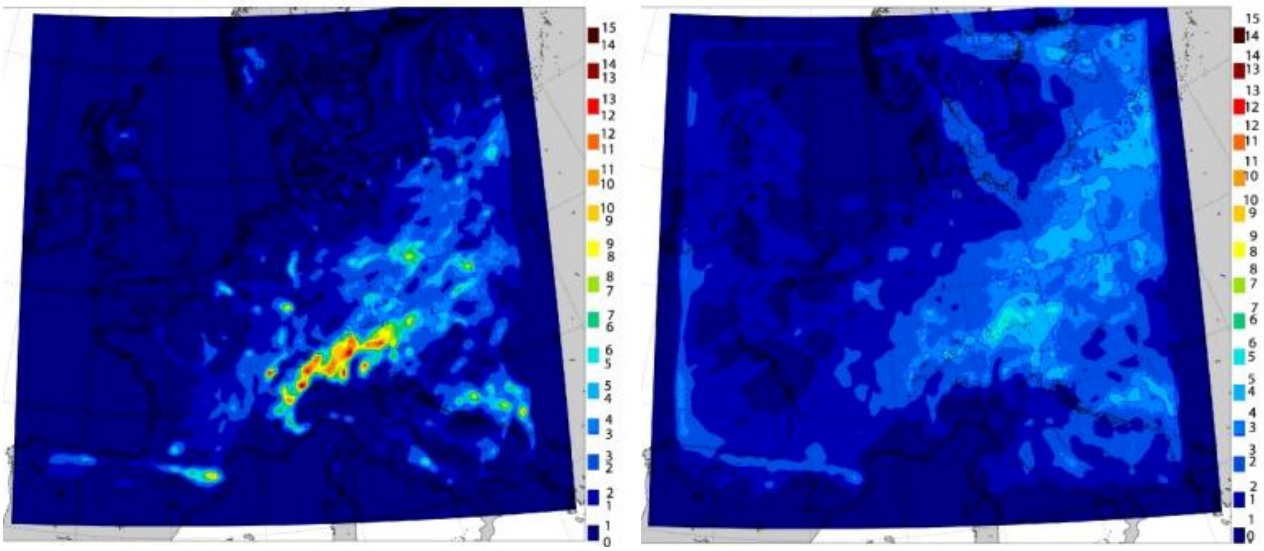

(a) *(b)*

Figure 37: *Accumulated precipitation (during 24 hour period) averaged over the forecast period: (a) convective precipitation (mm/24 hours); and (b) stratiform precipitation (mm/24 hours).*

Consider North-Eastern France and Belgium (Figure 36b). This area is located downwind of Paris and was influenced by the megacity sulfate emissions which are mixed upwards during daytime. In this region convective precipitation has changed (Figure 37) and cloud reflectivity increased substantially (Figure 36c) due to the indirect effects. Figure 38 displays the difference in cloud top temperature, lifting condensation level and vertically integrated cloud water. The clouds reach

higher levels and also extents further downwards as cloud water increase. These changes are consistent with more vigorous convection and longer cloud lifetime giving raise the observed decrease in cloud reflectance (Figure 36c).

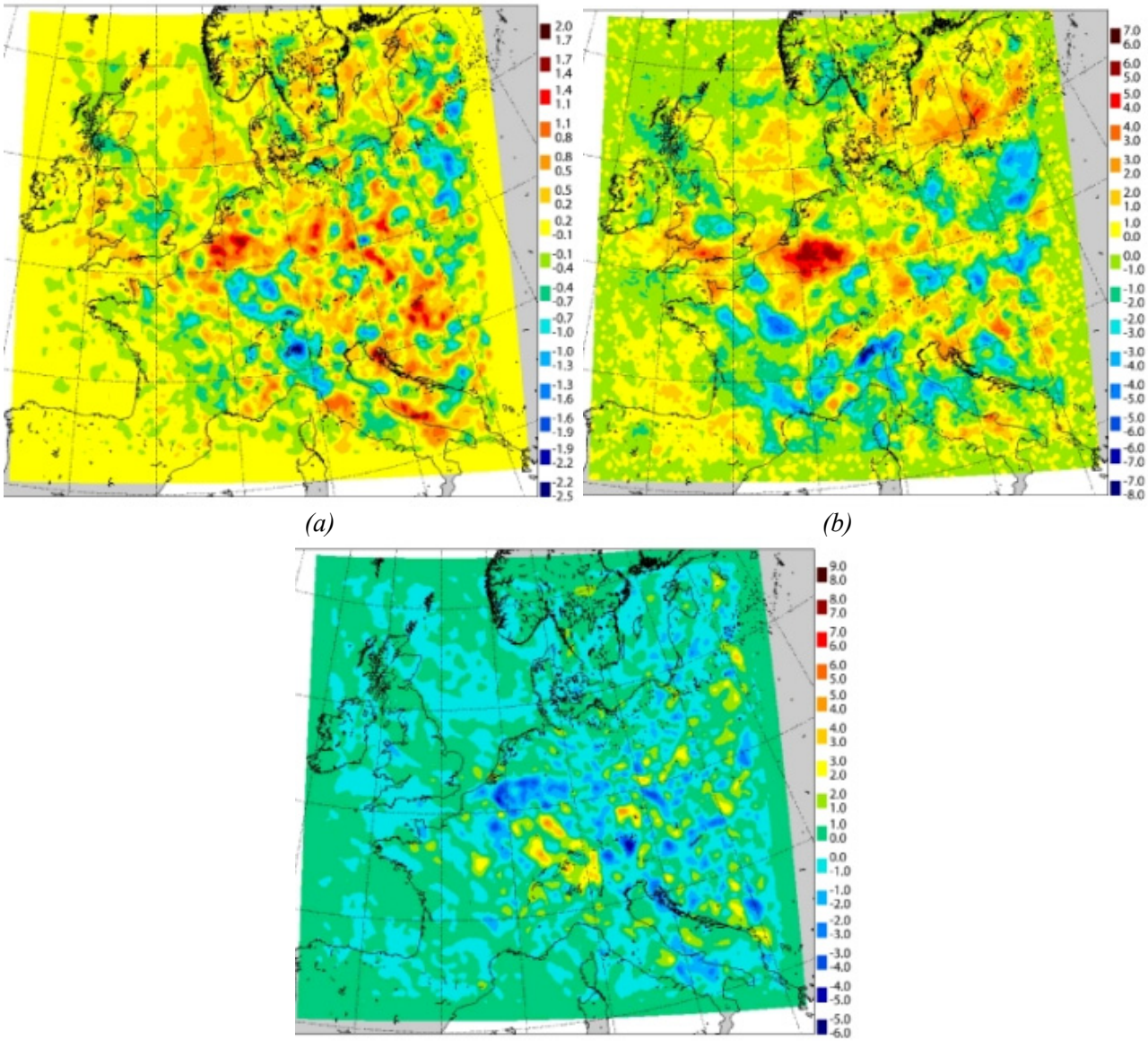

Figure 38: *(a) Difference (calculated as BASELINE minus 12IE) in cloud top temperature (°C), (b) difference in lifting condensation level (m), (c) difference in vertical integrated cloud water content (kg m^{-2}). All plots are taken as averages over the period 1 June 2009 to 30 June 2009.*

Figure 39 displays the sensible (Figure 39a) and latent heat (Figure 39c) fluxes along with the corresponding differences (Figure 39bd) between the runs. A negative flux is oriented from the surface to the atmosphere and hence leads to a cooling of the surface while a positive flux is directed into the surface. The latent fluxes are generally larger than the sensible ones in particular in the low pressure dominated region to the east of the domain. Urban areas stick out on the figures because urban areas are ascribed with desert properties in the model (dry and reflective) which thus affect the fluxes. In this region the precipitation changes induced by the aerosol effects led to a

decrease in upward latent heat fluxes which, an average, led to warming. The changes in SW radiation and cloud reflectivity; however, was larger and the region experienced a net cooling.

Next, consider the T_s decrease near and downwind of London and the temperature increase in mid-England originating near Birmingham (Figure 36b). In this region the change in cloud water path is modest (Figure 38c) and there is only little suppression of rain (Figure 37). Just north of London a region of cooling was found. The upward sensible heat flux decreased (Figure 39) and thus acts to warm the surface while an increase in upward latent heat flux (of similar magnitude) acted to cool the surface. Since, the latent fluxes are generally larger than the sensible fluxes the net result becomes a cooling of the surface. Just south of London an opposite situation exists..

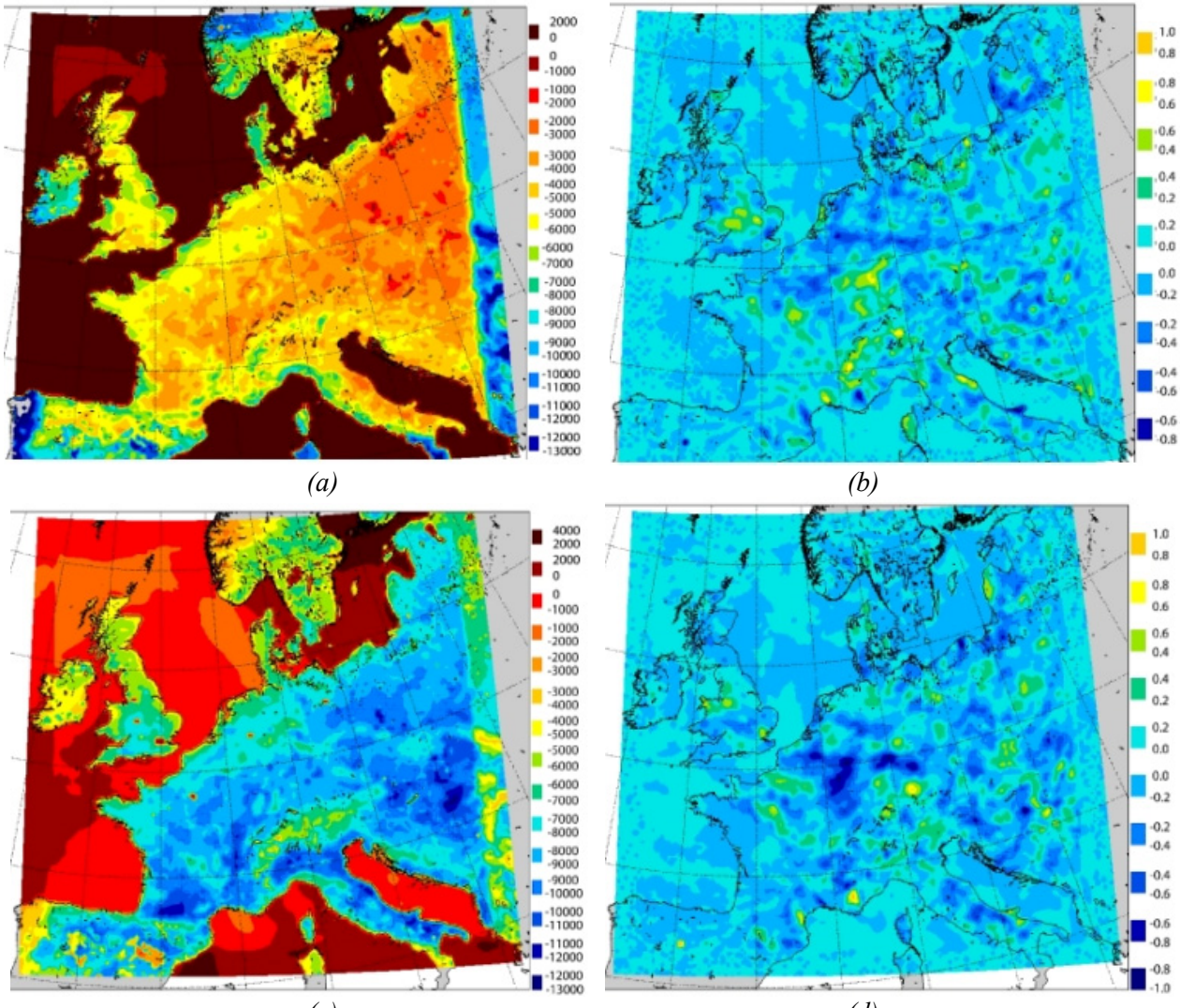

Figure 39: *(a) Daily accumulated sensible heat flux (x 10^3 W m^{-2}), (b) difference (calculated as BASELINE minus 12IE) in accumulated sensible heat flux (x 10^6W m^{-2}), and (c) daily accumulated latent heat flux (x 10^3 W m^{-2}), and (d) difference in accumulated latent heat flux (x 10^6 W m^{-2}) /all plots are averages over the period 1 June 2009 to 30 June 2009/.*

The aerosol effects induce a slight decrease in total precipitation which led to a decrease in the upward latent heat flux and thereby a slight net warming. By the same account the region in mid-England near Birmingham experienced a warming. The total precipitation decreased, the upward latent heat flux decreased accordingly while the upward sensible heat flux increased (similar in

magnitude) and the net effect became a warming in this area

10.1.6. Comparison with observations

In order to complement the above findings a comparison between temperature, dew point temperature and precipitation amount was made for the entire month. Figure 40 displays time series at 925 and 850 hPa of the observations, temperature and dew point temperature.

Both BASLINE and 12IE seems to predict the parameters well at these levels, however, at the end of the period models and temperature observations seem to diverge generating increased bias and RMSE. The error is evident at both levels and decrease upwards through the troposphere. Since, it is present in both runs it is assumed to be independent of the aerosol effects under consideration here. The BASELINE and 12IE runs seems quite similar in the statistics for these levels and there is no general improvement or degradation of the results, however, at individual stations some spread may be found. It is likely that the degradation is connected to a general degradation in precipitation predictions for both runs at the end of the forecast period (Figure 42).

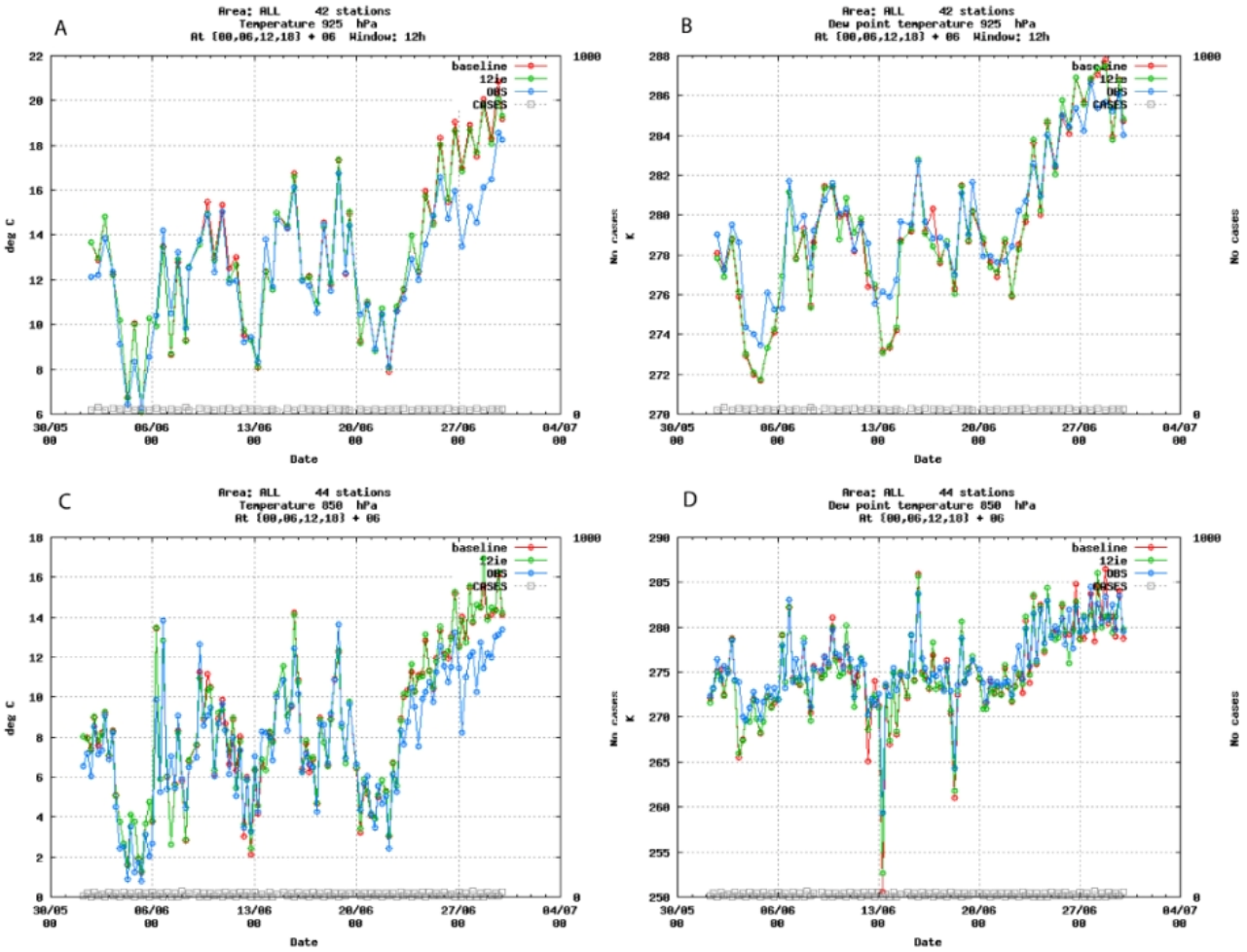

Figure 40: *Time series of domain averaged temperature at 925 hPa (A) and 850 hPa (C) and dew point temperature at 925 hPa (B) and 850 hPa (D) along with station averaged measurements.*

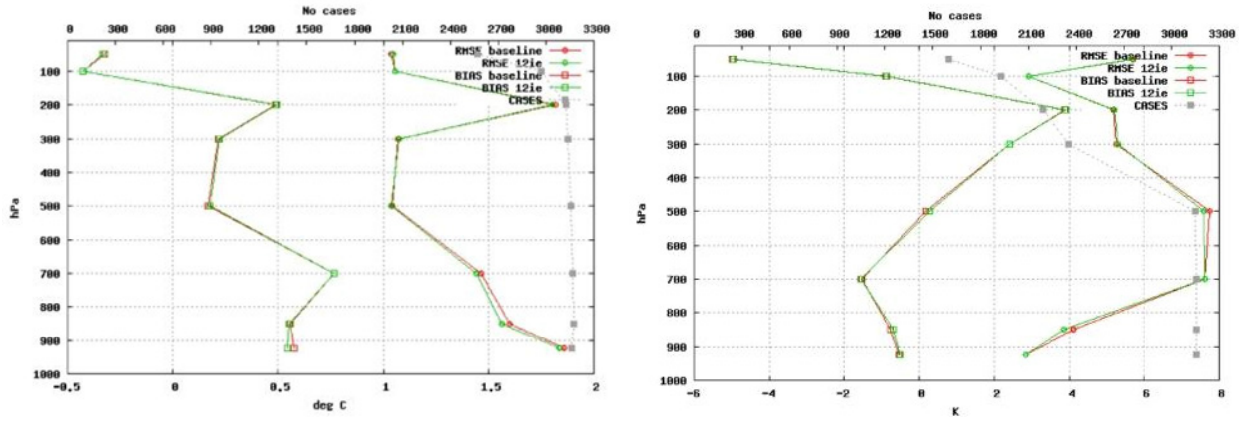

(a) (b)

Figure 41: *Domain averaged profiles of bias and rmse in temperature (a) and dew point temperature (b).*

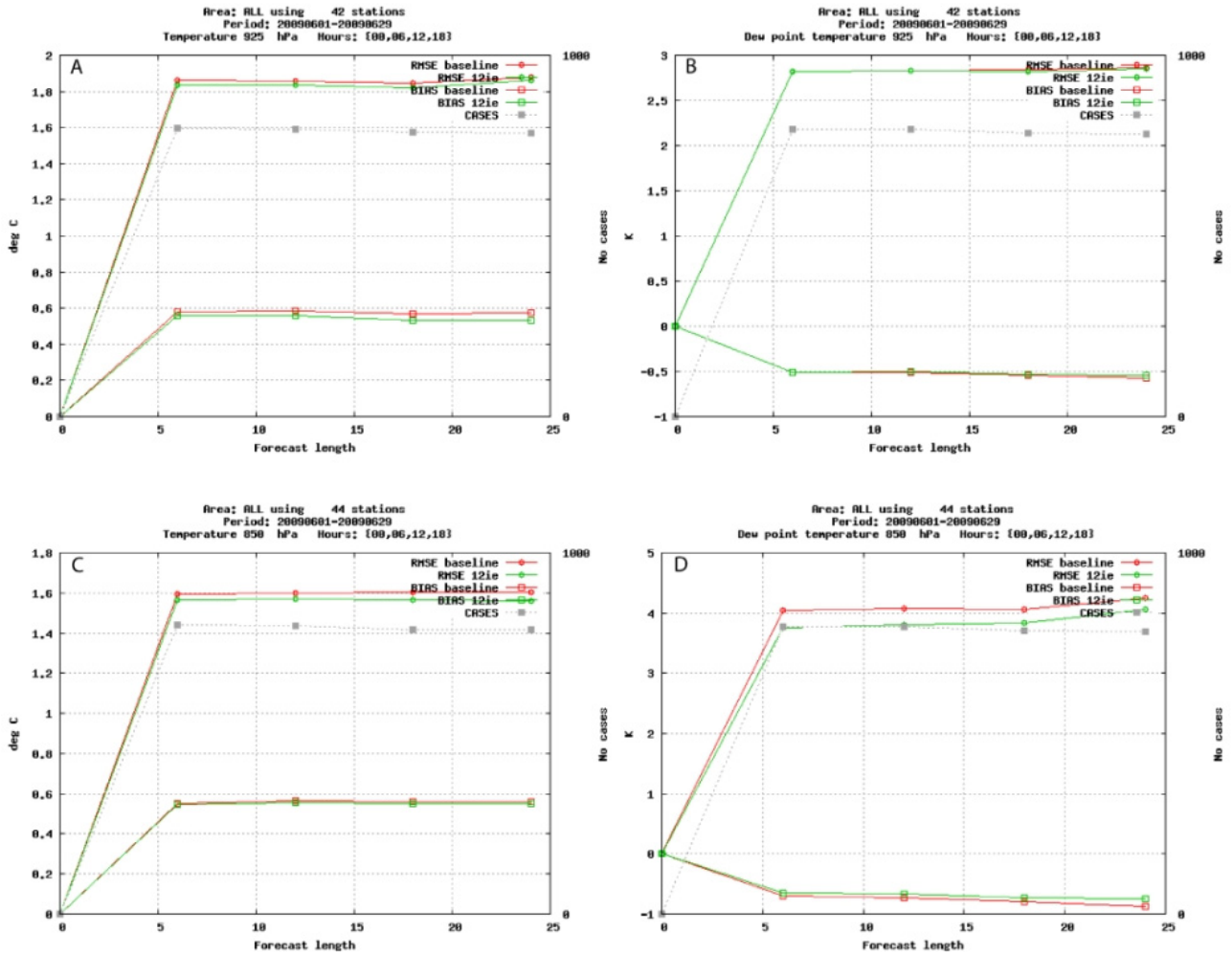

Figure 42: *Bias and root mean square error for temperature (A and C) and dew point temperature (B and D) at 925 (A and B) and 850 hPa (C and D) as a function of forecast length. All available stations and grid points were included.*

Taking averages over all stations containing profiling data Figure 41 shows that there is slight improvement (decreased bias and rmse) in the statistical scores for temperature near the surface while the largest deviation in dew point is found near the 500 hPa level.

Considering spatial statistics as a function of forecast time (Figure 42) at 925 and 850 hPa we found

that both dew point and temperature had slightly decreased bias (max increase of 0.12 K) and rmse (max decrease of about 0.28 K) during the forecast for the 12IE run. At the 925 hPa level dew point statistics remained constant between the two runs.

Figure 43 displays the precipitation rmse, bias and time series. There seems to be no general increase or decrease in the average precipitation performance. However, both runs seem to a tendency of over-predicting precipitation, in particular in the second half of the forecast period.

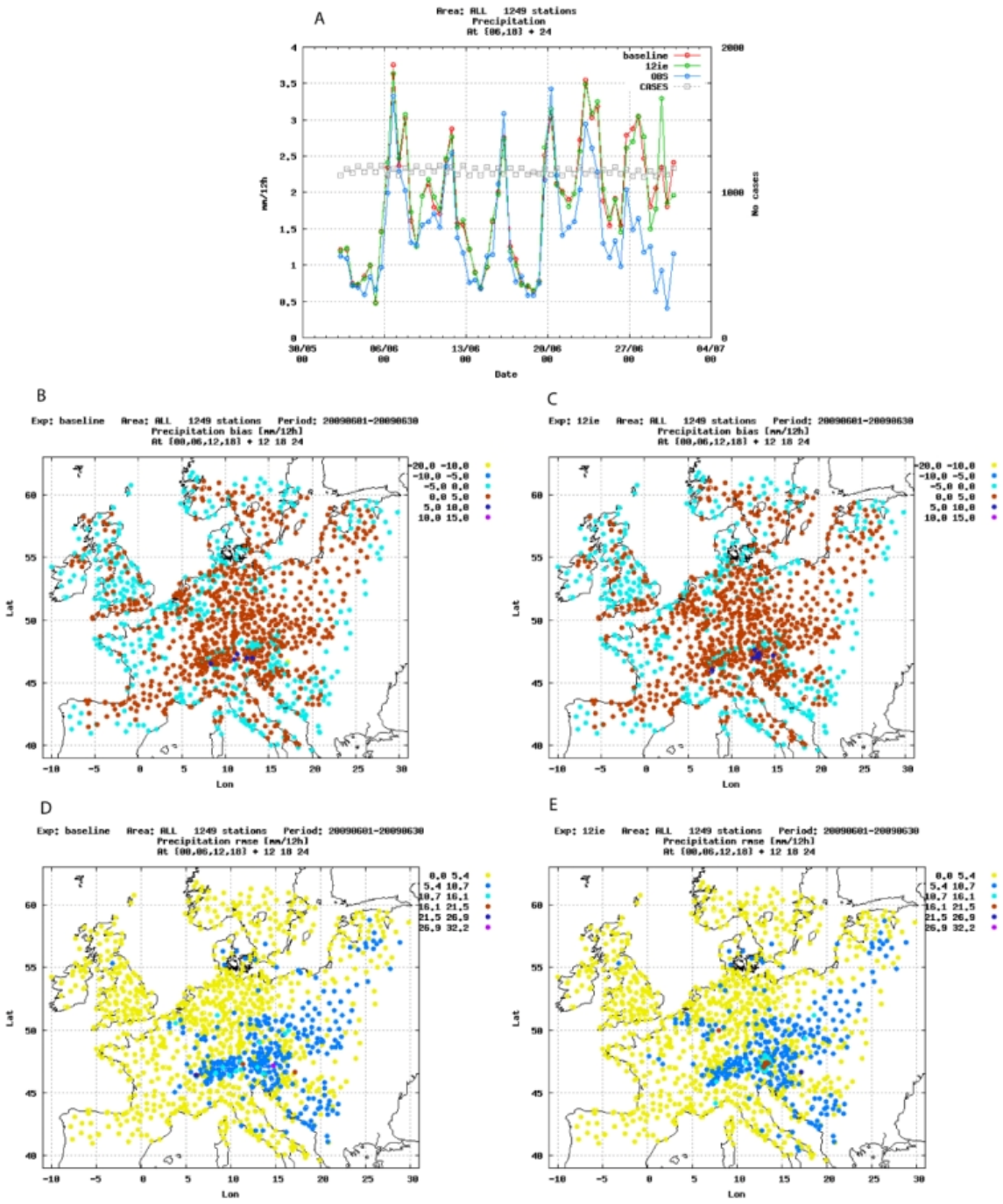

Figure 43: *Domain averaged precipitation as a function of time for the BASELINE, and12IE runs along with observations (A). Horizontal distribution of rmse for temperature (B) and dew point temperature (C) and the distribution of temperature bias (D) and dew point temperature bias (E).*

10.1.7. Summary and conclusions

In this experiment runs with and without the first and second aerosol indirect effects were compared. Averages were taken over the month of June 2009 and the average effect investigated. On average northern France and Belgium experienced a 0.5°C cooling as did a region just north of London and southern England while mid-England and a region just south of London was dominated by an average heating with a maximum of 0.5 degrees near Birmingham.

The cooling in northern France/Belgium resulted from larger reflection of incoming short wave radiation due to longer average cloud lifetime and more cloud droplets. The cooling north of London and the warming to the south of London were governed by changes in the latent heat fluxes due to changes of precipitation in the region. Similarly, the average warming in mid-England appeared because of decreased latent heat fluxes due to precipitation suppression.

Comparison of temperature, dew point temperature and precipitation with measurements did not reveal any time averaged increase in precipitation performance. However, considering statistical scores as a function of time revealed that temperature and dew point temperature retained slightly better scores during the forecast period.

The aerosol indirect effects led to both heating and cooling of the surface. In particular, suppression of precipitation led to stronger convective cells and thereby more precipitation on average. If the effect of cloud reflectivity is not dominant the surface temperature may be modulated by latent heat fluxes due suppression or enhancement of precipitation. It should be noted that this experiment considered only primary sulfate emissions. A more detailed study including secondary aerosols is expected to result in a larger temperature response due to an increased loading of activated aerosols.

10.2. Comparative studies of aerosol feedbacks vs. urban heat island effect for Paris MEGAPOLI summer campaign (July 2009).

By *Iratxe Gonzales-Aparicio, Alexander Baklanov, Roman Nuterman, Alexander Mahura, Ulrik Korsholm*

This research is devoted to the surface layer analysis in urban areas. The performance was carried out by means of long-term simulations using the Enviro-HIRLAM model for the Paris metropolitan area, considered as a Megacity.

The Enviro-HIRLAM (Environment – High Resolution Limited Area Model) is an online coupled numerical weather prediction and atmospheric chemical transport modelling system for research and forecasting of both meteorological and chemical weather (*Korsholm 2009, Korsholm et al 2008; Baklanov et al., 2009; Baklanov et al., 2008*). The meteorological and chemistry model solve

the governing equations describing by the main processes: emission, advection, horizontal and vertical diffusion, wet and dry deposition, convection, chemistry and aerosol feedbacks (*Korsholm 2009, Korsholm et al., 2008*). The system realisation includes the nesting of domains for higher resolutions, different types of urbanization, implementation of chemical mechanisms, aerosol dynamics and feedback mechanisms (*Korsholm 2009, Baklanov et al., 2008*).

Urban scale modelling with Enviro-HIRLAM is carried out using the Building Effect Parameterization (BEP, *Martilli et al., 2002*) module. The metropolitan area is represented by a combination of mentioned urban districts. Each district is represented as a combination of multiple streets and buildings of constant widths but with different heights. The parameterization includes computation of contributions from every type of urban surface (street canyon floor, roofs and walls of buildings) as well as vertical surface.

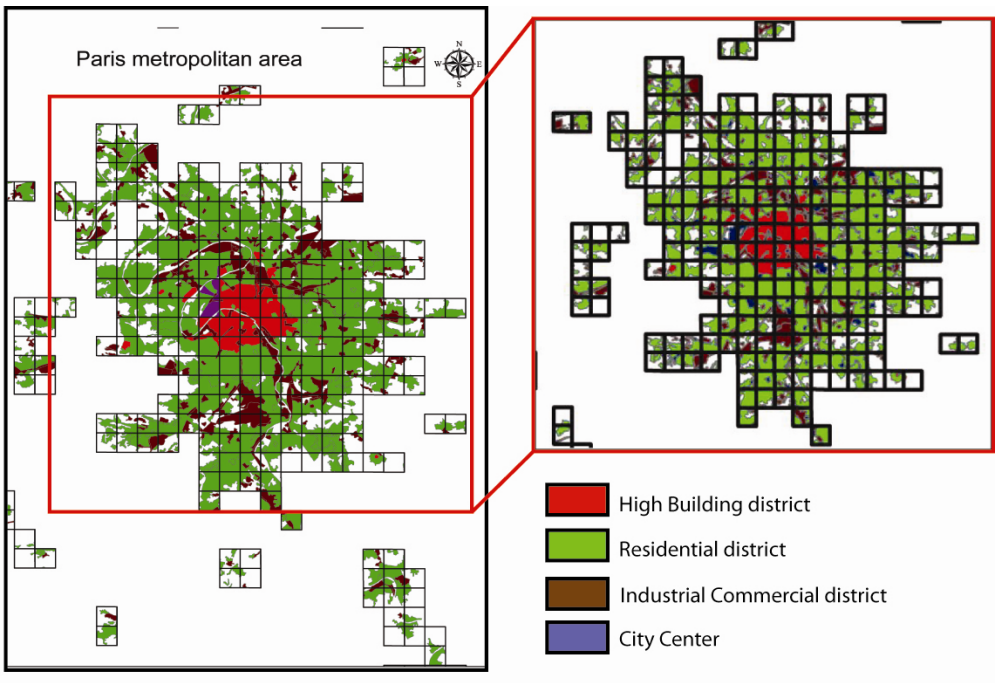

***Figure 44**: Reclassification into urban districts based on CORINE 2000 for the Paris metropolitan area*

Paris (France) is located inland of the country (Ile-de-France Region) over a semi-flat terrain. It is considered as a megacity (with population of 11.836 million inhabitants according to census 2007). Four urban districts were identified (*Mahura et al., 2010*): (1) city centre (CC) which included 13th, 15th and 19th arrondissement of the Paris Ile-de-France region; (2) high building district (HBD); (3) industrial commercial district (ICD) and (4) residential district (ReD). Figure 44 shows the urban reclassification of this city based on the CORINE 2000. The P01 modelling domain contained 65022 grids in total, where 3080 points are urban grids. The Paris metropolitan area was represented by 220 urban grid points and each urban grid was represented by the dominant urban district: HBD was attributed to 21 urban grids (9%); CC - 4 urban grids (2%); ICD - 30 urban grids (14%)

and ReD - 165 urban grids (75%).

High resolution (2.5 x 2.5 km for Paris) long-term runs for two specific months (during July 2009 and January-February 2010) with different wind conditions were performed. The main objectives were to evaluate the performance of the urbanized (with BEP module and Anthropogenic Heat Fluxes, calculated based on LUCY model, *Allen et al, 2010*) vs. non-urbanized and to estimate the influence of the city on formation of the meteorological fields for the air temperature, relative humidity at 2 m and wind speed at 10 m. Additionally, the scheme of sulphate aerosol dynamics was implemented to assess its indirect effects on meteorology. The simulations were performed in different modes:

1) Control run; i.e. without any modifications
2) Urban run which included BEP and Anthropogenic Heat Fluxes (AHF, 40 W/m2)
3) Feedbacks of the sulphate aerosols.
4) BEP + AHF and feedbacks of the sulphate aerosols

The impact of the cities on the meteorological variables was studied by evaluating the difference between outputs of the urbanized vs. control runs (see Figure 45-47). The impact of the feedbacks on meteorological variables was studied by assessing the difference between the outputs of the urbanized + feedbacks vs. urbanized runs for the Paris metropolitan area.

Before the urban canopy analysis, the comparison between the simulations vs. the observations was carried out for the temperature and relative humidity at 2 m and wind at 10 m. The comparison was performed on monthly basis (2nd – 31st July 2009) at the three different stations selected (urban - LHVP, suburban - SIRTA and rural CHARTRES). The Figure 45 shows the comparison of the temperature at 2 m on a monthly basis at the SIRTA site.

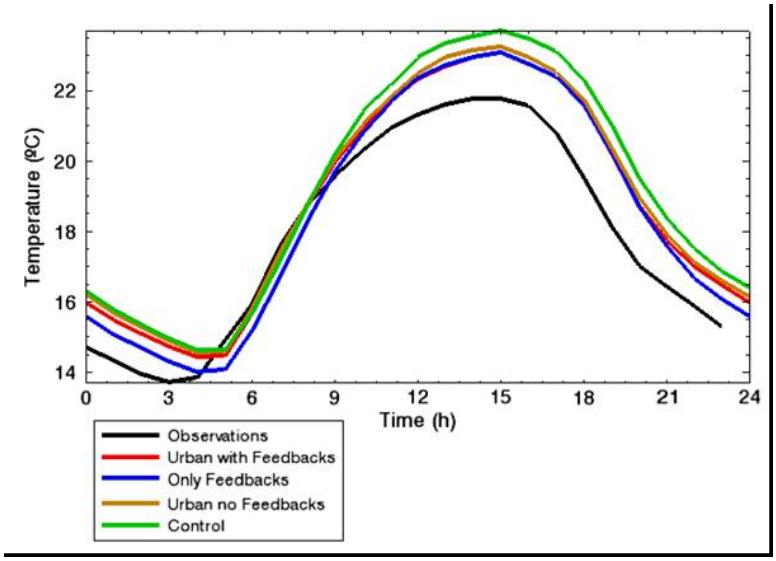

***Figure 45**: Comparison between the simulations (control runs, urban runs, aerosols run and urban+aerosol runs) vs. observations on monthly basis at SIRTA (sub-urban station) during July 2009.*

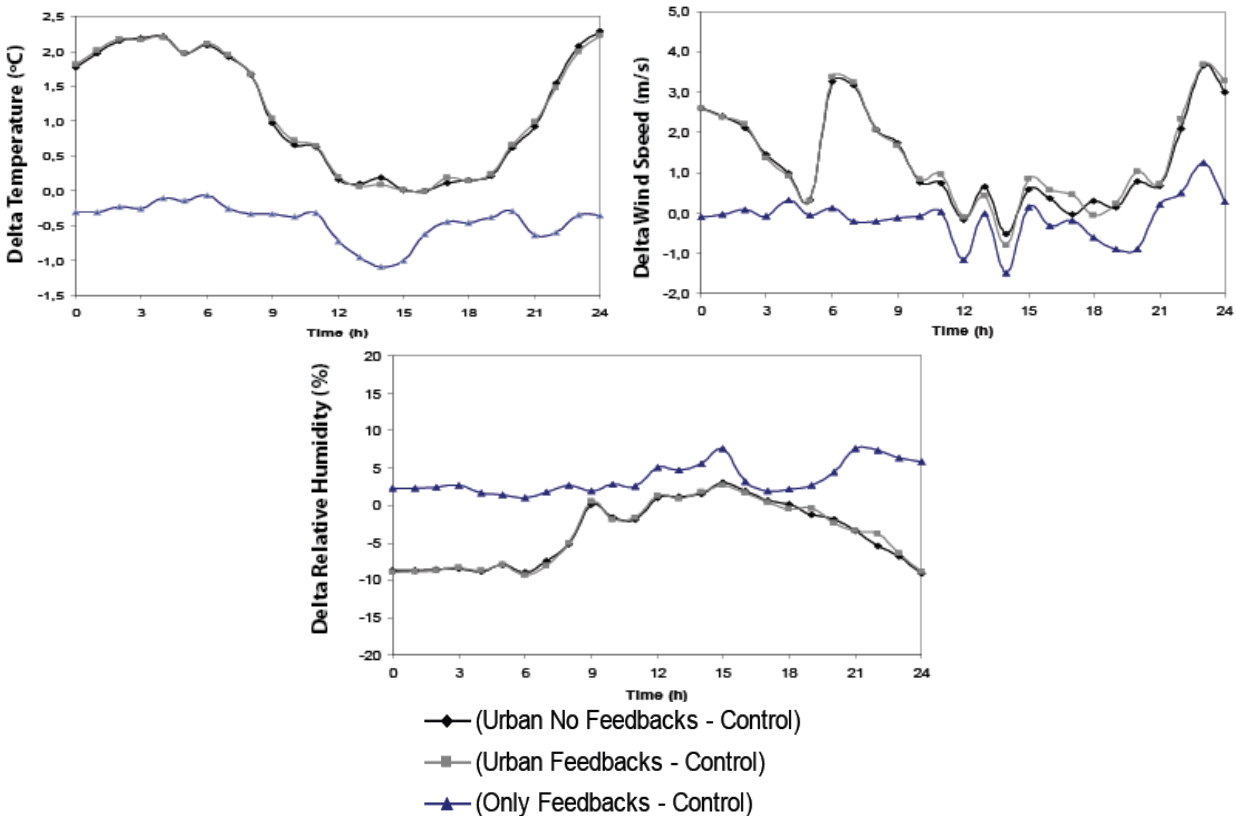

***Figure 46**: Difference plots for modified vs. control runs for (a) the 2 m temperature, (b) the 10 m wind, (c) the 2 m relative humidity on 28th July 2009.*

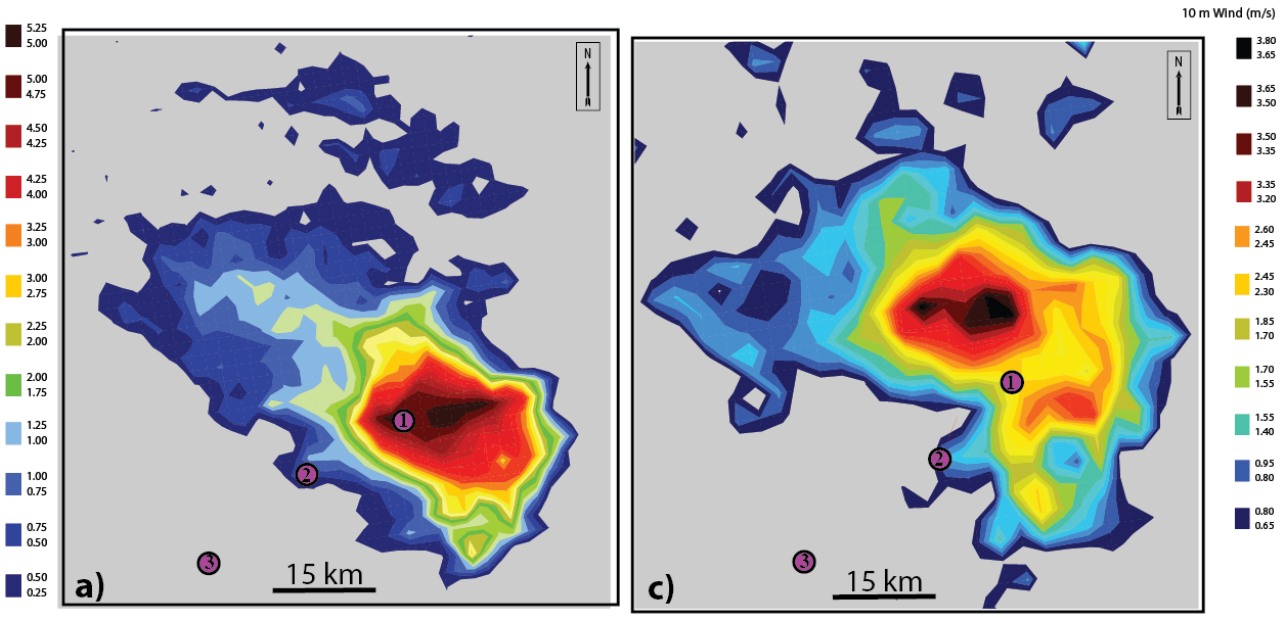

***Figure 47**: Difference plots for the (a) 2 m temperature (ºC) and (c) wind velocity (m/s) at 10 m for Paris metropolitan area between outputs of the urbanized (BEP + AHF) vs. control runs of the Enviro-HIRLAM model on the 21 July 2009 at 6 UTC.*

In the Paris metropolitan area, the wind flowed from South-East, transporting the plume of the UHI to the North-West. At the urban station (1-LHVP), on average, the 2 m temperature anomaly was 2.5 ºC (with a maximum of 2.75 ºC at 6 UTC) and the 10 m wind anomaly was 2.0 m/s (with a

maximum of 3.5 m/s at 6 UTC). However, at the sub-urban station (2-SIRTA), the maximum anomaly 2 m temperature was 0.2 ºC and the 10 m wind was 0.5 m/s. At the rural station (3-CHARTRES) the anomalies were negligible.

11. Application and Evaluation of the Regional CTM PMCAMx over the Paris and Mexico City Megacities

11.1. PMCAMx description

PMCAMx simulates advection, dispersion, gas-phase chemistry, emission, wet/dry deposition, aerosol dynamics and aqueous-phase chemistry of atmospheric compounds (*Gaydos et al., 2007; Karydis et al., 2007*). PMCAMx is the research version of the publicly available CAMx model. We summarize below the improvements of the model that took place during the MEGAPOLI project.

The amount of each inorganic species transferred between gas and aerosol phases is determined in PMCAMx by using the hybrid approach (*Capaldo et al., 2000*) for aerosol thermodynamics along with ISORROPIA II (*Fountoukis and Nenes, 2007*) which is a computationally efficient code that treats the thermodynamics of K^+-Ca^{2+}-Mg^{2+}-NH_4^+ -Na^+-SO_4^{2-}-NO_3^- -Cl^--H_2O aerosol systems. This should be contrasted with the bulk equilibrium approach and the ISORROPIA code use in the previous version (*Karydis et al., 2007*). According to the hybrid method, the aerosol particles with diameters less than the threshold diameter (1 μm for the purposes of this study) are simulated assuming equilibrium while for the particles larger than the threshold diameter the improved MADM model of *Pilinis et al. (2000),* as extended by *Gaydos et al. (2003),* is used, which ensures a stable solution, regardless if the particles are completely dry, with an aqueous phase or transition between acidic and neutral conditions.

For the organic aerosol components (OA) following *Tsimpidi et al. (2010),* a volatility distribution is applied to the emitted POA species with ten simulated volatility bins, ranging from 0 to 10^6 μg m^{-3} saturation concentration (all effective saturation concentrations in the VBS are at 298 K). This simulation also includes emissions of intermediate volatility organic compounds (IVOCs), which are distributed among the 10^4, 10^5, and 10^6 μg m^{-3} saturation concentration bins with emissions rates equal to 0.2, 0.5, and 0.8 times the original non-volatile POA emission rate, respectively. The gas-phase chemical mechanism in use, SAPRC-99, includes 77 gas-phase species (not including the gas- and particulate-phase organic species added for this study) and 217 reactions *(Carter, 2000).* SOA is split between aerosol formed from the condensation of the oxidation products of the volatile organic compounds (V-SOA), intermediate volatile organic compounds (I-SOA), and semi-

volatile organic compounds (S-SOA). The V-SOA is simulated with 4 volatility bins (1, 10, 100, 1000 μg m^{-3}), and 10 size bins (diameters range from 0.04 to 40 μm). I-SOA and S-SOA are described with 10 volatility bins (0 and 10^{-2}-10^{6} μg m^{-3}) and 10 size bins. The V-SOA yields used in PMCAMx-2008 are based on the NO_x-dependent stoichiometric yields of *Lane et al. (2008a)*. The corresponding parameters affecting V-SOA partitioning and removal processes, including effective Henry's law constants, molecular weights and enthalpies of vaporization, are taken from *Lane et al. (2008b)*. Those parameters for the S-SOA and I-SOA are obtained from *Shrivastava et al. (2008)*. Further gas-phase oxidation of SOA vapors (chemical aging) is modeled using a second-order reaction with hydroxyl radicals. To express the decrease of volatility with aging, products of this reaction are shifted down one volatility bin (factor of 10 reduction in effective saturation concentration). The base-case simulation ages S-SOA, I-SOA and V-SOA from anthropogenic sources using a rate constant k(298 K) = $40x10^{-12}$ cm^3 $molec^{-1}$ s^{-1} for S-SOA and I-SOA and k(298 K) = $40x10^{-12}$ cm^3 $molec^{-1}$ s^{-1} for V-SOA. No biogenic SOA aging is simulated based on both the available laboratory studies (*Ng et al., 2006; Presto et al., 2006*) and the results of *Lane et al. (2008b)*. Overall, the model, apart from the fresh primary organic aerosols (POA), simulates three types of oxygenated organic aerosols based on the initial volatility of the corresponding precursor compounds: S-SOA ($C^* \leq 10^2$ μg m^{-3}), I-SOA ($10^3 \leq C^* \leq 10^6$ μg m^{-3}), and V-SOA ($C^* > 10^6$ μg m^{-3}). A more comprehensive description of the organic aerosol module used by PMCAMx-2008 can be found in *Tsimpidi et al. (2010), Lane et al. (2008a, b) and Shrivastava et al. (2008)*.

11.2. Model application to Mexico City

PMCAMx was used to simulate air quality in the Mexico City Metropolitan Area (MCMA) during March of 2006 (MILAGRO study period). The first three days of each simulation have been excluded in order to limit the effect the initial conditions have on the results. The concentrations of the aerosol components at the boundaries of the domain were chosen based on results of the GISS-II' global CTM (*Racherla et al., 2006*) for the month of March. The modelling domain covers a 210x210x6 km region centered in the MCMA with 3x3 km grid resolution and fifteen vertical layers extending to 6 km. Inputs to the model include horizontal wind components, temperature, pressure, water vapor, vertical diffusivity, clouds, and rainfall, all computed offline by the MM5 meteorological model (*Grell et al., 1995*).

The emission inventory used is based on the MCMA 2004 official emission inventory (CAM, 2006) with improved dust and sodium chloride emissions, as well as new HONO emissions. The improved dust emissions are the only emissions which are different for each day of simulation and they were calculated based on the algorithm of *Draxler et al. (2001)*. The dust chemical composi-

tion including the levels of sodium, calcium, potassium, and magnesium cations, which are the reactive dust components, are determined based on the geological materials that produce fugitive dust emissions. Fugitive dust emitters in and around MCMA are considered to be unpaved and paved roads, agricultural soil, dried lake, asphalt, cement plants, landfill, gravel, and tezontle soil. The emission inventory has also been updated in order to include the anthropogenic emissions from the refineries, power plants and chemical companies in the Tula area located north of Mexico City and the biogenic emissions emitted from the forests northeast of the model domain. In order to account for partitioning of *primary organic emissions, the emission inventory was modified following the recommendations of Tsimpidi et al. (2010).* Table 1 shows the amount of the emitted organic material within the limits of the modelling domain. Anthropogenic and biogenic VOC emissions serve as anthropogenic and biogenic V-SOA precursors respectively. Nonvolatile ($C^* \leq 10^{-1}$ μg m^{-3}) organic compounds are in the aerosol phase and treated as POA emissions. Semivolatile (SVOC; $10 \leq C^* \leq 10^2$ μg m^{-3}) primary organic emissions partition between the aerosol and the gas phase. The material that remains in the aerosol phase and did not undergo chemical reactions during its atmospheric lifetime is fresh POA while the gas phase material is considered as S-SOA precursor. Finally, intermediate-volatility (IVOC; 10^3 μg $m^{-3} \leq C^* \leq 10^6$ μg m^{-3}) organic compounds exist largely in the gas phase at typical atmospheric conditions and are important I-SOA precursors as their oxidation can produce compounds with lower vapour pressures.

Table 1: *Organic compound emission rates in the Mexico City Metropolitan Area (MEGAPOLI Inventory) for March 2006.*

Organic compound	**Emission rate (tons d^{-1})**
Anthropogenic VOCs	2572
Biogenic VOCs	954
Intermediate volatile compounds	217
Semi-volatile compounds	35
Nonvolatile compounds	20

11.3. Overview of PMCAMx predictions for Mexico City

The predicted average ground-level concentrations of PM_1 sulfate, nitrate, ammonium, and chloride over the period of March 2006 are shown in Figure 1. The highest predicted sulfate concentrations are over the Tula vicinity (over 25 μg m^{-3}), coming from the large SO_2 sources from the industrial complexes in the area. In the center of Mexico City, there are no major SO_2 sources, and sulfate concentrations are lower (up to 5 μg m^{-3}). Nitrate is enhanced significantly in the urban area and immediate outflow (up to 3 μg m^{-3}), mostly produced from local photochemistry, indicating a strong urban source. Nitrate decreases with distance from the city, due to evaporation and deposition (of

HNO_3 vapor), remaining in low levels in the surroundings (lower than 1 μg m^{-3}). Ammonium concentrations peak at the center of Mexico City (2 μg m^{-3}) and the Tula vicinity (2.5 μg m^{-3}) existing mainly in the form of ammonium nitrate and ammonium sulfate respectively. Predicted PM_1 chloride concentrations are generally low (less than 0.5 μg m^{-3} in the entire model domain) with the highest values in the Texcoco dry Lake and the south area of the domain.

The results for the coarse (PM_{1-10}) sulfate, nitrate, ammonium, chloride, sodium, calcium, potassium, and magnesium are shown in Figure 2. The Texcoco dry lake is a significant source of potassium (1 μg m^{-3}), magnesium (1 μg m^{-3}), sodium (2 μg m^{-3}), and calcium (3 μg m^{-3}). Coarse calcium concentrations peak around Tolteca (7 μg m^{-3}), which is located around 70 km north of the Mexico City, due to the cement industries in the area. ISORROPIA II along with the hybrid approach assist in simulating the formation of PM_{1-10} nitrate and chloride describing interactions between these anions and the cations of mineral dust. The presence of calcium coming from the Tolteca vicinity as well as the rest of the mineral cations from the Texcoco Lake resulted in the formation of a significant amount of aerosol nitrate in the coarse mode with concentrations up to 3 μg m^{-3}. PM_{1-10} chloride is also high and its concentration exceeds 2 μg m^{-3} in Texcoco Lake. There is also a little ammonium in the coarse mode (less than 0.5 μg m^{-3}), because the coarse dust particles are alkaline. The soluble crustal elements increase the PM water content and thus favor the ammonium nitrate formation.

The predicted average ground-level concentration of PM_1 organic mass over the period of March 2006 is shown in Figure 3a. The organic mass peak values (approximately 20 μg m^{-3}) are in the center of Mexico City and in the Tula industrial area. The predicted organic mass concentration is the sum of the predicted concentration of primary organic aerosols which have been emitted in the atmosphere as particles (fresh POA) (Figure 3b) and the predicted concentrations of the oxygenated organic aerosol (Figure 3c) that has been created in the atmosphere through chemical reactions and corresponds to the sum of PMCAMx-2008 S-SOA, I-SOA, and V-SOA. The primary organic aerosol concentration is high in the center of Mexico City and in Tula, while it decreases rapidly from its sources mainly due to dilution and evaporation. As an example in the T0 urban site the predicted average fresh primary organic concentration is 4.4 μg m^{-3} while in the T1 suburban site it decreases to 1.2 μg m^{-3} and in the T2 rural site is lower than 1 μg m^{-3}. On the contrary, the predicted oxygenated organic aerosol concentration has a relatively more uniform spatial distribution with high values in the entire domain (Figure 3c). The highest values are predicted in the center of Mexico City (up to 7.5 μg m^{-3}), coming mainly from anthropogenic sources, and in the northeast corner of the domain, mainly from biogenic sources. In the suburban and rural areas, such as T1 and T2, the predicted oxygenated OA is also high, with concentrations around 6 μg m^{-3}. Anthropogenic V-SOA, I-SOA, and S-SOA, are predicted to be more photochemically processed and less volatile

downwind of the Mexico City center. In particular at T0 OA consists of 60% POA and 40% OOA. At T1 and T2, POA corresponds to 40% and 15% of total OA respectively.

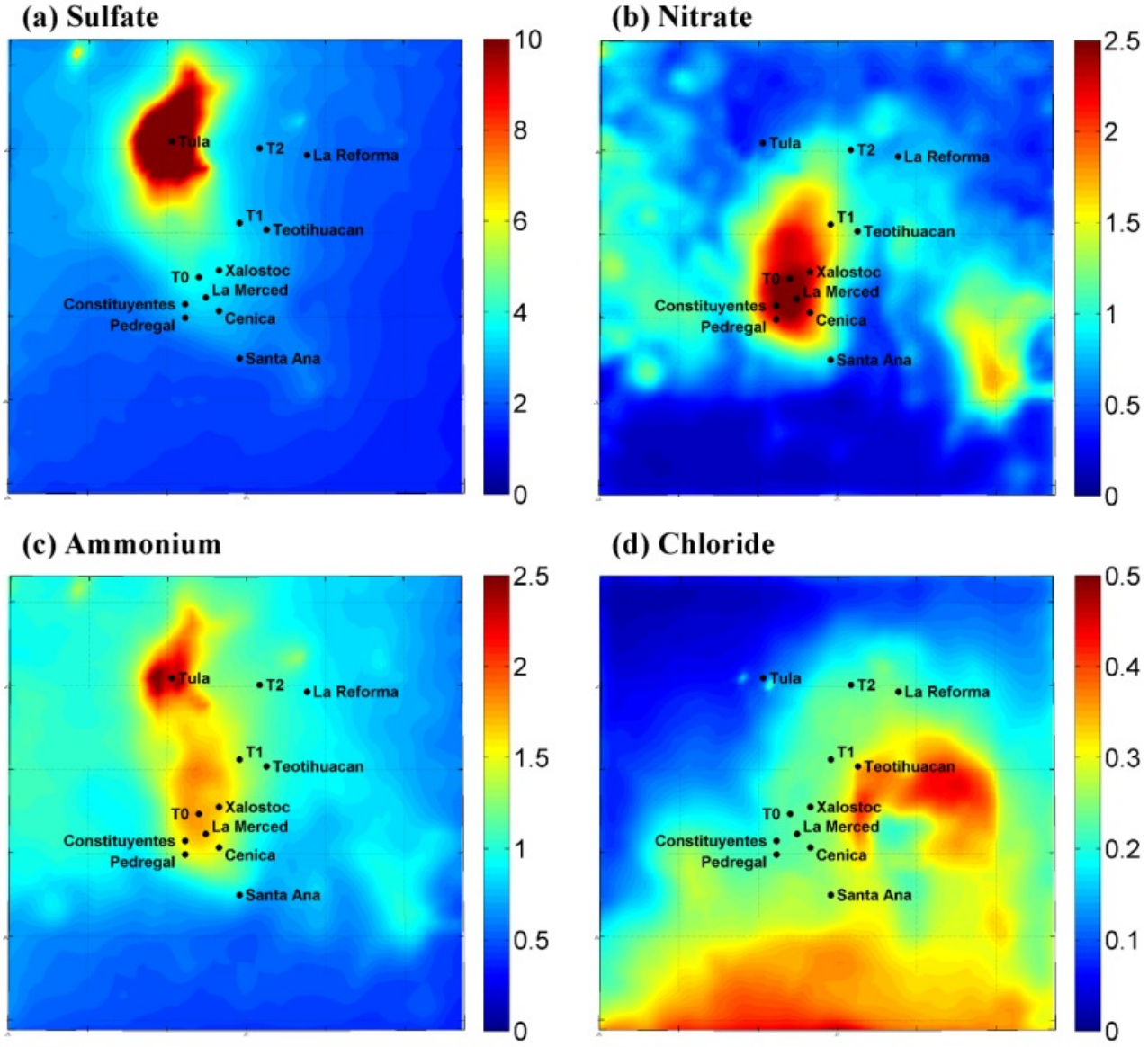

Figure 1: *Predicted average ground level concentrations of PM_1 (a) sulfate, (b) nitrate, (c) ammonium, and (d) chloride during 4-30 March 2006 in Mexico City.*

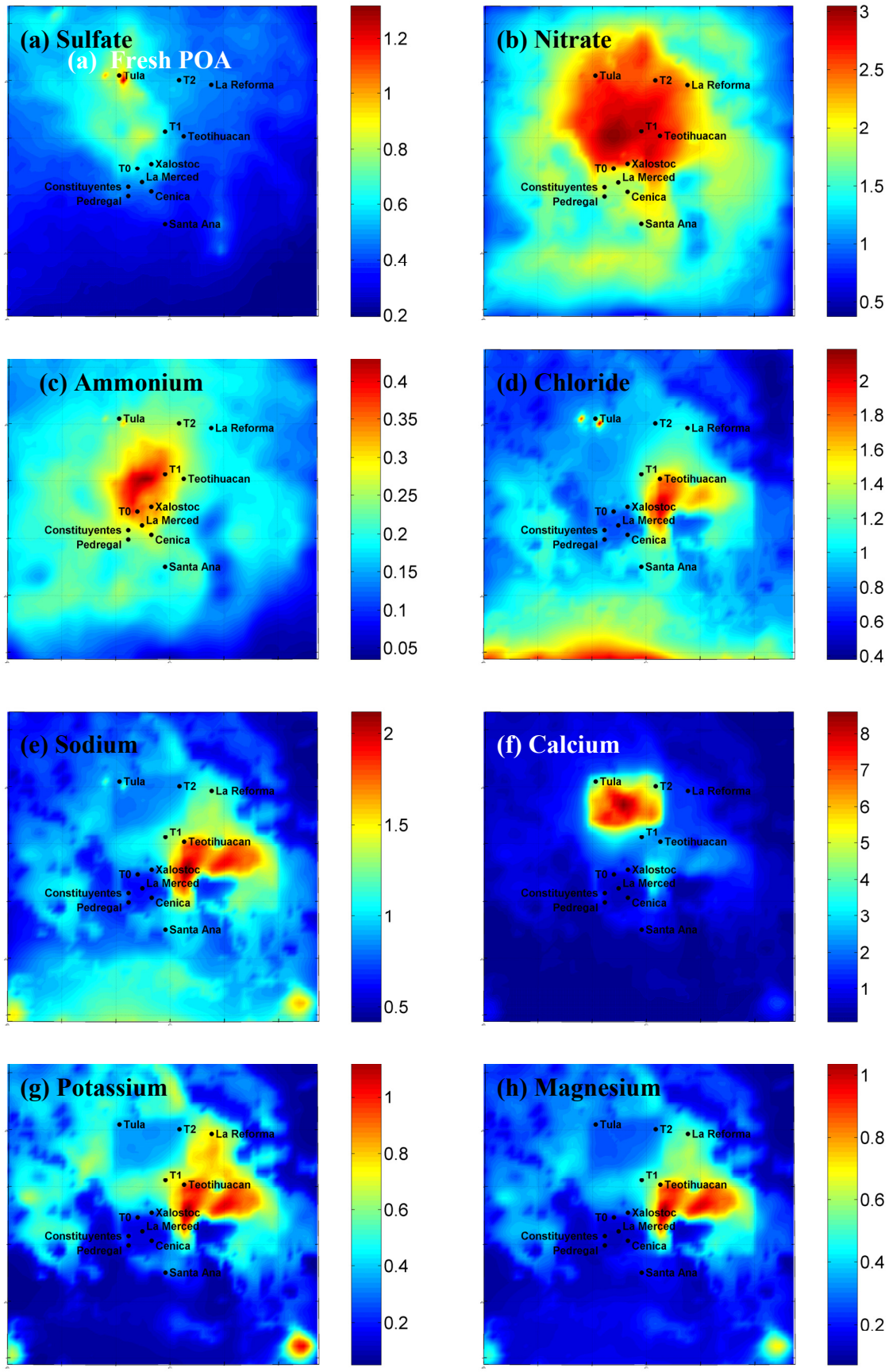

Figure 2: *Predicted average ground level concentrations of PM_{1-10} (a) sulfate, (b) nitrate, (c) ammonium, (d) chloride, (e) sodium, (f) calcium, (g) potassium, and (h) magnesium ($\mu g\ m^{-3}$) during 4-30 March 2006 in Mexico City.*

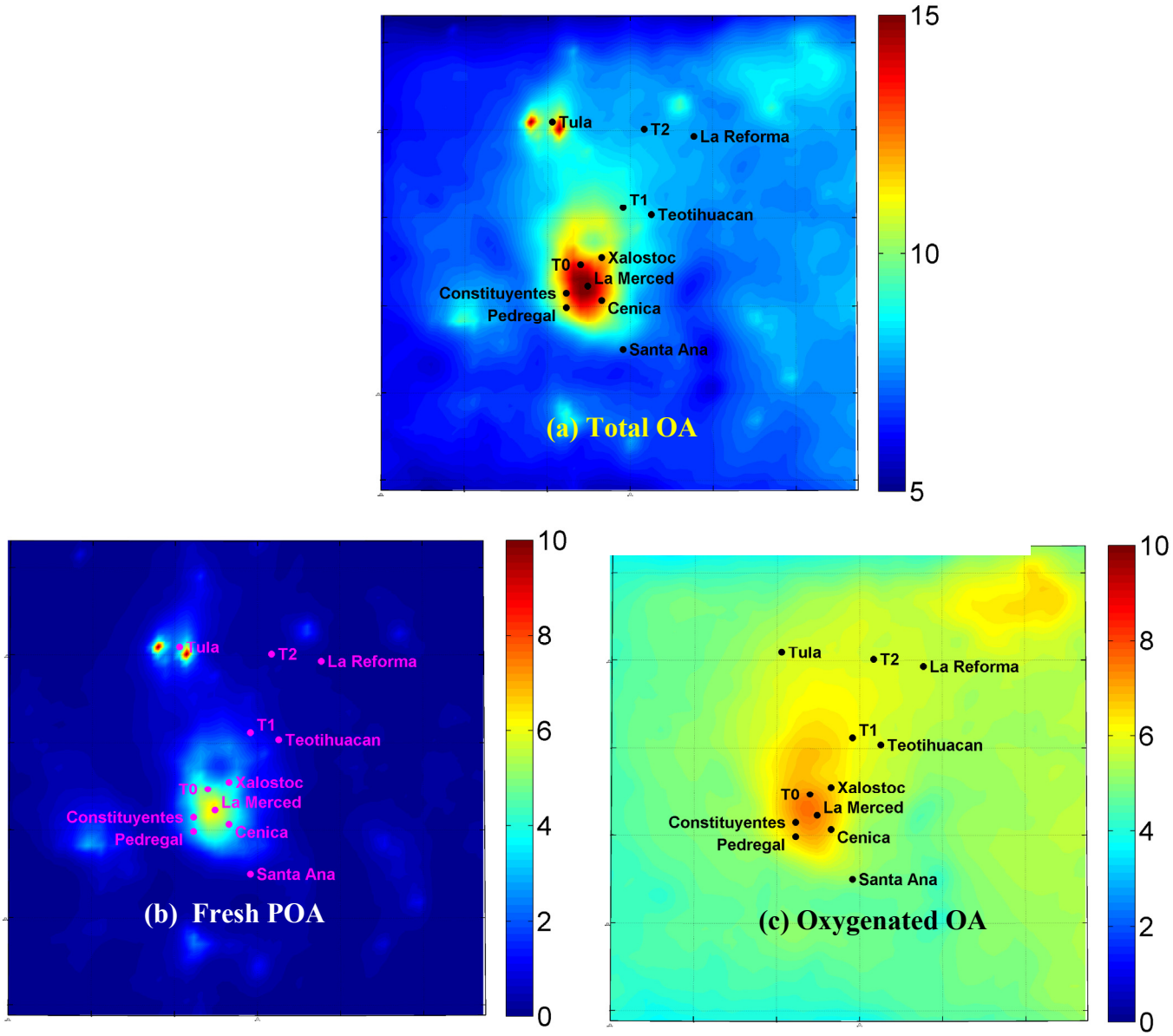

Figure 3: *Predicted average ground level concentrations of (a) PM_1 organic mass (μg m^{-3})* ***(b)*** *primary and* ***(b)*** *oxygenated organic aerosol concentrations (μg m^{-3}) in the Mexico City area during March 4^{th}-30^{th} of 2006.*

11.4. PMCAMx Evaluation in Mexico City for inorganic PM

The model predictions for PM_1 sulfate, nitrate, ammonium, and chloride were compared with measurements obtained during the MILAGRO field campaign at the T0 and T1 measurement sites (Aiken et al., 2009). The T0 monitoring station was located in the north-western part of the basin of Mexico City. It is an urban background site influenced by road traffic fresh emissions (300 m from four major roads surrounding it), domestic and residential emissions, but also potentially influenced by local industrial emissions and from the Tula industrial area (around 60 km to the north-

northwest). The model predictions for $PM_{2.5}$ sulfate, nitrate, ammonium, chloride, sodium, calcium, and magnesium were also compared with measurements that took place at T1 (Fountoukis et al., 2009). This is a suburban background site located around 50 km to the north of Mexico City, in an area isolated from major urban agglomerations but close to small populated agglomerations, and around 500 m from the closest road. The results of the comparison between the model predictions and the measurements are depicted in Figures 4-8.

Sulfate: The performance of the model for sulfate is encouraging in both T0 and T1 sites (Figure 4). In T0 the average predicted concentration is 3.7 μg m^{-3} while the observed average was 3.5 μg m^{-3}. Both the model and the measurements show little variability in the average diurnal sulphate concentration profile. In T1 the measured sulfate concentration was variable with concentration spikes up to 15 μg m^{-3} as the location of this station is closer to the Tula vicinity which is the major source of sulfate. The model does reproduce this behaviour even some of the spikes are not at the right times. This discrepancy between the measured and the predicted profiles is partially due to the use of the same emission inventory for SO_2 for every day. Errors in the meteorology were also identified as a major cause of some of the discrepancies between model predictions and measurements. For instance, during the 18th of March the model underpredicts sulfate in both measurement sites (Figures 4a, 4c). According to the measurements, the sulfate produced in Tula during the early morning of 18th was transported to the southeast and appeared in T1 (20 μg m^{-3}) and then in T0 (15 μg m^{-3}) at noon of the same day. On the other hand, there was not any peak in the predicted sulfate concentrations in T1 and T0 indicating potential problems during this period in the wind field used as input in PMCAMx-2008. The predicted average $PM_{2.5}$ sulfate concentration in T1 is 3.3 μg m^{-3} while the measured average is 4.4 μg m^{-3}.

Nitrate: Both PMCAMx-2008 and measurements suggest that nitrate peaks during noon at T0 (Figure 5a) and a couple of hours later at T1 with a lower concentration (Figure 5c). During nighttime, predicted nitrate remains low (a few μg m^{-3}) in both sites, which is consistent with the measurements. During noon, there are several high nitrate concentration (above 10 μg m^{-3}) measurement

periods in the dataset during which the model tends to underpredict the nitrate levels. Comparisons of the predicted and measured diurnal nitrate profiles at T0 (Figure 5b) suggest that the model underpredicts nitrate during noon as the predicted formation of nitrate during the early morning hours is not as rapid as the observations. This discrepancy is not the result of errors in the partitioning of the available nitric acid (Fountoukis et al., 2007) but to an underprediction of the total nitric acid. This is probably due to the predicted OH levels as they are slightly underestimated during early morning even though they are reasonably reproduced by the model during the rest of the day (not shown). Therefore the formation of HNO_3 during the day from the reaction of NO_2 with OH is limited in the model resulting eventually in an underprediction of the aerosol nitrate. Tsimpidi et al. (2010b) have shown that the HONO production is quite important for the production of OH into the early morning atmosphere in the MCMA, suggesting that a more accurate description of HONO sources is needed. The average predicted concentrations are 2.6 μg m^{-3} and 3.3 μg m^{-3} in T0 and T1 sites respectively while the observed averages were 3.5 μg m^{-3} and 3.2 μg m^{-3} respectively.

Ammonium: The ammonium predictions are quite sensitive to the ammonia emissions inventory, the predicted sulfate concentrations and the nitrate levels. The performance of the model is respectable in both sites (Figure 6) but it underpredicts ammonium concentrations during midday in T0 (Figure 6b), due to the underprediction in total nitric acid. In T0 the average predicted concentration is 1.7 μg m^{-3} while the observed average was 2.1 μg m^{-3}. Some of the difficulty in reproducing the hourly fluctuations of ammonium at T1 (Figure 6c) is due to the sulfate predictions as part of the ammonium in T1 exists in the aerosol phase in the form of ammonium sulfate. The predicted average $PM_{2.5}$ ammonium concentration in T1 is 1.3 μg m^{-3} while the measured average is 1.1 μg m^{-3}.

Chloride: Both observations and predictions suggest that chloride concentrations remain at low levels (up to 0.5 μg m^{-3}) most of the time in both the T0 and T1 sites (Figure 7). Nevertheless, there are some measured major spikes at T0 site during the morning rush hours that the model is unable to reproduce (Figure 7a). These spikes were observed mostly in the last week of the campaign.

Given that the model uses the same HCl emissions for every week day, it should be investigated if these emissions were, for some reason, higher during this week. During this period there is a clear decrease in the number of fires due to higher precipitation and humidity (Fast et al., 2007). Surprisingly enough, measured chloride is higher during this low fire period, which indicates that despite the source of chloride during fires (*DeCarlo et al., 2008*), urban sources and/or favourable partitioning conditions may be more important for this specie in the MCMA. Comparisons of the predicted and measured diurnal profiles at T0 (Figure 7b) suggest that the model underpredicts chloride. The average predicted concentration is 0.25 μg m^{-3} while the observed average was 0.35 μg m^{-3}. Given that the AMS measures only non refractory chloride, the model underprediction of the ambient chloride concentration is probably greater. Aiken et al. (2009) suggest that approximately two thirds of the chloride is due to NH_4Cl or species of similarly high volatility, while the rest may be due to more refractory species such as $PbCl_2$ that are not simulated by the model. In T1, the predicted average $PM_{2.5}$ chloride concentration is 0.3 μg m^{-3} while the measured average is 0.4 μg m^{-3}.

Dust components: Measurements of $PM_{2.5}$ sodium, calcium, and magnesium were only available at T1. PMCAMx-2008 shows on average a reasonable performance for these three dust components (Figure 8). However, there is a tendency towards overprediction, especially for calcium (Figure 8b), indicating a possible overestimation of the dust emissions that PMCAMx-2008 uses and probably errors in the contributions of the individual dust components or their size distribution. The predicted peaks appeared at T1 for sodium, calcium, and magnesium are in the range of 1 μg m^{-3}, 10 μg m^{-3}, and 0.5 μg m^{-3} respectively, while the measured peaks are in the range of range of 0.5 μg m^{-3} for sodium, 3 μg m^{-3} for calcium, and 0.3 μg m^{-3} for magnesium. Despite the above weakness, the model captures relative well not only the daily average concentrations of the dust components, but also their average diurnal variation, as both the predicted and the measured profiles are flat with almost constant concentration. The daily average predicted concentrations of $PM_{2.5}$ sodium, calcium, and magnesium at T1 are 0.4 μg m^{-3}, 1 μg m^{-3}, and 0.15 μg m^{-3} respectively, while the average measured concentrations of the same species are 0.3 μg m^{-3}, 0.7 μg m^{-3} and 0.15 μg m^{-3} respectively.

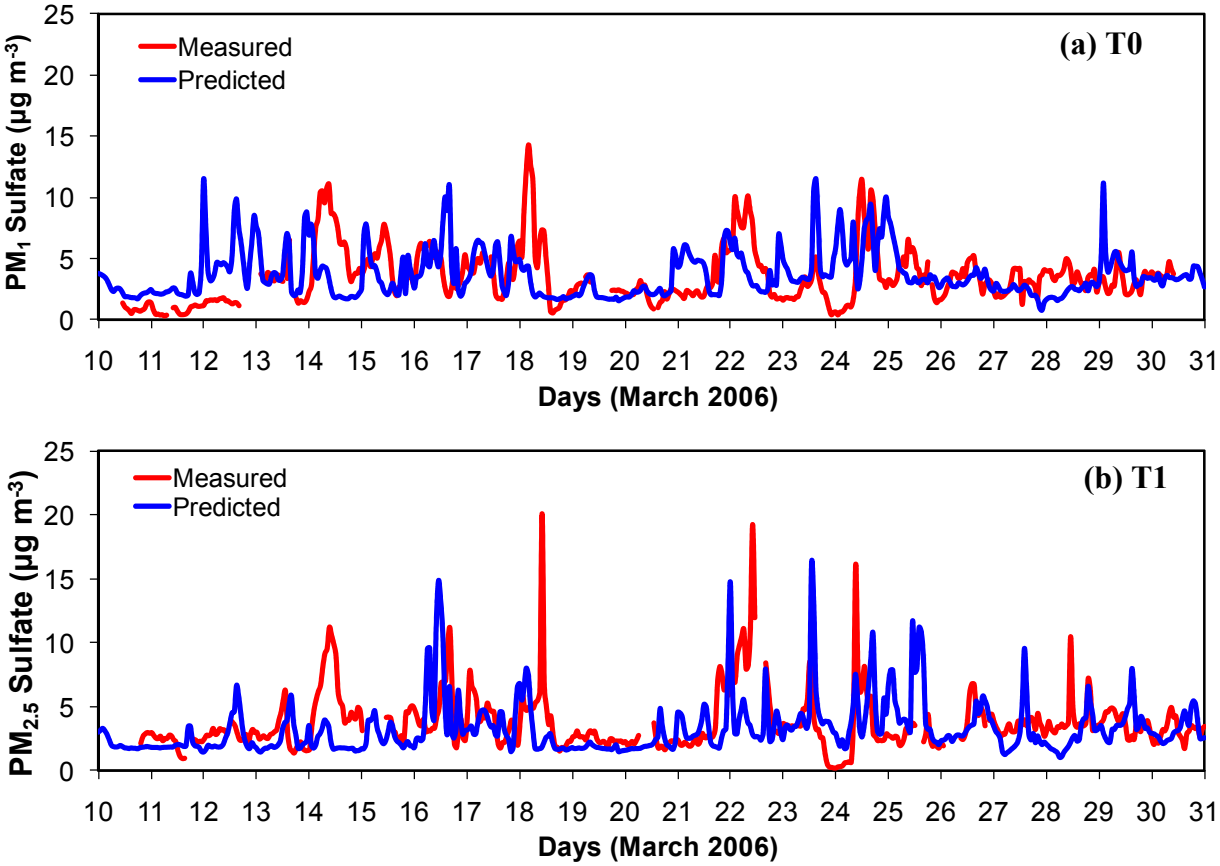

Figure 4: *Comparison of model hourly and diurnal predictions against measurements for PM_1 sulfate taken at T0 (a) and $PM_{2.5}$ sulfate taken at T1 (b), during the MILAGRO campaign.*

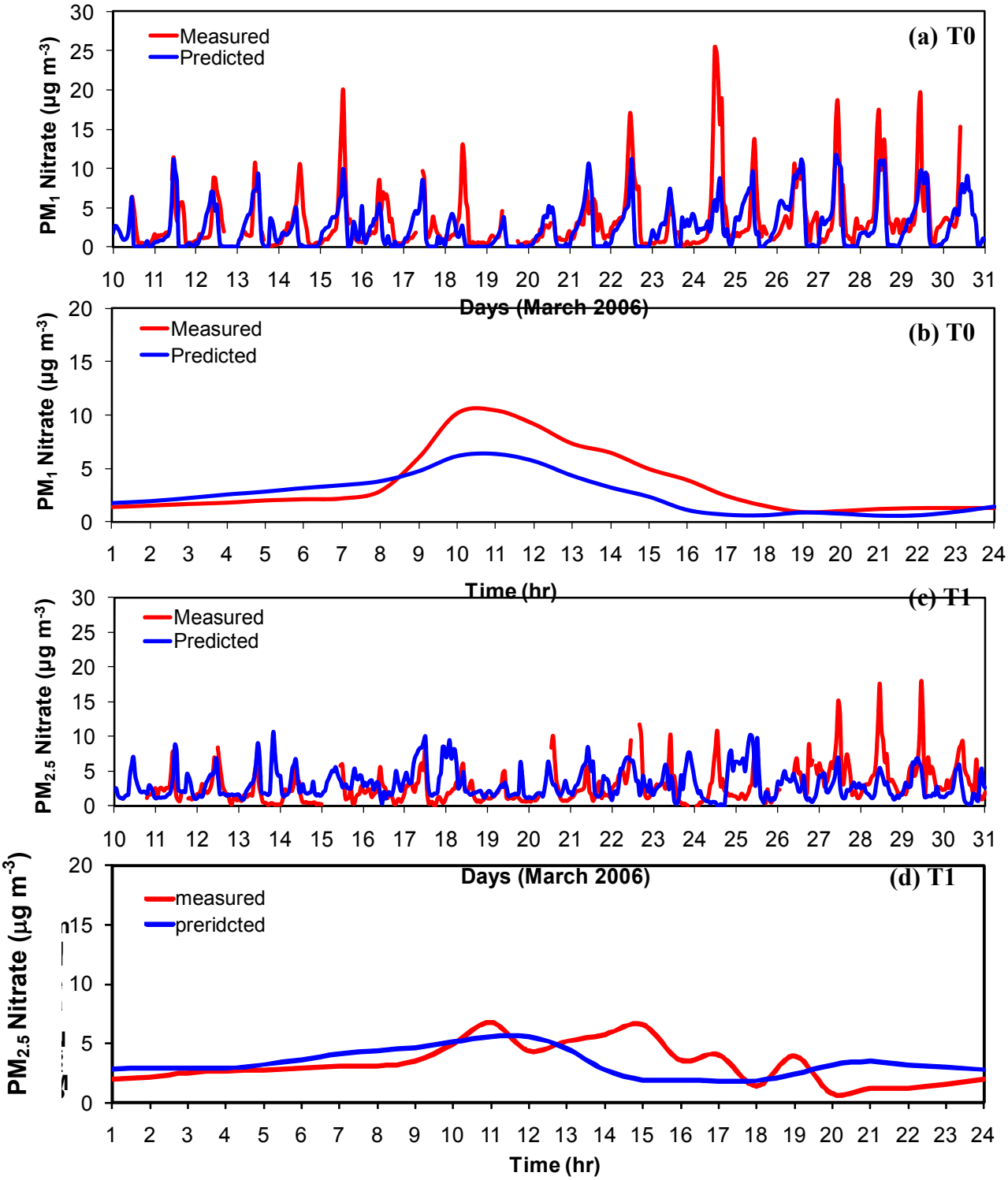

Figure 5: *Comparison of model hourly and diurnal predictions against measurements for PM_1 nitrate taken at T0 (a,b) and $PM_{2.5}$ nitrate taken at T1 (c,d) during the MILAGRO campaign.*

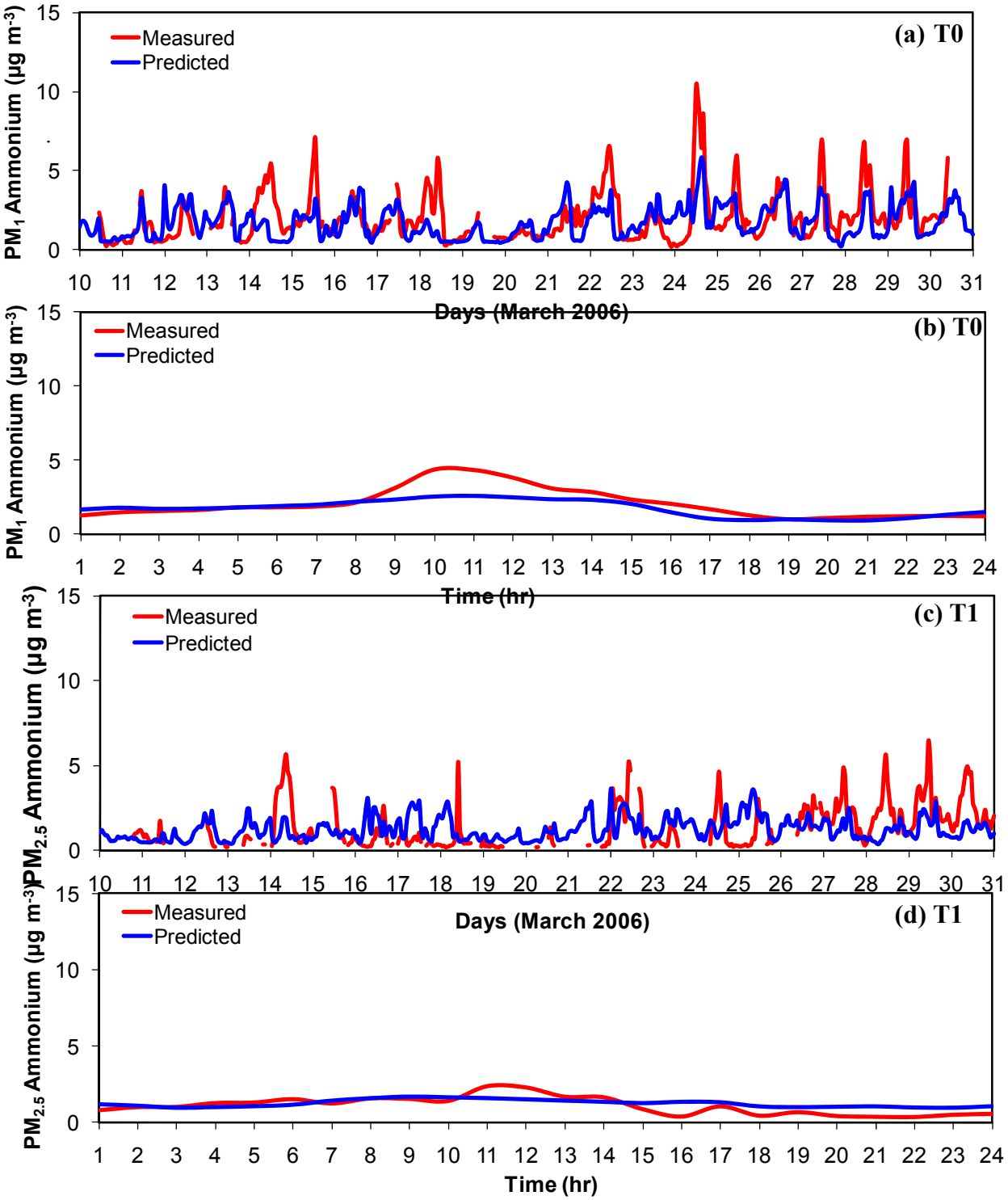

Figure 6: *Comparison of model hourly and diurnal predictions against measurements for PM_1 ammonium taken at T0 (a, b) and $PM_{2.5}$ ammonium taken at T1 (c, d) during the MILAGRO campaign.*

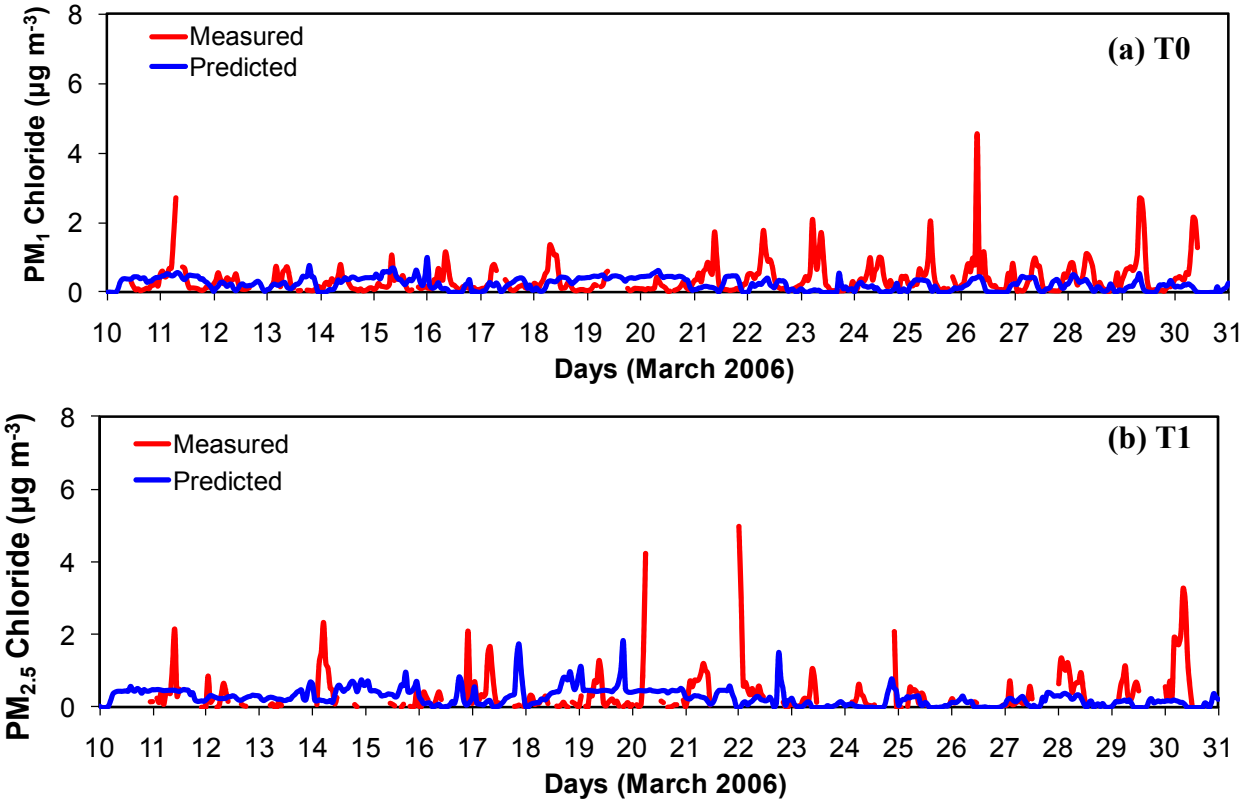

Figure 7: *Comparison of model hourly and diurnal predictions against measurements for PM_1 chloride taken at T0 (a) and $PM_{2.5}$ chloride taken at T1(b) during the MILAGRO campaign.*

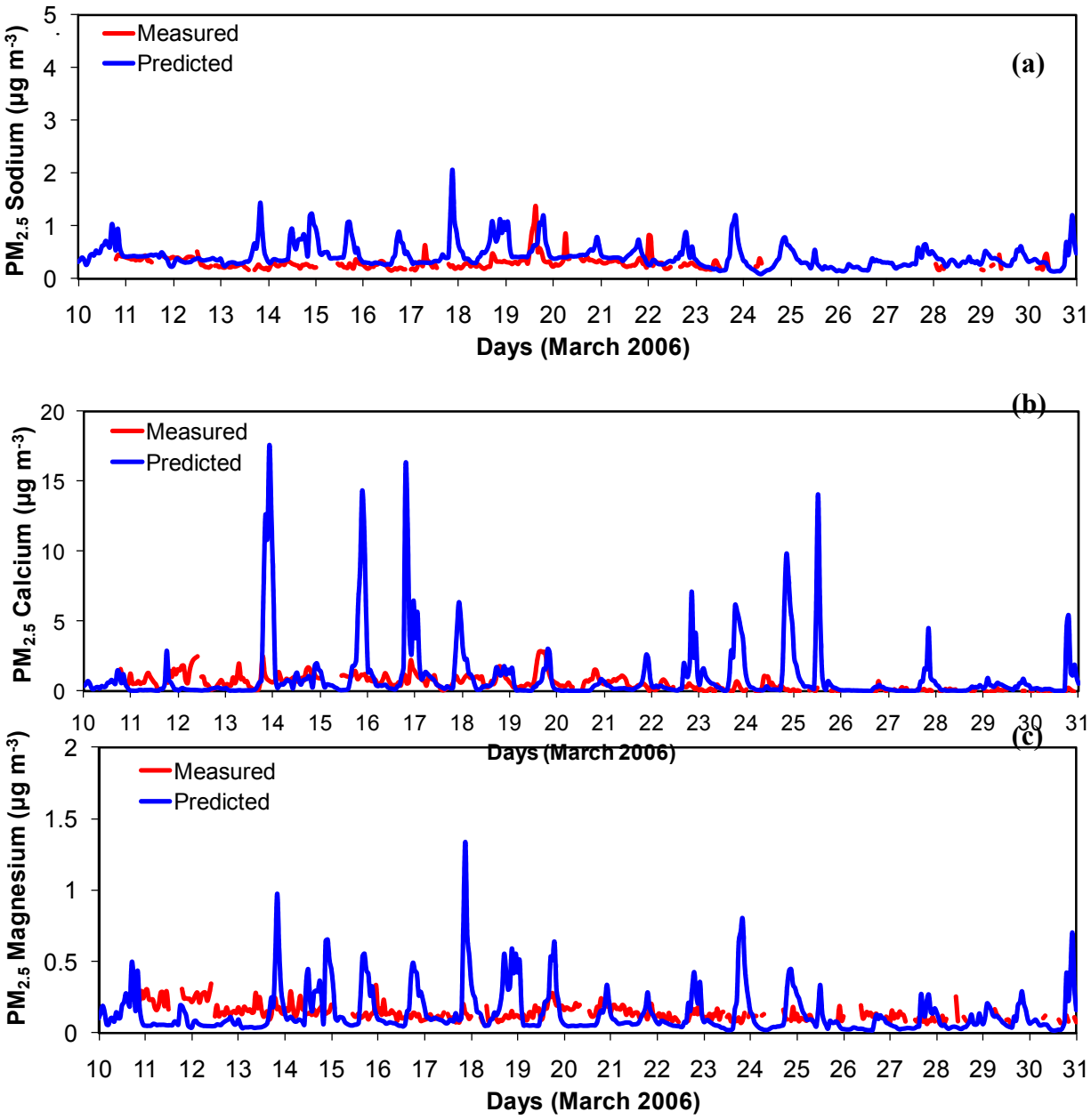

Figure 8: *Comparison of model hourly predictions against measurements for $PM_{2.5}$ (a) sodium, (b) calcium, (c) magnesium taken at T1 during the MILAGRO campaign.*

11.5. PMCAMx Evaluation in Mexico City for Organic PM

The results of the comparison of model predictions with the OA observations are depicted in Figure 9. The model does a reasonable job most of the time reproducing the observations in the T0 site, which is located in the urban center of Mexico City (Figure 9a). Nevertheless, the model is missing a few major spikes which appear early in the morning such as during the 11th, 18th, and 21st of the

month and are associated with biomass burning events (Aiken et al., 2009). Therefore, these under-predictions are related to the emission inventory currently used which does not contain explicitly temporally variable biomass burning emissions. These emissions are provided to the model through the boundary conditions which are time-independent. Both measurements and predictions though, suggest that organic mass has a high variation during the day. Organic mass concentrations are almost always higher than 10 μg m^{-3}, while during morning hours often exceed 25 μg m^{-3}.

In T1, which is a suburban site, the variation of organic mass concentrations is smaller than and not as regular as in the T0 site (Figure 9b). Most of this mass is coming from other areas and therefore depends mostly on the weather conditions. The model is able to reproduce the measured values within a few μg m^{-3} most of the time with concentrations ranging from 7 to 20 μg m^{-3}. Nevertheless PMCAMx-2008 underpredicts the organic mass during the period from the 18th to the 20th of the month. These are the days with the most favorable wind directions for T0-T1-T2 transport (Fast et al., 2007). The analysis of the measurements suggests that the organic mass produced in Mexico City center during the morning of 18th was transported to the north and appeared in T1 during the afternoon of the same day. On the other hand, the predictions in T1 show a reduction in organic mass during that day indicating errors by the meteorological model during this period. Errors in these inputs to PMCAMx result in corresponding problems in its predictions.

In the rural site T2 both the measured and predicted average OA concentrations are approximately 10-20% lower than the corresponding values at T1 (Figure 9c). Given the dilution expected during the transport of Mexico City originating OA between the two sites, this small decrease in OA concentrations is rather surprising. According to PMCAMx it reflects the ongoing generation of OOA and the importance of regional sources in this region. The dynamic range of OA in T2 is less than in T1. Overall, the model behaviour is satisfactory on average but it cannot reproduce the daily variations of organic mass accurately. T2 site is close to the north boundary of the model domain and given that the used boundary conditions are time-independent, the model cannot predict the hourly variations caused from sources north of the T2 site.

The predicted concentrations of biogenic V-SOA were compared against daily average measurement-based estimates of biogenic SOA at T0 and T1 sites (Stone et al., 2009). Overall, the PMCAMx predictions tent to be lower than the Stone et al. (2009) V-SOA estimates in both sites. The simulated biogenic V-SOA concentrations range from 0.1 to 1.1 μg m^{-3} at T0 and from 0.1 to 1.4 μg m^{-3} at T1. The measurement-based estimates range from 0.4 to 1.8 μg m^{-3} at T0 and from 0.4 to 2.2 μg m^{-3} at T1. These results suggest that biogenic SOA levels in the Mexico City region are far from negligible. In particular, the relative contribution of fresh biogenic V-SOA to total OA is predicted to be up to 15% north of Mexico City. The PMCAMx-predicted contribution of fresh biogenic V-SOA to fresh total SOA (sum of V-SOA, I-SOA, and S-SOA) is 20-30% within the city and up to 70% at the surrounding areas.

The predicted and measured diurnal average OA concentration profiles at T0, T1, and T2 sites during MILAGRO are depicted in Figure 10. These averages depend less on the day to day variability of the meteorology and the emissions and more on the major processes affecting the OA concentrations. In all cases, the model predictions are in agreement within experimental error with the measurements. The diurnal profile at the urban site T0 (Figure 10a) has two peaks; the major one during morning, related to the primary emissions, and a second less pronounced peak in the afternoon, mainly due to photochemical processes. The same peaks appear in the diurnal profile of OA at the suburban site T1 (Figure 10b), the levels of which are smaller compared to those in the T0 site. The first peak is related to the local sources while the peak in the afternoon is caused by the OA which was transported there from the urban center and the local photochemistry. Finally, both the measured and the predicted organic mass at the rural site T2 (Figure 10c), increase slightly late in the afternoon mainly due to transport of emissions and also photochemistry. As expected, there is no morning peak, given the absence of local sources in area around and immediately upwind of T2.

The AMS spectra were analyzed with the PMF technique (*Paatero and Tapper, 1994*) as described by *Ulbrich et al. (2009)* and *Aiken et al. (2009)* separating total organic aerosol (OA) into hydrocarbon-like organic aerosol (HOA, a POA surrogate), oxidized organic aerosol (OOA, a

surrogate for SOA) and biomass burning organic aerosol (BBOA) for three locations in Mexico City: T0, T1, and PTP.

This specification allows a more in-depth evaluation of modeled OA components as they have different temporal emission and formation patterns. HOA appears to have the AMS mass spectral fingerprint for primary combustion particles from urban sources, and also includes particles from other relatively reduced sources such as meat cooking and trash (plastic) burning (Mohr et al., 2009). Therefore the AMS fresh HOA can be compared with the PMCAMx-2008 POA which is the fraction of the emissions that is in the aerosol phase without having undergone any chemical reactions (Figure 11). At T0, PMCAMx-2008 successfully reproduces the observed HOA variation characterized by an early morning peak associated with traffic (Figure 11a). Both, the average predicted POA concentration and the AMS-HOA concentration during March 2006 at T0 are close to 4.5 μg m^{-3}. The agreement is still reasonable at T1 where the average POA and AMS-HOA concentrations are approximately 1.3 μg m^{-3}. However the predicted morning POA peaks 2 hours later than observed (Figure 11b). At PTP, larger discrepancies between observed and modeled POA values are found. The average predicted POA concentration during March 2006 is 1.7 μg m^{-3} while the PMF analysis resulted in 2.9 μg m^{-3} HOA during the same periods at PTP. The predicted morning POA peaks 2 hours earlier than observed. The late arrival of the measured pollutants over the elevated PTP site is associated with the growth of the PBL above 900 m (station's altitude). Therefore, this discrepancy suggests potential problems in describing the vertical mixing in the complex terrain around PTP in the early morning hours.

OOA often contains a more volatile and less processed oxygenated OA fraction which shows high correlation with photochemical products such as O_3, O_x, glyoxal, and ammonium nitrate (*Volkamer et al., 2006, 2007; Aiken et al., 2008, Lanz et al., 2007; Ulbrich et al., 2009; Dzepina et al., 2009*). However, a significant fraction of the OOA consists of more oxygenated organics (*Aiken et al., 2008*) which are assumed here to have initially formed far from Mexico City. Therefore, the AMS OOA is compared with the sum of the PMCAMx-2008 S-SOA, I-SOA,

V-SOA, and transported oxygenated OA. Figure 12 presents the comparison of average diurnal profiles of predicted oxygenated organic components and the PMF-estimated OOA at the 3 locations, T0, T1 and PTP. The shape of the OOA diurnal profile features a strong enhancement in concentrations during the morning associated with an active photochemical production of oxygenated organic aerosols close to the emissions (i.e. T0, PTP). The diurnal variability is less pronounced at the peripheral T1 station and displays a more gradual increase of concentrations during the day. Figure 12 confirms that the predicted oxygenated organic aerosol values and their associated variability range are in reasonable agreement with the observed ones. Both predicted and observed OOA levels gradually decrease downwind of the city with monthly average concentrations ranging from 7.5 μg m^{-3} at T0 respectively to 6.3 μg m^{-3} and 4.6 μg m^{-3} at T1 respectively. At T0 and PTP the predicted formation of OOA during the early morning hours is not as rapid as the PMF estimates. This discrepancy can be partially attributed on the predicted OH levels as they are slightly underestimated during early morning even though they are reasonably reproduced by the model during the rest of the day (not shown). A sensitivity study to the HONO emissions used by the model suggests that the HONO production and emissions are relatively important for the production of OH and SOA in the early morning. The comparison at T1 and PTP suggests a model tendency to overpredict OOA concentration during early afternoon. At PTP the average monthly predicted OOA concentration is 6.6 μg m^{-3} while the PMF analysis resulted in 5.9 μg m^{-3} OOA on average during the same period.

Overall, the predicted chemical composition of OA is generally consistent with the PMF analysis. However, PMCAMx-2008 tends to predict high oxygenated OA. Given that the AMS PMF results are also subject to error this comparison of the predictions of these two methods is quite encouraging. Future simulations though, should use a larger domain along with an accurate biomass burning emission inventory in order to increase the precision not only of the estimated BBOA but also of the SOA produced from fire emitted VOCs, I-VOCs, and S-VOCs.

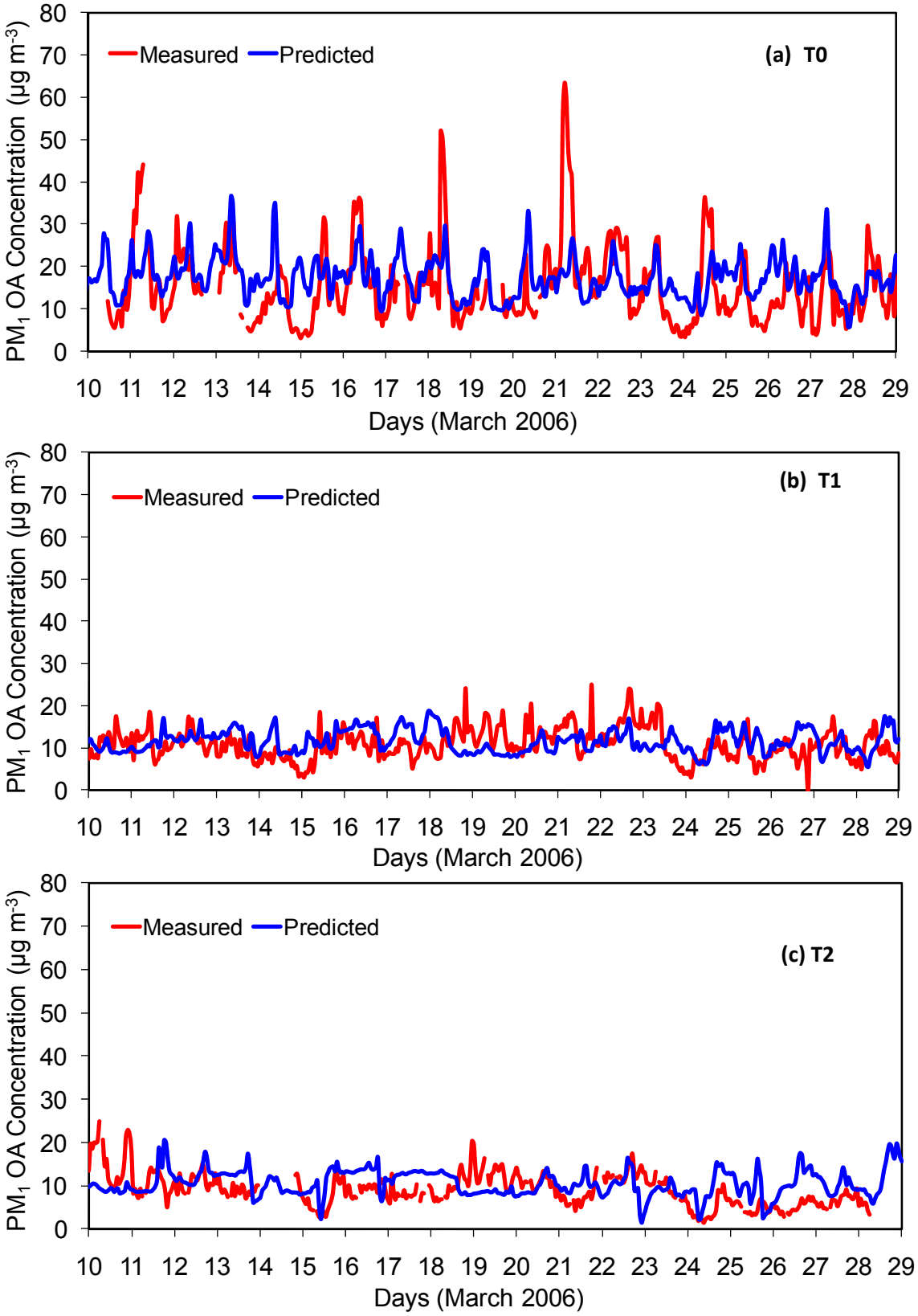

Figure 9: *Comparison of model predictions with hourly measurements for total PM_1 organic mass concentration taken during the MILAGRO campaign in March 2006 at a) T0 (urban site), b) T1 (suburban site), and c) T2 (rural site) on ground level.*

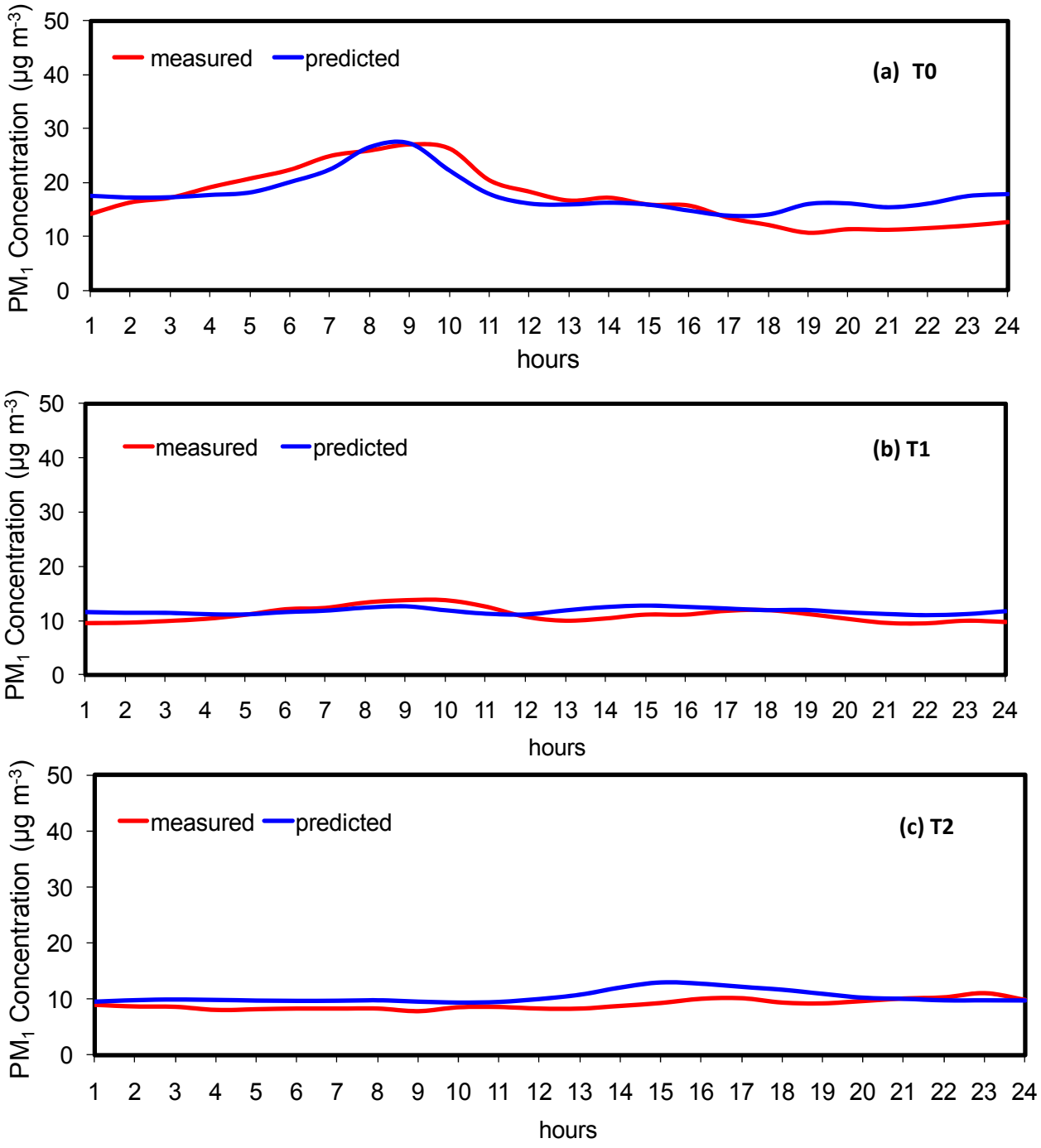

Figure 10: *Comparison of model diurnal predictions with hourly measurements for total PM_1 organic aerosols against measurements taken during the MILAGRO campaign in March 2006 at a) T0 (urban site), b) T1 (suburban site), and c) T2 (rural site) on ground level.*

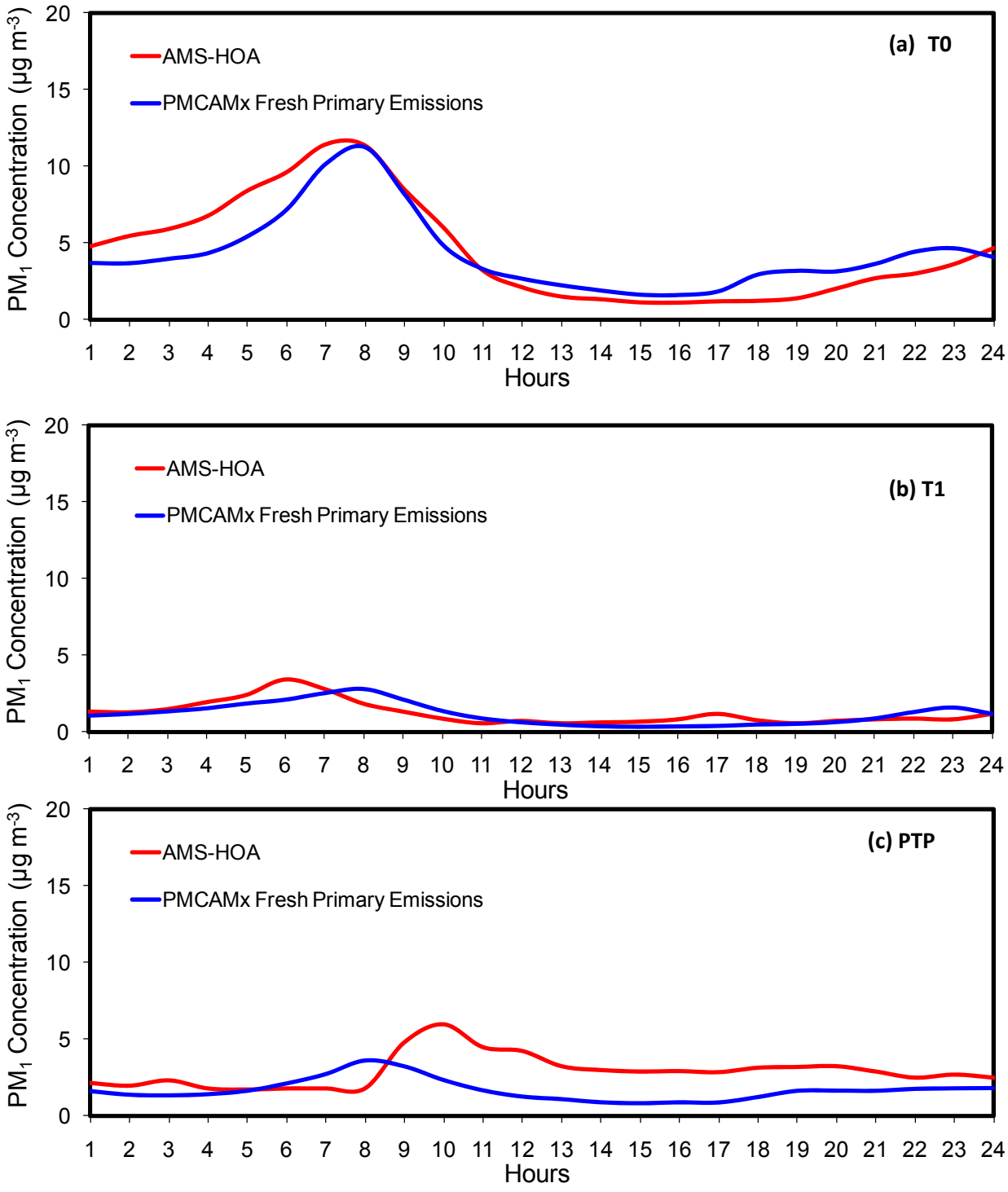

Figure 11. *Comparison of model episode average diurnal predictions for PM_1 local primary organic aerosols against AMS-HOA taken during the MILAGRO campaign in 4-30 of March 2006 at a) T0, b) T1 and c) PTP.*

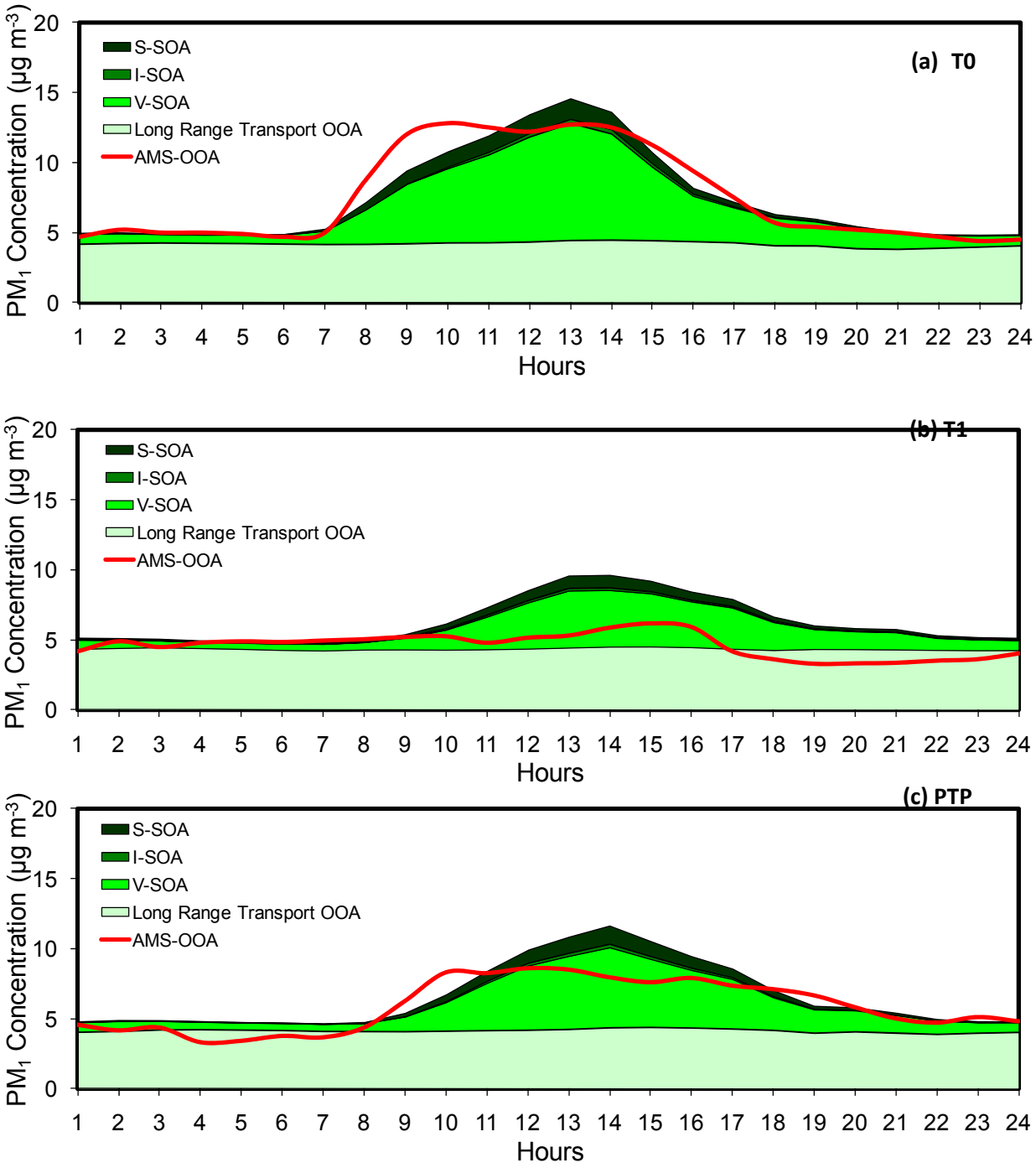

Figure 12. *Comparison of model episode average diurnal predictions for PM_1 oxygenated organic aerosols (sum of Long Range Transport Oxygenated OA, V-SOA, I-SOA, and S-SOA) against AMS-OOA taken during the MILAGRO campaign in 4-30 of March 2006at a) T0, b) T1 and c) PTP.*

11.6. PMCAMx application to Europe focusing on Paris

The PMCAMx modelling domain covers a 5400 × 5832 km^2 region in Europe with 36 × 36 km grid resolution (150 × 162 cells) and 14 vertical layers covering approximately 6 km. The model was set to run with coarse grid spacing (36 × 36 km) over the wide European domain, while within the same run, a fine grid nest was applied in the Paris greater area with a higher resolution (4 × 4 km). The Paris subdomain covers a total area of 216 × 180 km^2 (54 × 45 cells) with the city center placed centrally in the subdomain (Fig. 13). PMCAMx-2008 was set to perform simulations on a rotated polar stereographic map projection. The first three days of each simulation were excluded from the analysis to limit the effect of the initial conditions on the results. The boundary condition organic aerosol (BC-OA) is expected to consist of both SOA and oxidized POA. Here we assume that the BC-OA is all oxidized and half of it is biogenic OA and the other half oxidized primary OA (*Kanakidou et al., 2005; Farina et al., 2010*). All concentrations reported here are under ambient temperature and pressure conditions.

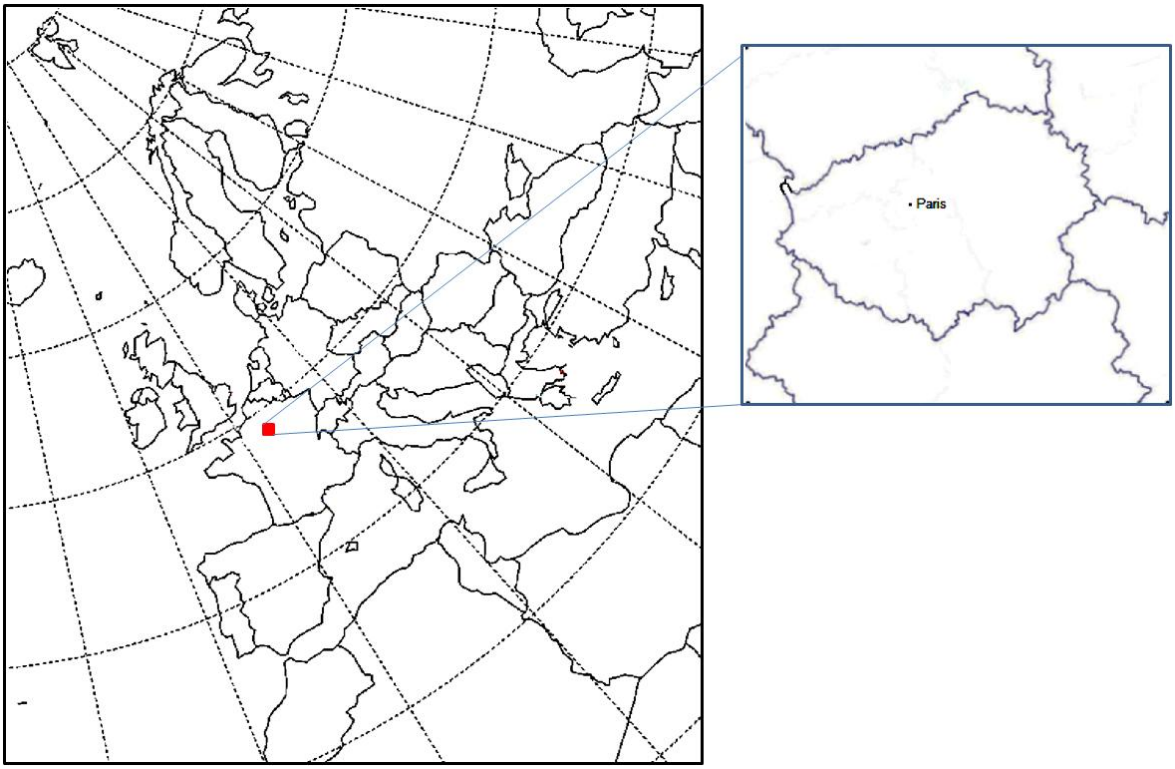

Figure 13. *PMCAMx modelling domain for Europe and subdomain for the Paris greater area.*

The necessary inputs to the model include horizontal wind components, vertical diffusivity, temperature, pressure, water vapor, clouds and rainfall. The meteorological model WRF (Weather Research and Forecasting; *Skamarock et al., 2005*) was used to create the above inputs. WRF was

driven by static geographical data and dynamic meteorological data (near real-time and historical data generated by the Global Forecast System (1x1 deg)). 27 sigma-p layers up to 0.1 bars were used in the vertical dimension. Each layer of PMCAMx is aligned with the layers used in WRF. The WRF July 2009 run was periodically re-initialized (every 3 days) to ensure accuracy in the corresponding fields that are used as inputs in PMCAMx.

Anthropogenic and biogenic hourly emission gridded fields were developed for the European domain for gases and primary particulate matter both for the master and nested model domains. Volatile organic compounds are split based on the SAPRC 99 chemical mechanism. Anthropogenic gas emissions that were used to develop the gridded fields include land emissions from the GEMS dataset (*Visschedijk et al., 2007*) as well as international shipping emissions. Anthropogenic particulate matter mass emissions of organic and elemental carbon are based on the Pan-European Carbonaceous Aerosol Inventory. A variety of emission sources are identified in the two inventories, including industrial, domestic, agricultural and traffic. Three different datasets are combined in order to produce the biogenic gridded emissions for the model. Emissions from ecosystems are produced by MEGAN (Model of Emissions of Gases and Aerosols from Nature) (Guenther et al., 2006). MEGAN inputs include the leaf area index, the plant functional type and the emission factors while the weather data needed for MEGAN are provided from the WRF model. Since sea surface covers a considerable portion of the domain, the marine aerosol model developed by O' Dowd et al. (2008) has been used to estimate mass fluxes for both accumulation and coarse mode including the organic aerosol fraction. Wind speed data from WRF and chlorophyll-a concentrations are the inputs needed for the marine aerosol model. The OA emissions in PMCAMx were distributed by volatility using the volatility distributions of *Tsimpidi et al. (2010).*

11.7. Predicted concentration fields for Paris and evaluation

Figure 14 shows the PMCAMx average ground-level concentrations for PM_1 total mass, OA, sulfate, ammonium, nitrate, and elemental carbon during July 2009 over the Paris greater area. Among the PM_1 species, organic matter is the dominant PM_1 species in the domain with a peak value of 2 μg m^{-3} close to the city center (LHVP site). The model predicts an almost uniform distribution of PM_1 aerosol sulfate with an average value of 0.9 μg m^{-3} and a similar pattern in the concentration map of ammonium and nitrate. An average of 0.5 μg m^{-3} is predicted for PM_1 EC concentrations in the domain, although higher values are predicted locally (up to 1.7 μg m^{-3} in the city center). PMCAMx-2008 predicts an average OA to sulfate mass ratio of 1.6 over the Greater Paris Area and a maximum at the city center where the PM_1 OA mass is predicted to be 2.1 times greater than the PM_1 sulfate levels. Oxidized POA is predicted to be the dominant OA component

during this period contributing 51% to the total oxygenated OA (sum of OPOA, SOA and BC-OA) in the modelling domain of Paris. Biogenic SOA comprises on average 38% of the total predicted OA over the domain while more than 40% of the total oxygenated OA consists of bSOA. Anthropogenic SOA concentrations are predicted to be generally low in the modelling domain (8% contribution to total PM_1 OA on average). The model predicts an almost uniform distribution of aged organic aerosol transported into the domain from the boundaries (~0.4 μg m^{-3}).

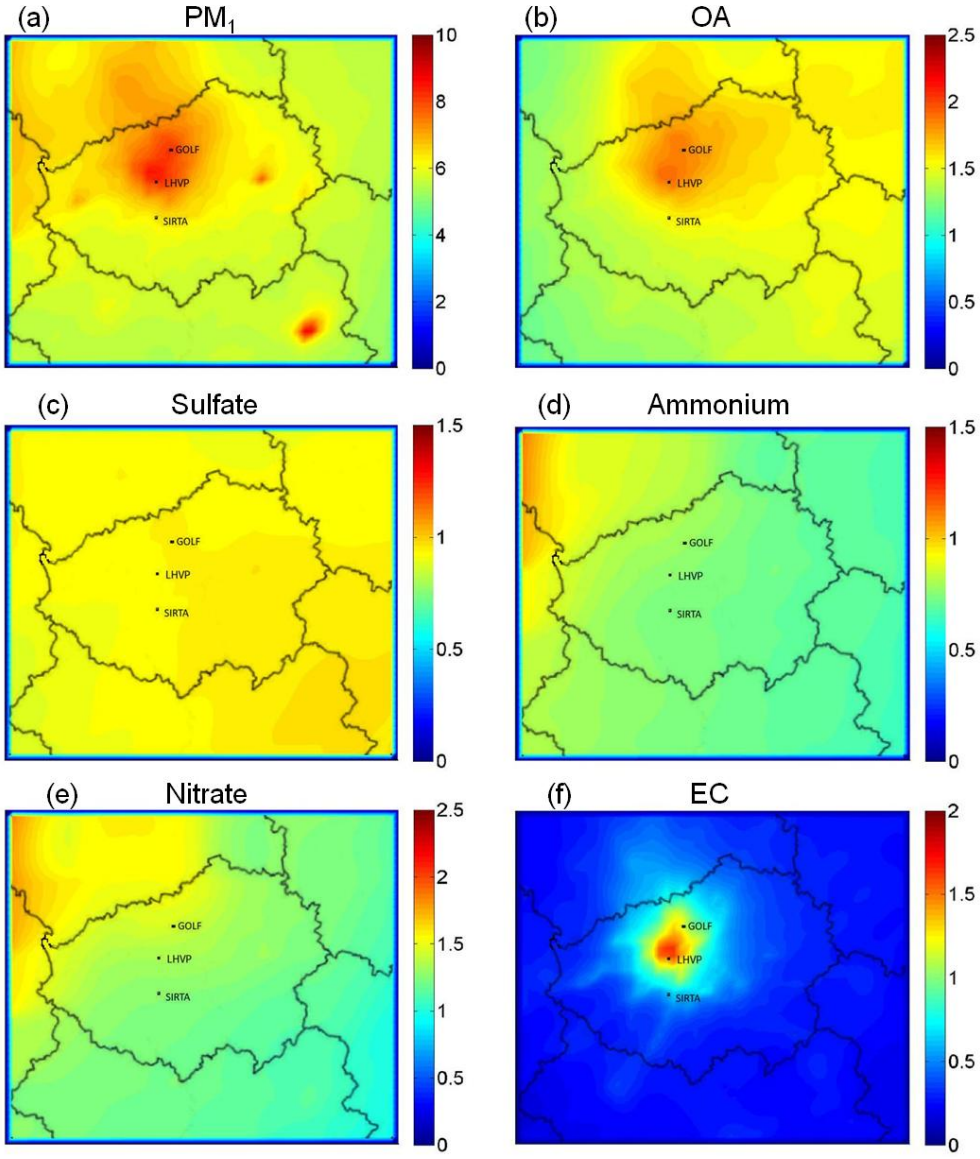

Figure 14. *Ground-level concentration predictions averaged over the entire simulation period (1-30 July 2009) for PM_1 in the Paris area (a) total aerosol mass, (b) sulfate, (c) nitrate, (d) ammonium and EC (in μg m^{-3}). Different scales are used.*

The model results of PMCAMx are compared against measurements from 3 ground sites in the Paris Greater Area. Figures 15-17 show predicted vs. measured (AMS) time series of PM_1 OA at the LHVP (city center), SIRTA and the GOLF site respectively. PMCAMx predictions agree

reasonably well with the AMS measurements. The monthly average predicted concentration for total PM_1 OA is 2.4 μg m^{-3} at LHVP, 1.4 μg m^{-3} at SIRTA, and 1.8 μg m^{-3} at the GOLF site compared to the observed average of 3.4 μg m^{-3}, 1.2 μg m^{-3}, and 3 μg m^{-3} respectively. Figures 18-20 show predicted vs. measured time series of EC at the LHVP, SIRTA and the GOLF site respectively. The model overpredicts EC during the rush hour for some days in the city center and predicts an average value of 1.2 μg m^{-3} compared to an observed monthly average of 0.8 μg m^{-3}. At the SIRTA and GOLF sites the agreement is better. For sulfate the agreement is also encouraging with an average predicted value of ~0.9 μg m^{-3} at all three sites compared to observed averages of 0.8 μg m^{-3}, 0.5 μg m^{-3} and 1.2 μg m^{-3}, respectively.

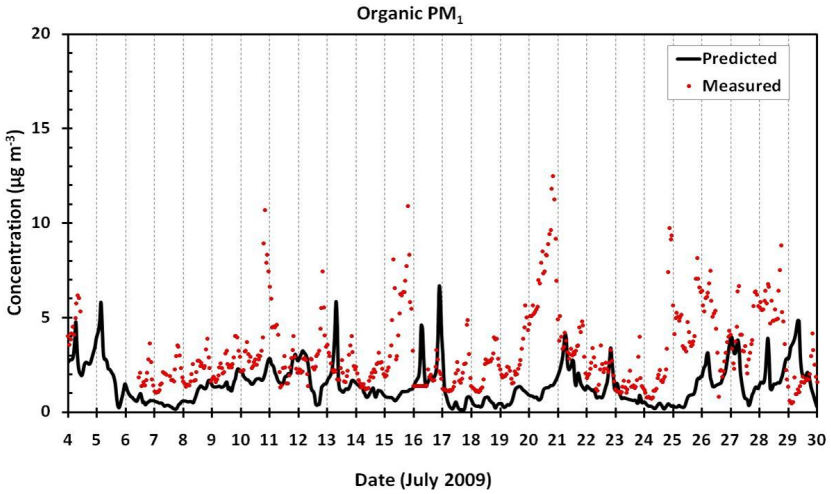

Figure 15: *Comparison of model predictions with measurements of PM_1 OA (in μg m^{-3}) taken at the LHVP site during July 2009.*

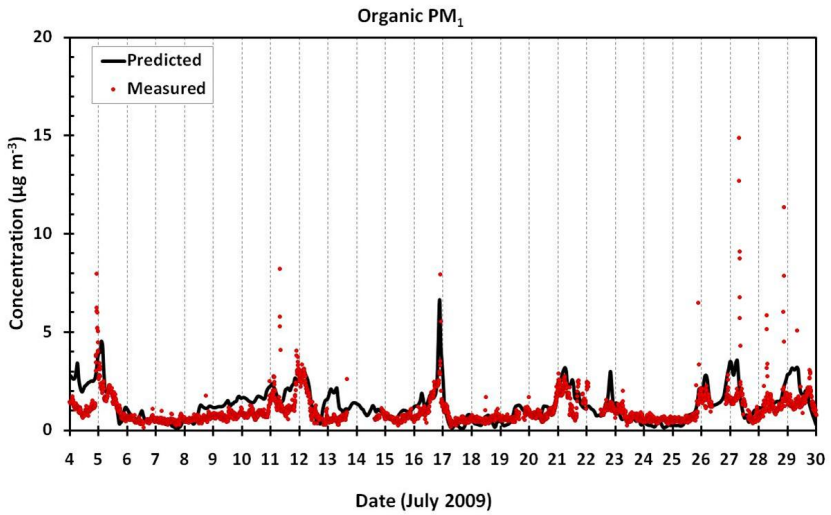

Figure 16: *Comparison of model predictions with measurements of PM_1 OA (in μg m^{-3}) taken at the SIRTA site during July 2009.*

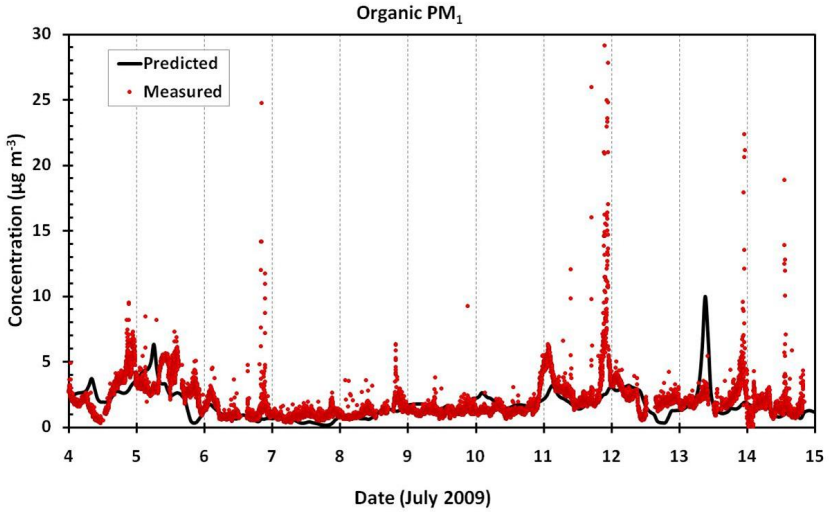

Figure 17: *Comparison of model predictions with measurements of PM_1 OA (in µg m^{-3}) taken at the GOLF site during July 2009.*

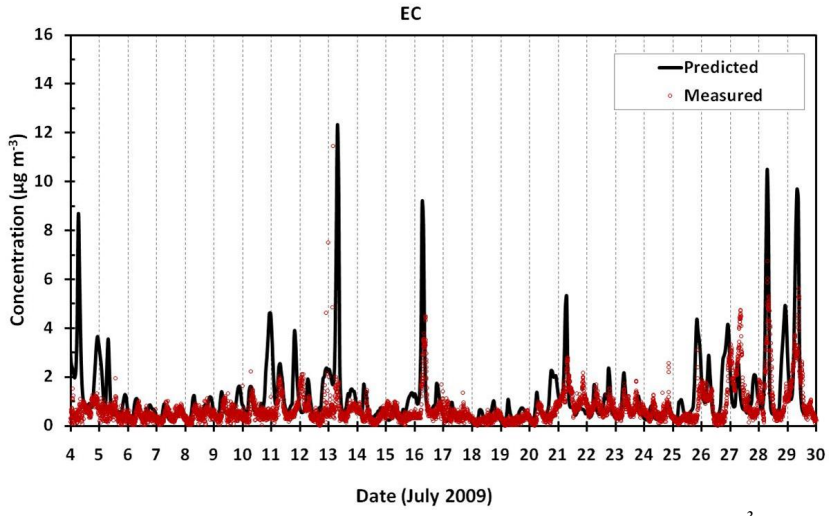

Figure 18: *Comparison of model predictions with measurements of EC (in µg m^{-3}) taken at the LHVP site during July 2009.*

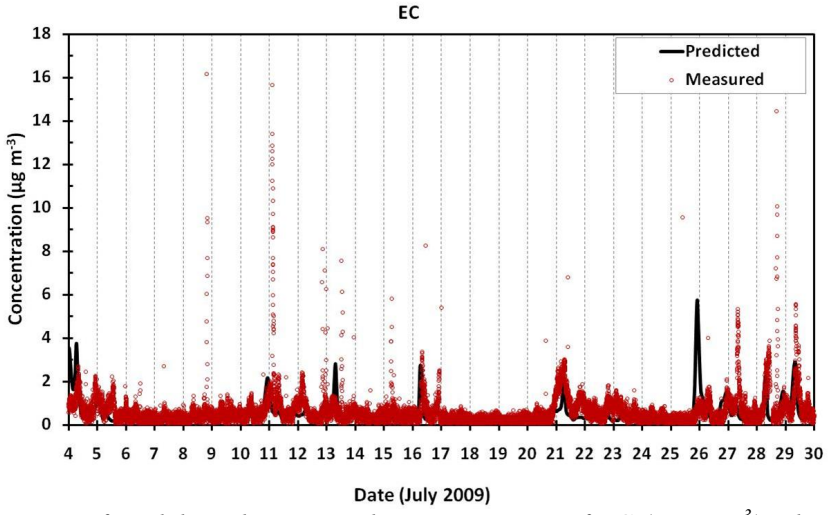

Figure 19: *Comparison of model predictions with measurements of EC (in µg m^{-3}) taken at the SIRTA site during July 2009.*

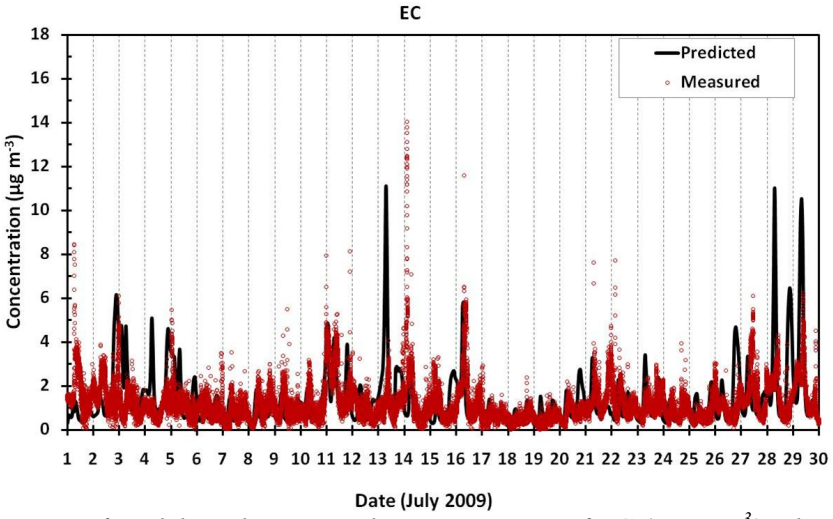

Figure 20: *Comparison of model predictions with measurements of EC (in µg m^{-3}) taken at the GOLF site during July 2009.*

12. Operational Chemical Weather Forecasting Models in Europe

Methods that include a combination of weather forecasting and atmospheric chemistry simulations are here referred to as chemical weather forecasting (CWF). We have selected 18 operational CWF models on regional and continental scales in Europe for a more detailed analysis, This selection of models includes most of the models used in MEGAPOLI (such as Enviro-HIRLAM, FARM, LOTOS-EUROS, SILAM and WRF-CMAQ). This section is based on an extensive review article that is available at ACPD (*Kukkonen et al., 2011*).

We have collected the information in a structured form, and inter-compared and evaluated the mathematical structure of these models. This information makes it possible to evaluate the relative advantages and limitations of the various modelling systems, modelling approaches and sub-models. We have also surveyed the most prominent gaps of knowledge in this field, and suggested potential priorities for future research directions.

Recently, an overview has been published on existing integrated mesoscale meteorological and chemical transport modelling systems in Europe *(Baklanov et al., 2008a)*. However, this study did not aim at an intercomparison of the mathematical structure of the various modelling systems. *Baklanov (2008b)* suggested a more extended definition and concept of CWF, considering the chemical weather as a two-way interaction between the meteorological and chemical composition of the atmosphere based on on-line coupled models.

There are currently several tens, possibly more than a hundred, chemical weather forecasting and information systems (CWFIS's) on a local, regional and continental scale in Europe and worldwide.

An extensive amount of literature exists regarding the properties of individual models, their evaluation against various datasets, and various model applications. However, the literature is scarce regarding the scientific evaluation of such models. With a scientific evaluation, we refer here to the detailed analysis and evaluation of the mathematical structure of such models or modelling systems, in terms of the underlying physics and chemistry of atmospheric pollution.

The literature is also very sparse regarding the inter-comparisons of the properties of several, or even a few, models. However, in most cases, it is far from obvious which modelling option or sub-module is the optimal solution for a specific task. A systematic review of the various available modelling alternatives is therefore urgently needed, to be able to evaluate the advantages and limitations of the various methods.

This study has three main aims. The first is to gather information on the selected operational CWF models in harmonized formats. The second aim is to preliminarily evaluate, and to provide information that makes it possible for the readers to evaluate the relative strengths and limitations of the various sub-models and modelling systems. The third is to highlight and survey the most prominent gaps of knowledge in this field, and to suggest potential priorities for future research directions. This following section focuses on the third aim and only on some selected emerging areas and future research challenges in this area.

12.1. Emerging areas and future challenges

The evaluation of emissions is one of the main sources of the uncertainties in the predictions of the CWF models. First of all, improvement is required for the emission inventories for aerosols, VOCs and organic species. Most of the regional emission inventories currently consider PM_{10} and $PM_{2.5}$; however, primary aerosol emissions definitely need to be further specified in terms of the aerosol size distributions, chemical composition and their source origins. In particular, particulate black carbon (BC) and organic carbon (OC) should be specified. The modelling of the natural emissions of PM—for example, dust events in arid or semi-arid areas, wild-land fires and sea spray—are emerging areas of further research.

Knowledge of the emissions of relevant organic species and their atmospheric chemistry limits the understanding of secondary organic aerosols, which are of importance for both air quality and climate change. Correspondingly, the models for aerosol formation and dynamics need to be implemented into CWF models, and the chemical mechanisms used in CWF models should be substantially improved to be able to simulate sufficiently accurately such processes.

The lack of harmonisation of emission inventories at European and national levels is one of the main obstacles to the quantitative inter-comparison of the predictions of operational CWF sys-

tems. The horizontal resolution of the emission inventories can currently be reasonably accurate for regional CWFs. However, the temporal variability of emissions and the vertical distribution of the heights of the emission sources are not considered accurate in all cases, and these aspects of the emission inventories need to be improved.

The on-line integration of NWP with atmospheric aerosol and chemical transport models is one of possible directions to include the feedbacks of air pollution (e.g., those due to aerosols) on meteorological processes and climate forcing, and further on the atmospheric chemical composition.

An important aspect in the regional applications of the CWF models is the type of initial and boundary conditions used. The use of climatic conditions is one of the common practices, but implementing boundary conditions obtained from global air quality models is currently a significant challenge. This challenge consists of obtaining the required parameters (especially regarding the properties of particulate matter) from the global model computations within a sufficient temporal and spatial resolution.

A fast-growing research area is inverse modelling of emissions using adjoint methods and 4D-VAR. Inverse modelling is being used, especially in global modelling, for monitoring atmospheric constituents, but its benefit for weather and chemical weather forecasting has also been demonstrated. Research on both inverse modelling and data assimilation has been boosted by the availability of satellite-retrieved measurements, which have brought new aspects into assimilation of chemical components. Global spatial coverage, better representativeness of the measured area and gradually improving resolution are the main virtues of these data. In contrast, censoring by clouds, relatively poor time resolution (e.g. two times daily over one spot) and inaccuracies or even errors of the retrieval process are the main drawbacks. An overview of European research on remote sensing of tropospheric constituents has been presented by *Burrows and Borrell (2009).*

Observations of chemical weather are fragmented within the existing European and global landscape of initiatives and infrastructures. This fragmentation reflects the historical development of understanding and the widening spectrum of environmental issues under investigation during the last decades, but also exists to some extent because of the limited resources and the lack of cooperation between countries (*Tørseth and Fahre Vik, 2009*). As is evident from the emergence of chemical data assimilation, the limited availability of measurement data has significant consequences for the pace of progress of research and development in that area.

First, although a relatively new field, CWF is developing quickly, touching upon research, development, and operational forecasting. Although CTM models can be coupled to NWP models either off-line or on-line, a scientific perspective of CWF would argue for an eventual migration from off-line modelling (where the CTM is run after the NWP model is completed) to on-line modelling, allowing coupling and integration of the physical and the chemical components of CWFISs. Spe-

cifically, better and more complete representations of physical and chemical processes and interactions in models are needed. When compared to weather forecasting, CWF has still a long way to go. A key challenge appears to rather be the dimensionality and complexity of the problem itself. For example, the traditional set of prognostic state variables in weather forecasting (e.g., temperature, wind, precipitation) expands to hundreds of prognostic variables because of the number of chemical species involved. In particular, resolving, simulating, and parameterizing processes is no longer limited to relatively well-known physical processes, but is compounded by a huge amount of both chemical and physical processes (e.g., interactions between species, emission, deposition, radiation). This fact has important ramifications for predictability, data assimilation, and ensemble prediction, where scientific and technological progress in CW is slower than in traditional meteorology. Importantly, progress is also inhibited by the lack of or insufficient monitoring of many relevant species and the lack of well-established monitoring data-exchange mechanisms. It is reassuring to know that COST ES0602 and other initiatives are working to address these issues.

Second, numerous well-validated operational CWFISs operate in Europe, addressing the needs of a large spectrum of users from governmental organizations to the individual citizen (e.g., *Karatzas and Kukkonen, 2009*). How is the output from CWF models assessed and interpreted for the end users ? Moreover, how do we interact with those users to provide the needed services? With the ability to assess and explore ensemble prediction systems comes the challenge in communicating probabilistic chemical weather forecasts.

Successful CWFIS services will also need to aggregate and integrate information and deliver it in a way that is comprehensible, user-friendly, timely, and reliable. As a first step, the European open-access CWF portal (http://www.chemicalweather.eu/Domains) integrates existing CWFISs offered by numerous institutions within Europe. This portal provides a direct gateway to the individual resources and is intended to complement and support other European initiatives, such as the GMES Atmospheric Service.

Conclusions

The presented multi-model ensemble has allowed:

(i) to perform an objective inter-comparison of the predictions of the participating models (made within the scope of this WP5 and the WP 7, deliverable 7.3)

(ii) to estimate the extent to which the predictions of the individual models can be improved by means of multi-model ensemble

(iii) to compare different methods of the ensemble treatment to find out the relative strengths and weaknesses of each method.

It was found that the individual models are performing generally similarly for well-verified gaseous pollutants, such as NO_2, SO_2, and O_3. Out of these, the most difficult pollutant to be modelled was SO_2, for which all models have shown very low correlation with the observed time series, being generally close to the mean values. A series of specifics of some of the models were identified and communicated to the model developing groups for investigation.

Contrary to previous findings with other multi-model ensembles, the results showed that vertical profiles of the models are quite comparable, so that the difference between the predicted fields does not increase significantly with height above the surface.

In line with the previous experience, the differences between the model predictions for the compounds not verified routinely can be very large. More efforts are evidently needed to better understand and verify the modelling systems for these species.

It was demonstrated that application of even simple ensemble based estimates leads to improvement of the predictions. However, the effect varies among the compounds. The strongest improvement was obtained for optimising ensemble treatment applied to $PM_{2.5}$ and PM_{10} predictions where these methods eliminated the under-estimation and kept the predicted spatial pattern of the concentrations. Neutral impact was found for SO_2 whereas for O_3 the ensemble average appeared to be superior to the optimising methods. The reasons for such behaviour are under investigations.

Model simulations around the Paris area clearly benefit from emission inventories based on nesting information from local inventories. For particulate matter, the average concentrations over Paris are much lower in this case due to another spatial distribution of the anthropogenic emissions. Comparison with observations shows that with these ‘nested’ emissions, the diurnal cycle is represented better.

A general offset between the PM observations and the simulations largely remains due to missing aerosol components in the models. It could be compensated by empirical approaches and data assimilation procedures but the favoured solution is further research on emission of PM and their precursors, quantification of missing sources and processes to avoid being right for the wrong reasons.

References

Albrecht, B., 1989. Aerosols, Cloud Microphysics and Fractional Cloudiness. Science, 245, 1227-1230.

Allen L., Beevers S., Lindberg F., lamarino M., Kitiwiron N., Grimond GSB., 2010: Global to City Scale Urban Anthropogenic Heat Flux: Model and variability. Sci. Report, 1-87.

Andreae, M. O. and Crutzen, P. J.: Atmospheric aerosols: biogeochemical sources and role in atmospheric chemistry, Science, 276, 1052-1058, 1997.

Andreae, M., O., D. Rosenfeld, P. Artaxo, A. A. Costa, G. P. Frank, K. M. Longo, M. A. F. Silva-Dias, 2004. Smoking Rain Clouds over the Amazon. Science, 303, 1337 - 1342.

Atkinson, R. and Arey, J.: Atmospheric degradation of volatile organic compounds, Chem. Rev., 103, 4605-4638, 2003.

Baklanov A., Grimmond S., Mahura A., Athanassiadou M., (Eds) 2009: Meteorological and air Quality Models for Urban Areas. Springerdoi 10.1007/978-3-642-00298-4.

Baklanov A., Korsholm U., Mahura A., Petersen C., Gross A., 2008: Enviro-HIRLAM online couplied modelling of urban meteorology and air pollution, Adv.Sci. Res., 2, 41-46.

Baklanov A., Mahura A., Sokhi R., (Eds.) (2010): Integrated Systems Of Meso-Meteorological And Chemical Transport Models, 190p., Springer, In press

Baklanov, A., Fay, B., Kaminski, J., and Sokhi, R., Pechinger, U., De Ridder, K., Delcloo, A., Smith Korsholm, U., Gross, A., Männik, A., Kaasik,M., Sofiev, M., Reimer, E., Schlünzen, H., Tombrou, M., Bossioli, E., Finardi, S., Maurizi, A., Castelli, S.T., Finzi, G., Carnevale, C., Pisoni,E., Volta, M., Struzewska, J., Kaszowski, W., Godlowska, J., Rozwoda, W., Miranda, A.I., San José, R., Persson, C., Foltescu, V., Clappier,A., Athanassiadou, M., Hort, M.C., Jones, A., Vogel, H., Suppan, P., Knoth, O., Yu, Y., Chemel, C., Hu, R.-M., Grell, G., Schere, K., Manins, P., Flemming, J.: Overview of Existing Integrated (Off-line and On-line) Mesoscale Meteorological and Chemical Transport Modelling Systems in Europe, WMO TD No. 1427, 2008a.

Baklanov, A., Korsholm, U., Mahura, A., Petersen, C., Gross, A.: Enviro-HIRLAM: on-line coupled modelling of urban meteorology and air pollution, Adv. Sci. Res., 2, 41-46, 2008b.

Baltensperger, U., Kalberer, M., Dommen, J., Paulsen, D., Alfarra, M. R., Coe, H., Fisseha, R., Gascho, A., Gysel, M., Nyeki, S., Sax, M., Steinbacher, M., Prevot, A. S. H., Sjogren, S., Weingartner, E., and Zenobi, R.: Secondary organic aerosols from anthropogenic and biogenic precursors, Faraday Discuss., 130, 265-278, 2005.

Boucher, O., U. Lohmann, 1995. The sulfate-CCN-cloud albedo effect, a sensitivity study with two general circulation models. Tellus, 47B, 281-300.

Burrows, J. and Borrell, P. (Eds.): The Remote Sensing of Tropospheric Constituents form Space. ACCENT-TROPOSAT-2: Activities 2007-8 & Final Report. ACCENT Secretariat, Urbino 2009. http://troposat.iup.uni-heidelberg.de/AT2/AT2/reports.htm.

Capaldo, K. P., Pilinis, C., and Pandis, S. N.: A computationally efficient hybrid approach for dynamic gas/aerosol transfer in air quality models, Atmos. Environ., 34, 3617-3627, 2000.

Carter, W. P. L.: Programs and Files Implementing the SAPRC-99 Mechanism and its Associates Emissions Processing Procedures for Models-3 and Other Regional Models: http://pah.cert.ucr.edu/~carter/SAPRC99.htm, last access: 31 January 2000.

Coakley, J. A., C. D. Walsh, 2002. Limits to the aerosol indirect radiative effect derived from observations of ship tracks. J. Atmos. Sci., 59, 668-680.

Donahue, N. M., Robinson, A. L., Stanier, C. O., and Pandis, S. N.: Coupled partitioning, dilution, and chemical aging of semivolatile organics. Environ. Sci. Technol., 40, 2635-2643, 2006.

Dzepina, K., Volkamer, R. M., Madronich, S., Tulet, P., Ulbrich, I. M., Zhang, Q., Cappa, C. D., Ziemann, P. J., and Jimenez, J. L.: Evaluation of recently-proposed secondary organic aerosol models for a case study in Mexico City, Atmos. Chem. Phys., 9, 5681-5709, 2009.

ENVIRON: User's Guide to the Comprehensive Air Quality Model with Extensions (CAMx), Version 4.02, Report, ENVIRON Int. Corp., Novato, Calif. Available at: http://www.camx.com, 2003.

Fahey, K. and Pandis, S. N.: Optimizing model performance: variable size resolution in cloud chemistry modeling, Atmos. Environ., 35, 4471–4478, 2001.

Fan, J., R. Zhang, W. Tao, K. I. Mohr, 2008. Effects of aerosol optical properties on deep convective clouds and radiative forcing. J.G.R., 113, D08209, doi:10.1029/2007JD009257.

Farina, S. C., Adams, P. J., and Pandis, S. N.: Modeling global secondary organic aerosol formation and processing with the volatility basis set: Implications for anthropogenic secondary organic aerosol, J. Geophys. Res., 115, D09202, doi:10.1029/2009JD013046, 2010.

Feingold, G., B., Stevens, W. R., Cotton, A. R. Frish, 1996. The relationship between drop in-cloud residence time and drizzle production in numerically simulated stratocumulus clouds. J. Atmos. Sci., 53, 1108-1122.

Ferek, R., J., D. A. Hegg, P. V. Hobbs, P. A. Durkee, K. Nielsen, 1998. Measurements of ship induced tracks in clouds off the Washington coast. J. Geophys. Res., 103, 23199-23206.

Gaydos, T., Koo, B., and Pandis, S. N.: Development and application of an efficient moving sectional approach for the solution of the atmospheric aerosol condensation/evaporation equations. Atmos. Environ., 37, 3303-3316, 2003.

Gonzalez-Aparicio I., Nuterman R., Korsholm U., Mahura A. , Hidalgo J. , Baklanov A., 2010: Land-use database Processing approach for meso-scale urban NWP Model Initialization. Sci. Report: ISBN: 978-87-7478-593-4.

Guenther, A., Karl, T., Harvey, P., Wiedinmyer, C., Palmer, P. I., and Geron, C.: Estimates of global terrestrial isoprene emissions using MEGAN (Model of Emissions of Gases and Aerosols from Nature), Atmos. Chem. Phys., 6, 3181-3210, 2006.

Han Q., W. B. Rossow, J. Zeng, R. Welch, 2002. Three different behaviours of liquid water path of water clouds in aerosol-cloud interactions. J. Atmos. Sci., 59, 726-735.

Hidalgo, J., P. Grégorie, V. Masson, 2008. Urban-breeze circulation during the CAPITOUL experiment: Experimental data analysis approach. Met. and Atm. Phys., 102, 223-241.

Hildebrandt, L., Donahue, N. M., and Pandis, S. N.: High formation of secondary organic aerosol from the photo-oxidation of toluene, Atmos. Chem. Phys., 9, 2973-2986, 2009.

Huffman, J. A., Docherty, K. S., Aiken, A. C., Cubison, M. J., Ulbrich, I. M., DeCarlo, P. F., Sueper, D., Jayne, J. T., Worsnop, D. R., Ziemann, P. J., and Jimenez, J. L.: Chemically-resolved aerosol volatility measurements from two megacity field studies, Atmos. Chem. Phys., 9, 7161–7182, 2009a.

Huffman, J. A., Docherty, K. S., Mohr, C., Cubison, M. J., Ulbrich, I. M., Ziemann, P. J., Onasch, T. B., and Jimenez, J. L.: Chemically-resolved volatility measurements of organic aerosol from different sources, Environ. Sci. Technol., 43, 5351-5357, 2009b.

Jayne, J. T., Leard, D. C., Zhang, X. F., Davidovits, P., Smith, K.A., Kolb, C.E., Worsnop, D.R.: Development of an aerosol mass spectrometer for size and composition analysis of submicron particles, Aerosol Sci. Tech., 33, 49-70, 2000.

Kanakidou, M., Seinfeld, J. H., Pandis, S. N., Barnes, I., et al.: Organic aerosol and global climate modeling: a review, Atmos. Chem. Phys., 5, 1053-1123, 2005.

Karatzas, K., and Kukkonen, J. (Eds.): Quality of life information services towards a sustainable society for the atmospheric environment, COST Action ES0602, Workshop Proceedings, Sofia Publications S.A., Thessaloniki, Greece, ISBN: 978-960-6706-20-2. 118 pp, 2009.

Karydis, V. A., Tsimpidi, A. P., Fountoukis, C., Nenes A., Zavala, M., Lei, W., Molina, L. T., and Pandis, S. N.: Simulating the fine and coarse inorganic particulate matter concentrations in a polluted megacity, Atmos. Environ., 44, 608-620, 2010.

King, M. D., L. F. Radke, P. V. Hobbs, 1993. Optical properties of marine stratocumulus clouds modified by ships. J. Geophys. Res., 98, 2729-2739.

Koo, B., Pandis, S. N., and Ansari, A.: Integrated approaches to modeling the organic and inorganic atmospheric aerosol components, Atmos. Environ., 37, 4757-4768, 2003.

Korsholm U.S., 2009: Integrated modeling of aerosol indirect effects. Development and application of an o nline couled chemical weather model. PhD thesis.

Korsholm U.S., Baklanov A., Gross A. and Sorensen J.H. , 2008: On the importance of the meteorological coupling interval in dispersion modelling during ETEX-1, Atmos. Environ., doi: 1016/ j.atmosenv.2008.11.017.

Korsholm U.S., Mahura A., Baklanov A., (2010): Effect of Paris on regional weather: Monthly averaged changes in surface temperature due to aerosol indirect effects of primary aerosol emissions in Western Europe. Geophysical Research Abstracts, Vol. 12, EGU2010-10650.

Kukkonen, J., Balk, T., Schultz, D. M., Baklanov, A., Klein, T., Miranda, A. I., Monteiro, A., Hirtl, M., Tarvainen, V., Boy, M., Peuch, V.-H., Poupkou, A., Kioutsioukis, I., Finardi, S., Sofiev, M., Sokhi, R., Lehtinen, K., Karatzas, K., San José, R., Astitha, M., Kallos, G., Schaap, M., Reimer, E., Jakobs, H., and Eben, K., (2011): Operational, regional-scale, chemical weather forecasting models in Europe, Atmos. Chem. Phys. Discuss., 11, 5985-6162. http://www.atmos-chem-phys-discuss.net/11/5985/2011/

Lane, T. E., Donahue, N. M., and Pandis, S. N.: Effect of NOx on secondary organic aerosol concentrations, Environ. Sci. Technol., 42, 6022-6027, 2008b.

Lane, T. E., Donahue, N. M., and Pandis, S. N.: Simulating secondary organic aerosol formation using the volatility basis-set approach in a chemical transport model, Atmos. Environ., 42, 7439-7451, 2008a.

Lipsky, E. M. and Robinson, A. L.: Effects of dilution on fine particle mass and partitioning of semivolatile organics in diesel exhaust and wood smoke, Environ. Sci. Technol., 40, 155-162, 2006.

Lu, M. L., J. H. Seinfeld, 2005. Study of the aerosol indirect effect by large-eddy simulation of marine stratocumulus. J. Atmos. Sci., 62, 3909-3932.

Martilli A., Clappier A., Rotach M.W., 2002: An Urban Surface Ex-change Parameterisation for Mesoscale Models, Boundary-Layer Meteorol. 104, 261-304.

Martin, G. M., D. W. Johnson, A. Spice, 1994. The measurement and parameterization of effective radius of droplets in warm stratocumulus clouds. J. Atm. Sci., 51, 1823-1842.

Masson, V., L. Gomes, G. Pigeon, C. Liousse, V. Pont, J. P. Lagouarde, J. Voogt, J. Salmond, T. R. Oke, J. Hildago, D. Legain, O. Garrouste, C. Lac, O. Connan, X. Briottet, S. Lachérade, P. Tulet, 2008. The Canopy and Aerosol Particles Interactions in TOulouse Urban Layer (CAPITOUL) experiment. Met. and Atm. Phys., 102, 135-137.

Murphy, B. N. and Pandis, S. N.: Simulating the formation of semivolatile primary and secondary organic aerosol in a regional chemical transport model, Environ. Sci. Technol., 43, 4722-4728, 2009.

Nenes, A., Pandis, S. N., and Pilinis, C.: ISORROPIA: a new thermodynamic equilibrium model for multiphase multicomponent inorganic aerosols, Aquatic Geochemistry, 4, 123-152, 1998.

Ng, N. L., Canagaratna, M. R., Zhang, Q., Jimenez, J. L., Tian, J., Ulbrich, I. M., Kroll, J. H., Docherty, K. S., Chhabra, P. S., Bahreini, R., Murphy, S. M., Seinfeld, J. H., Hildebrandt, 15 L., DeCarlo, P. F., Lanz, V. A., Prevot, A. S. H., Dinar, E., Rudich, Y., and Worsnop, D. R.: Organic aerosol components observed in Northern hemisphere datasets from aerosol mass spectrometry, Atmos. Chem. Phys., 10, 4625-4641, 2010.

Ng, N. L., Kroll, J. H., Keywood, M. D., Bahreini, R., Varutbangkul, V., Flagan, R. C., and Seinfeld, J. H.: Contribution of first- versus second-generation products to secondary organic aerosols formed in the

oxidation of biogenic hydrocarbons, Environ. Sci. Technol., 40, 2283-2297, 2006.

O'Dowd, C. D., Langmann, B., Varghese, S., Scannell, C., Ceburnis, D., and Facchini, M. C.: A Combined Organic-Inorganic Sea-Spray Source Function, Geophys. Res. Lett., 35, L01801, doi:10.1029/2007GL030331, 2008.

Paatero, P. and Tapper, U.: Positive matrix factorization: a nonnegative factor model with optimal utilization of error estimates of data values, Environmetrics, 5, 111-126, 1994.

Paatero, P.: Least squares formulation of robust non-negative factor analysis, Chemometr. Intell. Lab., 37, 23-35, 1997.

Pandis, S. N., Wexler, A. S., and Seinfeld, J. H.: Secondary organic aerosol formation and transport. 2. Predicting the ambient secondary organic aerosol size distribution, Atmos. Environ., 27A, 2403-2416, 1993.

Pilinis, C., Capaldo, K. P., Nenes, A., and Pandis, S. N.: MADM - a new multicomponent aerosol dynamics model. Aerosol Science and Technology 32, 482–502, 2000.

Platnick, S., P. A. Durkee, K. Nielsen, J. P. Taylor, S. C. Tsay, M. D. King, R. J. Ferek, P. V. Hobbs, J. W. Rottman, 2000. The role of background cloud microphysics in the radiative formation of shiptracks. J. Atmos. Sci., 57, 2607-2624.

Pun, B. K., Wu, S. Y., Seigneur, C., Seinfeld, J. H., Griffin, R. J., and Pandis, S. N.: Uncertainties in modeling secondary organic aerosols: Three-dimensional modeling studies in Nashville/Western Tennessee, Environ. Sci. Technol., 37 (16), 3647-3661, doi:10.1021/es0341541, 2003.

Radke, L., F., J. A. Jr. Coakley, M. D. King, 1989. Direct and remote sensing observations of the effects of ships on clouds. Science, 246, 1146-1149.

Rasch, P., J. Kristjansson, 1998, A comparison of the {CCM3} Model Climate using diagnosed and predicted condensate parameterizations, J. Climate, 11, 1587-1614.

Roberts, G. C., Andreae, M. O., Zhou, J., and Artaxo, P.: Cloud condensation nuclei in the Amazon Basin: "Marine" conditions over a continent?, Geophys. Res. Lett., 28(14), 2807-2810, 2001.

Robinson, A. L., Donahue, N. M., Shrivastava, M. K., Weitkamp, E. A., Sage, A. M., Grieshop, A. P., Lane, T. E., Pierce, J. R., Pandis, S. N.: Rethinking organic aerosol: semivolatile emissions and photochemical aging, Science, 315, 1259-1262, 2007.

Sass, B. H., L. Rontu, P. Räisänen, 1994. HIRLAM-2 Radiation Scheme: Documentation and Tests. Norrköping, December 1994 (www.hirlam.org).

Sass, B., 2002. A research version of the STRACO cloud scheme. Danish Meteorological Institute, Technical report no. 02-10 (http://www.dmi.dk/dmi/index/viden/dmi-publikationer/videnskabeligerapporter.htm).

Seinfeld, J, H., S. N. Pandis, 1998. Atmospheric Chemistry and Physics, 2nd Ed., John wiley and Sons, Inc., Hoboken.

Shrivastava, M. K., Lane, T. E., Donahue, N. M., Pandis, S.N., and Robinson, A. L.: Effects of gas-particle partitioning and aging of primary emissions on urban and regional organic aerosol concentrations, J. Geophys. Res., 113, D18301, doi:10.1029/2007JD009735, 2008.

Skamarock, W. C., Klemp, J. B., Dudhia, J., Gill, D. O., Barker, D. M., Wang, W., and Powers, J. G.: A Description of the Advanced Research WRF Version 2, NCAR Technical Note (http://www.mmm.ucar.edu/wrf/users/docs/arw_v2.pdf), 2005.

Stanier, C. O., Donahue, N. M., and Pandis, S. N.: Parameterization of secondary organic aerosol mass fraction from smog chamber data, Atmos. Environ., 42, 2276-2299, 2008.

Takegawa, N., Miyazaki, Y., Kondo, Y., Komazaki, Y., Miyakawa, T., Jimenez, J. L., Jayne, J. T., Worsnop, D. R., Allan, J. D., and Weber, R. J.: Characterization of an Aerodyne Aerosol Mass Spectrometer (AMS): Intercomparison with other aerosol instruments, Aerosol Sci. Tech., 39 (8), 760-770, 2005.

Tijm, S., 2009. Hirlam pseudo satellite images. HIRLAM newsletter, no. 46 (www.hirlam.org)

Tørseth, K., and Fahre Vik A.: An Overview of WG1: "Exchange of AQ Forecasts and input data". In: Quality of life information services towards a sustainable society for the atmospheric environment, COST Action ES0602, Workshop Proceedings, Karatzas, K., and Kukkonen, J. (Eds.), Sofia Publications S.A., Thessaloniki, Greece, ISBN: 978-960-6706-20-2, pp. 39-42, 2009.

Tsimpidi, A. P., Karydis, V. A., Zavala, M., Lei, W., Molina, L., Ulbrich, I. M., Jimenez, J. L., and Pandis, S. N.: Evaluation of the volatility basis-set approach for the simulation of organic aerosol formation in the Mexico City metropolitan area, Atmos. Chem. Phys., 10, 525-546, 2010.

Twomey, S., 1971. Pollution and the Planetary Albedo. Atm. Env., 8, 1251-1256.

Undén, P., L. Rontu, H. Järvinen, H., P. Lynch, J. Calvo, G. Cats, J. Cuhart, K. Eerola et al., 2002. HIRLAM-5 Scientific Documentation. December 2002, HIRLAM-5 project report, SMHI, Norrköping, Sweden (www.hirlam.org).

van der Gon D., H.A.C., A.J.H.Visschedijk , H van der Brugh, R. Droge (2009): A High Resolution Gridded European Emission Database for the year 2005, TNO Report

Visschedijk, A. J. H., Zandveld, P., and Denier van der Gon, H. A. C.: TNO Report 2007 A-R0233/B: A high resolution gridded European emission database for the EU integrated project GEMS, Netherlands, Organization for Applied Scientific Research, 2007.

Wesely, L. M., 1989. Parameterization of surface resistances to gaseous dry deposition in regional-scale numerical models, Atm. Env., 23, 1293-1304.

Wong, K. K., R. A.Dirks, 1978. Mesoscale Perturbations on Airflow in the Urban Mixing Layer. Amer. Met. Soc., 677-688.

Wyser, K., L. Rontu, H. Savijärvi, 1999. Introducing the Effective Radius into a Fast Radiation Scheme of a Mesoscale Model. Contr. Atmos. Phys., 72, 205-218.

Zhang, Q., Canagaratna, M. C., Jayne, J. T., Worsnop, D. R., and Jimenez, J. L: Time and size-resolved chemical composition of submicron particles in Pittsburgh Implications for aerosol sources and processes, J. Geophys. Res., 110, D07S09, doi:10.1029/2004JD004649, 2005a.

Zhang, Q., Jimenez, J. L., Canagaratna, M. R., et al.: Ubiquity and dominance of oxygenated species in organic aerosols in anthropogenically-influenced Northern Hemisphere midlatitudes, Geophys. Res. Lett., 34, L13801, doi:10.1029/2007GL029979, 2007.

Zhang, Q., Worsnop, D. R., Canagaratna, M. R., and Jimenez, J. L.: Hydrocarbon-like and oxygenated organic aerosols in Pittsburgh: insights into sources and processes of organic aerosols, Atmos. Chem. Phys., 5, 3289-3311, 2005b.

Previous MEGAPOLI reports

Previous reports from the FP7 EC MEGAPOLI Project can be found at: http://www.megapoli.info/

Collins W.J. (**2009**): Global radiative forcing from megacity emissions of long-lived greenhouse gases. Deliverable 6.1, *MEGAPOLI Scientific Report 09-01*, 17p, *MEGAPOLI-01-REP-2009-10, ISBN: 978-87-992924-1-7*
http://megapoli.dmi.dk/publ/MEGAPOLI_sr09-01.pdf

Denier van der Gon, HAC, AJH Visschedijk, H. van der Brugh, R. Dröge, J. Kuenen (**2009**): A base year (2005) MEGAPOLI European gridded emission inventory (1st version). Deliverable 1.2, *MEGAPOLI Scientific Report 09-02*, 17p, *MEGAPOLI-02-REP-2009-10, ISBN: 978-87-992924-2-4*
http://megapoli.dmi.dk/publ/MEGAPOLI_sr09-02.pdf

Baklanov A., Mahura A. (Eds) (**2009**): First Year MEGAPOLI Dissemination Report. Deliverable 9.4.1, *MEGAPOLI Scientific Report 09-03*, 57p, *MEGAPOLI-03-REP-2009-12, ISBN: 978-87-992924-3-1*
http://megapoli.dmi.dk/publ/MEGAPOLI_sr09-03.pdf

Allen L., S Beevers, F Lindberg, Mario Iamarino, N Kitiwiroon, CSB Grimmond (**2010**): Global to City Scale Urban Anthropogenic Heat Flux: Model and Variability. Deliverable 1.4, *MEGAPOLI Scientific Report 10-01*, *MEGAPOLI-04-REP-2010-03,* 87p, *ISBN: 978-87-992924-4-8*
http://megapoli.dmi.dk/publ/MEGAPOLI_sr10-01.pdf

Pauli Sievinen, Antti Hellsten, Jaan Praks, Jarkko Koskinen, Jaakko Kukkonen (**2010**): Urban Morphological Database for Paris, France. Deliverable D2.1, *MEGAPOLI Scientific Report 10-02*, *MEGAPOLI-05-REP-2010-03,* 13p, *ISBN: 978-87-992924-5-5*
http://megapoli.dmi.dk/publ/MEGAPOLI_sr10-02.pdf

Moussiopoulos N., Douros J., Tsegas G. (Eds.) (**2010**): Evaluation of Zooming Approaches Describing Multiscale Physical Processes. Deliverable D4.1, *MEGAPOLI Scientific Report 10-03*, *MEGAPOLI-06-REP-2010-01, 41p, ISBN: 978-87-992924-6-2*
http://megapoli.dmi.dk/publ/MEGAPOLI_sr10-03.pdf

Mahura A., Baklanov A. (Eds.) (**2010**): Hierarchy of Urban Canopy Parameterisations for Different Scale Models. Deliverable D2.2, *MEGAPOLI Scientific Report 10-04*, *MEGAPOLI-07-REP-2010-03, 50p, ISBN: 978-87-992924-7-9*
http://megapoli.dmi.dk/publ/MEGAPOLI_sr10-04.pdf

Dhurata Koraj, Spyros N. Pandis (**2010**): Evaluation of Zooming Approaches Describing Multiscale Chemical Transformations. Deliverable D4.2, *MEGAPOLI Scientific Report 10-05*, *MEGAPOLI-08-REP-2010-01, 29p, ISBN: 978-87-992924-8-6*
http://megapoli.dmi.dk/publ/MEGAPOLI_sr10-05.pdf

Igor Esau (**2010**): Urbanized Turbulence-Resolving Model and Evaluation for Paris. Deliverable D2.4.1, *MEGAPOLI Scientific Report 10-06*, *MEGAPOLI-09-REP-2010-03, 20p, ISBN: 978-87-992924-9-3*
http://megapoli.dmi.dk/publ/MEGAPOLI_sr10-06.pdf

Grimmond CSB., M. Blackett, M.J. Best, et al. (**2010**): Urban Energy Balance Models Comparison. Deliverable D2.3, *MEGAPOLI Scientific Report 10-07*, *MEGAPOLI-10-REP-2010-03, 72p, ISBN: 978-87-993898-0-3*
http://megapoli.dmi.dk/publ/MEGAPOLI_sr10-07.pdf

Gerd A. Folberth, Steve Rumbold, William J. Collins, Tim Butler (**2010**): Determination of Radia-

tive Forcing from Megacity Emissions on the Global Scale. Deliverable D6.2, *MEGAPOLI Scientific Report 10-08*, *MEGAPOLI-11-REP-2010-03, 19p, ISBN: 978-87-993898-1-0*

http://megapoli.dmi.dk/publ/MEGAPOLI_sr10-08.pdf

Thomas Wagner, Steffen Beirle, Reza Shaiganfar (**2010**): Characterization of Megacity Impact on Regional and Global Scales Using Satellite Data. Deliverable D5.1, *MEGAPOLI Scientific Report 10-09*, *MEGAPOLI-12-REP-2010-03, 25p, ISBN: 978-87-993898-2-7*

http://megapoli.dmi.dk/publ/MEGAPOLI_sr10-09.pdf

Baklanov A., Mahura A. (Eds.) (**2010**): Interactions between Air Quality and Meteorology, Deliverable D4.3, *MEGAPOLI Scientific Report 10-10, MEGAPOLI-13-REP-2010-03, 48p, ISBN: 978-87-993898-3-4*

http://megapoli.dmi.dk/publ/MEGAPOLI_sr10-10.pdf

Baklanov A. (Ed.) (**2010**): Framework for Integrating Tools. Deliverable D7.1, *MEGAPOLI Scientific Report 10-11, MEGAPOLI-14-REP-2010-03, 68p, ISBN: 978-87-993898-4-1*

http://megapoli.dmi.dk/publ/MEGAPOLI_sr10-11.pdf

Sofiev M., Prank M., Vira J., and MEGAPOLI Modelling Teams (**2010**): Provision of global and regional concentrations fields from initial baseline runs. Deliverable D5.2*, MEGAPOLI Technical Note 10-12, MEGAPOLI-15-REP-2010-03, 10p.*

http://megapoli.dmi.dk/publ/MEGAPOLI_sr10-12.pdf

H.A.C. Denier van der Gon, J. Kuenen, T. Butler (**2010**): A Base Year (2005) MEGAPOLI Global Gridded Emission Inventory (1st Version). Deliverable D1.1*, MEGAPOLI Scientific Report 10-13, MEGAPOLI-16-REP-2010-06, 20p, ISBN: 978-87-993898-5-8*

http://megapoli.dmi.dk/publ/MEGAPOLI_sr10-13.pdf

Lawrence M. G., Butler T. M., Collins W., Folberth G., Zakey A., Giorgi F. (**2010**): Meteorological Fields for Present and Future Climate Conditions. Deliverable D6.5*, MEGAPOLI Technical Note 10-14, MEGAPOLI-17-REP-2010-09, 9p.*

http://megapoli.dmi.dk/publ/MEGAPOLI_sr10-14.pdf

Beekmann M., Baltensperger U., and the MEGAPOLI campaign team (**2010**): Database of Chemical Composition, Size Distribution and Optical Parameters of Urban and Suburban PM and its Temporal Variability (Hourly to Seasonal). Deliverable D3.1*, MEGAPOLI Scientific Report 10-15, MEGAPOLI-18-REP-2010-10, 21p, ISBN: 978-87-993898-6-5*

http://megapoli.dmi.dk/publ/MEGAPOLI_sr10-15.pdf

Beekmann M., Baltensperger U., and the MEGAPOLI campaign team (**2010**): Database of the Impact of Megacity Emissions on Regional Scale PM Levels. Deliverable D3.4*, MEGAPOLI Scientific Report 10-16, MEGAPOLI-19-REP-2010-10, 29p, ISBN: 978-87-993898-7-2*
http://megapoli.dmi.dk/publ/MEGAPOLI_sr10-16.pdf

Kuenen J., H. Denier van der Gon, A. Visschedijk, H. van der Brugh, S. Finardi, P. Radice, A. d'Allura, S. Beevers, J. Theloke, M. Uz-basich, C. Honoré, O. Perrussel (**2010**): A Base Year (2005) MEGAPOLI European Gridded Emission Inventory (Final Version). Deliverable D1.6*, MEGAPOLI Scientific Report 10-17, MEGAPOLI-20-REP-2010-10, 37p, ISBN: 978-87-993898-8-9*

http://megapoli.dmi.dk/publ/MEGAPOLI_sr10-17.pdf

Karppinen A., Kangas L., Riikonen K., Kukkonen J., Soares J., Denby B., Cassiani M., Finardi S., Radice P., (**2010**): Evaluation of Methodologies for Exposure Analysis in Urban Areas and Application to Selected Megacities. Deliverable D4.4, *MEGAPOLI Scientific Report 10-18, MEGAPOLI-21-REP-2010-11, 29p, ISBN: 978-87-993898-9-6*

http://megapoli.dmi.dk/publ/MEGAPOLI_sr10-18.pdf

Soares J., A. Karppinen, B. Denby, S. Finardi, J. Kukkonen, M. Cassiani, P. Radice, M.Williams

(**2010**): Exposure Maps for Selected Megacities. Deliverable D4.5, *MEGAPOLI Scientific Report 10-19, MEGAPOLI-22-REP-2010-11, 26p, ISBN: 978-87-92731-00-5*
http://megapoli.dmi.dk/publ/MEGAPOLI_sr10-19.pdf

Rumbold S.T., W.J. Collins, G.A. Folberth (**2010**): Comparison of Coupled and Uncoupled Models. Deliverable D6.4, *MEGAPOLI Scientific Report 10-20, MEGAPOLI-23-REP-2010-11, 15p, ISBN: 978-87-92731-01-2*
http://megapoli.dmi.dk/publ/MEGAPOLI_sr10-20.pdf

Baklanov A., Mahura A. (Eds) (**2010**): Second Year MEGAPOLI Dissemination Report. Deliverable D9.4.2, *MEGAPOLI Scientific Report 10-21*, *MEGAPOLI-24-REP-2010-12, 89p, ISBN: 978-87-92731-02-9*
http://megapoli.dmi.dk/publ/MEGAPOLI_sr10-21.pdf

Moussiopoulos N., Douros J., Tsegas G. (Eds) (**2010**): Evaluation of Source Apportionment Methods. Deliverable D4.6, *MEGAPOLI Scientific Report 10-22*, *MEGAPOLI-25-REP-2010-12, 54p, ISBN: 978-87-92731-03-6*
http://megapoli.dmi.dk/publ/MEGAPOLI_sr10-22.pdf

Theloke J., M.Blesl, D. Bruchhof, T.Kampffmeyer, U. Kugler, M. Uzbasich, K. Schenk, H. Denier van der Gon, S. Finardi, P. Radice, R. S. Sokhi, K. Ravindra, S. Beevers, S. Grimmond, I. Coll, R. Frie-drich, D. van den Hout (**2010**): European and megacity baseline scenarios for 2020, 2030 and 2050. Deliverable D1.3, *MEGAPOLI Scientific Report 10-23, MEGAPOLI-26-REP-2010-12, 57p, ISBN: 978-87-92731-04-3*
http://megapoli.dmi.dk/publ/MEGAPOLI_sr10-23.pdf

Galmarini S., Vinuesa J.F., Cassiani M., Denby B., Martilli A., (**2011**): Evaluation of Sub-Grid Models with Interactions between Turbulence and Urban Chemistry. *Recommendations for Emission Inventories Improvement*. Deliverable D2.6, *MEGAPOLI Scientific Report 11-01*, *MEGAPOLI-27-REP-2011-01, 41p, ISBN: 978-87-92731-05-0*
http://megapoli.dmi.dk/publ/MEGAPOLI_sr11-01.pdf

Butler T., H.A.C. Denier van der Gon, J. Kuenen (**2011**): The Base Year (2005) Global Gridded Emission Inventory used in the EU FP7 Project MEGAPOLI (Final Version). Deliverable D1.5, *MEGAPOLI Scientific Report 11-02*, *MEGAPOLI-28-REP-2011-01, 27p, 978-87-92731-06-7*
http://megapoli.dmi.dk/publ/MEGAPOLI_sr11-02.pdf

Schlünzen K.H., M. Haller (Eds) (**2011**): Evaluation of Integrated Tools. Deliverable D7.2 *MEGAPOLI Scientific Report 11-03, MEGAPOLI-29-REP-2011-03, 50p, 978-87-92731-07-4*
http://megapoli.dmi.dk/publ/MEGAPOLI_sr11-03.pdf

Sofiev M., M. Prank, J. Kukkonen (Eds) (**2011**): Evaluation and Improvement of Regional Model Simulations for Megacity Plumes. Deliverable D5.3, *MEGAPOLI Scientific Report 11-04, MEGAPOLI-30-REP-2011-03, 88p, 978-87-92731-08-1*
http://megapoli.dmi.dk/publ/MEGAPOLI_sr11-04.pdf

MEGAPOLI

Megacities: Emissions, urban, regional and Global Atmospheric POLlution and climate effects, and Integrated tools for assessment and mitigation

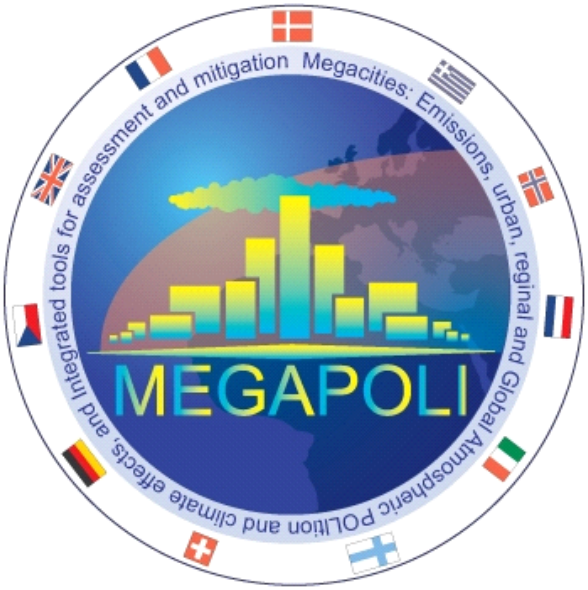

EC FP7 Collaborative Project

2008-2011

Theme 6: Environment (including climate change)
Sub-Area: ENV-2007.1.1.2.1:
Megacities and regional hot-spots air quality and climate

MEGAPOLI Project web-site

http://www.megapoli.info

MEGAPOLI Project Office

Danish Meteorological Institute (DMI)
Lyngbyvej 100, DK-2100
Copenhagen, Denmark
E-mail: alb@dmi.dk
Phone: +45-3915-7441
Fax: +45-3915-7400

MEGAPOLI Project Partners

- **DMI** - Danish Meteorological Institute (Denmark) - Contact Persons: *Prof. Alexander Baklanov (co-ordinator), Dr. Alexander Mahura (manager)*
- **FORTH** - Foundation for Research and Technology, Hellas and University of Patras (Greece) - *Prof. Spyros Pandis (vice-coordinator)*
- **MPIC** - Max Planck Institute for Chemistry (Germany) - *Dr. Mark Lawrence (vice-coordinator)*
- **ARIANET** Consulting (Italy) – *Dr. Sandro Finardi*
- **AUTH** - Aristotle University Thessaloniki (Greece) - *Prof. Nicolas Moussiopoulos*
- **CNRS** - Centre National de Recherche Scientifique (incl. LISA, LaMP, LSCE, GAME, LGGE) (France) – *Dr. Matthias Beekmann*
- **FMI** - Finnish Meteorological Institute (Finland) – *Prof. Jaakko Kukkonen*
- **JRC** - Joint Research Center (Italy) – *Dr. Stefano Galmarini*
- **ICTP** - International Centre for Theoretical Physics (Italy) - *Prof. Filippo Giorgi*
- **KCL** - King's College London (UK) – *Prof. Sue Grimmond*
- **NERSC** - Nansen Environmental and Remote Sensing Center (Norway) – *Dr. Igor Esau*
- **NILU** - Norwegian Institute for Air Research (Norway) – *Dr. Andreas Stohl*
- **PSI** - Paul Scherrer Institute (Switzerland) – *Prof. Urs Baltensperger*
- **TNO**-Built Environment and Geosciences (The Netherlands) – *Prof. Peter Builtjes*
- **MetO** - UK MetOffice (UK) – *Dr. Bill Collins*
- **UHam** - University of Hamburg (Germany) – *Prof. Heinke Schluenzen*
- **UHel** - University of Helsinki (Finland) – *Prof. Markku Kulmala*
- **UH-CAIR** - University of Hertfordshire, Centre for Atmospheric and Instrumentation Research (UK) – *Prof. Ranjeet Sokhi*
- **USTUTT** - University of Stuttgart (Germany) – *Prof. Rainer Friedrich*
- **WMO** - World Meteorological Organization (Switzerland) – *Dr. Liisa Jalkanen*
- **CUNI** - Charles University Prague (Czech Republic) – *Dr. Tomas Halenka*
- **IfT** - Institute of Tropospheric Research (Germany) – *Prof. Alfred Wiedensohler*
- **UCam** - Centre for Atmospheric Science, University of Cambridge (UK) – *Prof. John Pyle*

Work Packages

WP1: Emissions
(H. Denier van der Gon, P. Builtjes)
WP2: Megacity features
(S. Grimmond, I. Esau)
WP3: Megacity plume case study
(M. Beekmann, U. Baltensperger)
WP4: Megacity air quality
(N. Moussiopoulos)
WP5: Regional and global atmospheric composition
(J. Kukkonen, A. Stohl)
WP6: Regional and global climate impacts
(W. Collins, F. Giorgii)
WP7: Integrated tools and implementation
(R. Sokhi, H. Schlünzen)
WP8: Mitigation, policy options and impact assessment
(R. Friedrich, D. van den Hout)
WP9: Dissemination and Coordination
(A. Baklanov, M. Lawrence, S. Pandis)